Supporting Information for

Substituents Make a Difference: 6,6''-modified Terpyridine Complexes with Helix Configuration and Enhanced Emission

Fan Fu,[a] Die Liu,[b]* Lili Zhao,[c] Huili Li,[c] Xinyu Bai,[c] Mingzhao Chen,[c] Zhilong Jiang,[c] Peiyang Su,[c] Wanying Zhong,[c]Yiming Li,[b] Jun He,[a]* Pingshan Wang[b]*

[a] School of Chemical Engineering and Light Industry, Guangdong University of Technology, Guangzhou 510006, China.

[b] College of Chemistry and Chemical Engineering, Central South University, Changsha, Hunan-410083, China

[c] Institute of Environmental Research at Greater Bay Area, Guangzhou University, Guangdong-510006, China

Table of contents

Materials and General Methods

Absorption spectra were measured with Hitachi (model U-3010) UV-Vis spectrophotometer in a 1-cm quartz cell. Emission spectra were measured with Edinburgh (FS5) fluorescence spectrophotometer in a 1-cm quartz cell under the following conditions: EX Slit, 5.0 nm; EM Slit, 3.0 nm; PMT Voltage, 240 V for complex $L2_2$-Zn and EX Slit, 3.0 nm; EM Slit, 0.66 nm; PMT Voltage, 240 V for complex $L2_2$-M. PL quantum yields and transient PL decay are measured using Edinburgh Instruments FS30 spectrometer, Fluorescence transient spectrum measured by Edinburgh FLS980.CD spectra were measured by Chirascan,

NMR spectra were recorded on a Bruker ADVANCE 400 or 600 NMR Spectrometer. ^{1}H NMR chemical shifts are reported in ppm downfield from tetramethyl silane (TMS) reference using the residual protonated solvent, as an internal standard.

Mass spectra of complexes and ligands were determined on Waters Synaptic G2 Mass Spectrometer with traveling wave ion mobility (TWIM) under the following conditions: ESI capillary voltage, 3.5 kV; cone voltage, 35 V; desolation gas flow, 800 L/h. TWIM-MS was measured with IM traveling wave height, 25 V; and IM traveling wave velocity, 1000 m/s.

Single crystals were mounted on glass fiber. Intensity data were collected using a Bruker AXS-KAPPA APEX II diffractometer with graphite monochromate Mo-Ka (l ¼ 0.710-73 Å) radiation and Cu-Ka (l ¼ 0.710-73 Å). Data were collected using omega scans of 0.5 per frame, and full spheres of data were obtained. Cell parameters were retrieved using Bruker SMART software and refined using Bruker SAINT on all the observed reflections. Absorption corrections were applied using SADABS. Structures were solved by direct methods using the SHELXS-97 package and refined with SHELXL-97 Calculations were performed using the WinGX System Version 1.80.03. The remaining hydrogen atoms were inserted in calculated positions. Least square refinements, with anisotropic thermal motion parameters for all the nonhydrogen atoms and isotropic for the remaining atoms, were employed. CCDC 2170550 **($L2_2$-Co)**, 2170551 (**$L2_2$-Ni)**, 2170552 (**$L2_2$-Cu)**, 2170553 (**$L2_2$-Zn)**, 2170554 (**$L2_2$-Fe)**, 2169764 (**$L2_2$-Mn)**, 2210926 (**$L1_2$-Co)** contain the supplementary crystallographic data of this paper. These data can be obtained free of charge from the Cambridge Crystallographic Data Centre via w.ccdc.cam. ac.uk/data request/cif. Crystal data and details of data collections are reported in Table S3.

All chemicals were purchased from commercial suppliers and used without further purification unless otherwise specified. Benzaldehyde and 1-(6-bromopyridin-2-yl) ethan-1-one were purchased from Bide Pharmatech Company.

Density functional theory (DFT) calculations were carried out by using the Gaussian 09 package [1]. Ground-state geometries were fully optimized with PBE0 functional, 6-31G (d, p) basis set for C, H, O, N atoms and LANL2DZ basis set for Zn atoms. Time-dependent density functional theory (TD-DFT) was employed to calculate excited states using the same basis set. The implicit solvation models (SMD) of water and the dispersion corrections with Grimme's D3(BJ) method [2] were taken into consideration in all calculations. The orbital diagrams were prepared using with the Multiwfn software [3] and VMD package [4].

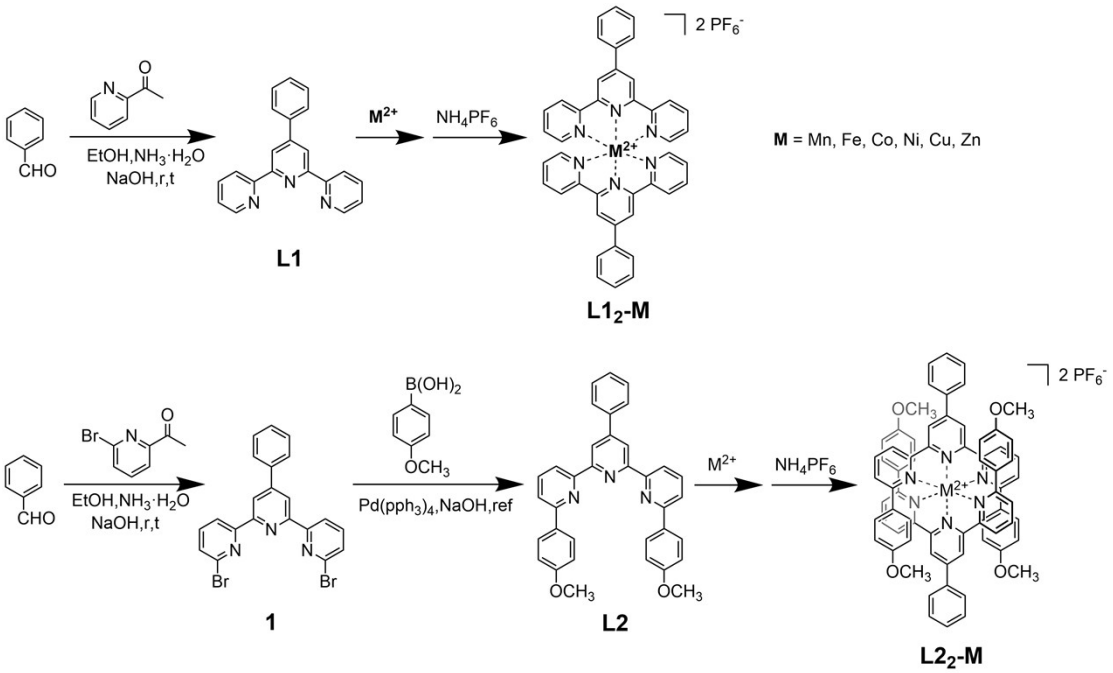

Scheme S1 Synthesis of complex **$L1_2$-M** and **$L2_2$-M** (**M^{2+}** = Mn^{2+}, Fe^{2+}, Co^{2+}, Ni^{2+}, Cu^{2+}, Zn^{2+}), ligand **L1** was synthesized according to the literature procedures.[5]

1

Compound 1. To a solution of benzaldehyde (1.1 g, 10 mmol) in EtOH (60 mL), 1- (6-bromopyridin-2-yl) ethan-1-one (4.9 g, 24.5 mmol) and NaOH powder (2g, 50mmol) was added. After stirring at room temperature for 24 h, aqueous NH_3•H_2O (28%, 25 mL) was added, the resulting mixture was refluxed for 20 h. After cooling to room temperature, The solid was collected by suction filtration and was washed with CH_3OH to give the product as a white solid: 2.042g, 43.7%) ◦ ^{1}H NMR (400 MHz, $CDCl_3$, ppm): δ = 8.69 (s, 2H), 8.59 (d, *J* = 7.6 Hz, 2H), 7.87 (d, *J* = 7.6 Hz, 2H), 7.72(t, J= 15.6Hz, 2H), 7.53 (m, 5H); ^{13}C NMR (126 MHz, $CDCl_3$, ppm): δ = 157.3, 154.4, 150.9, 141.7, 139.2, 138.2, 129.2, 129.0, 128.2, 127.4, 120.0, 119.9.

Ligand L2. To a flask containing **1** (0.2g, 0.43 mmol), (4-methoxyphenyl) boronic acid (0.26 g, 1.7 mmol) and NaOH (0.14 g,3.5 mmol), A mixed solvent (40mL) of THF/H_2O (10:1, v/v) was added. Then Pd (PPh_3)$_4$ (0.21 g, 0.18 mmol) was added, the system was pumped and backfilled with nitrogen. The mixture was refluxed for 2 days under N_2. After cooling to 25 °C, the mixture was extracted with $CHCl_3$ and the combined organic extract was evaporated in vacuo to dryness giving a reside that was washed with CH_3OH, Then subjected to column chromatography (Al_2O_3, CH_2Cl_2/MeOH = 100:1), Then the major fraction was recrystallized from a mixture of CH_2Cl_2 / MeOH to give **L2** (64%), As a white solid: 0.14 g (0.81 mmol); ^{1}H NMR (400 MHz, $CDCl_3$, ppm) δ = 8.82 (s, 2H), 8.53 (d, *J* = 8.4 Hz, 2H), 8.09 (d, *J* = 8.8 Hz, 4H), 7.85(m, 4H), 7.69 (d, J= 8.8Hz, 2H) , 7.51 (t, J= 14.8Hz, 2H),7.43 (t, J= 14.8Hz, H), .6.99 (d, J= 8.8Hz, 4H) .3.83 (s, 6H); ^{13}C NMR (126 MHz, $CDCl_3$, ppm): δ = 160.5, 156.15 156.1, 155.8, 150.3, 139.2, 137.5, 132.1, 129.0, 128.8, 128.3, 127.5, 119.6, 119.2, 119.0, 114.1, 55.4.

NMR spectra of ligands L1 and L2

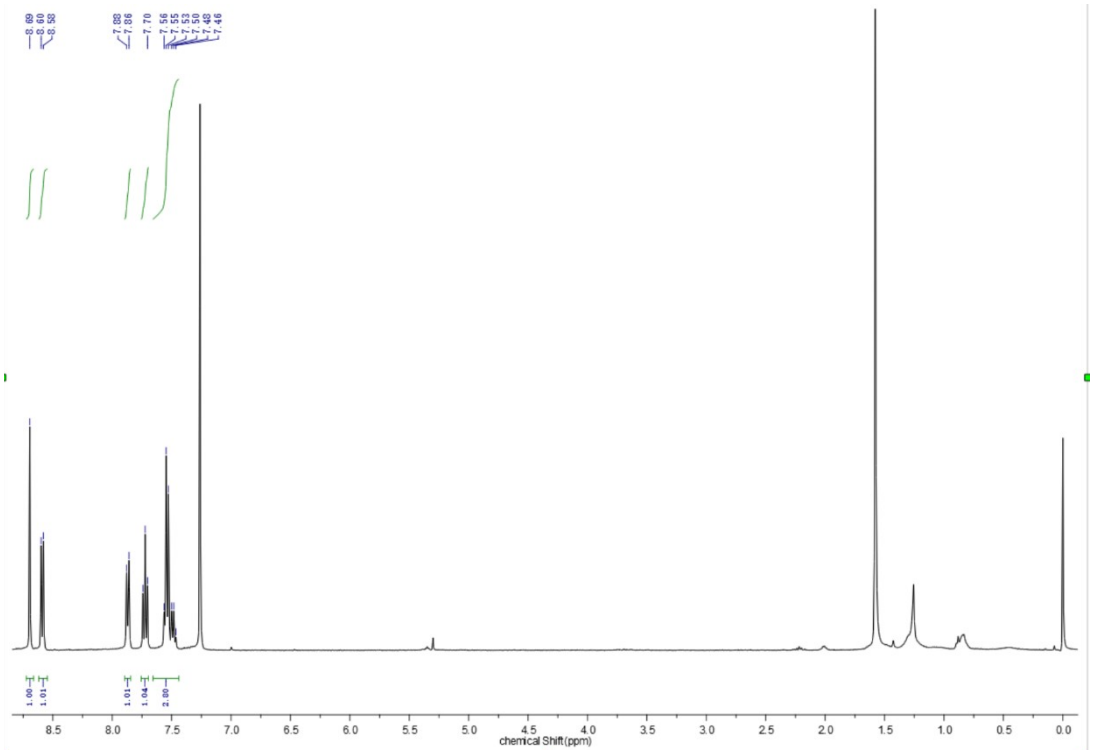

Fig. S1 ^{1}H NMR spectra of ligand **L1** in $CDCl_3$.

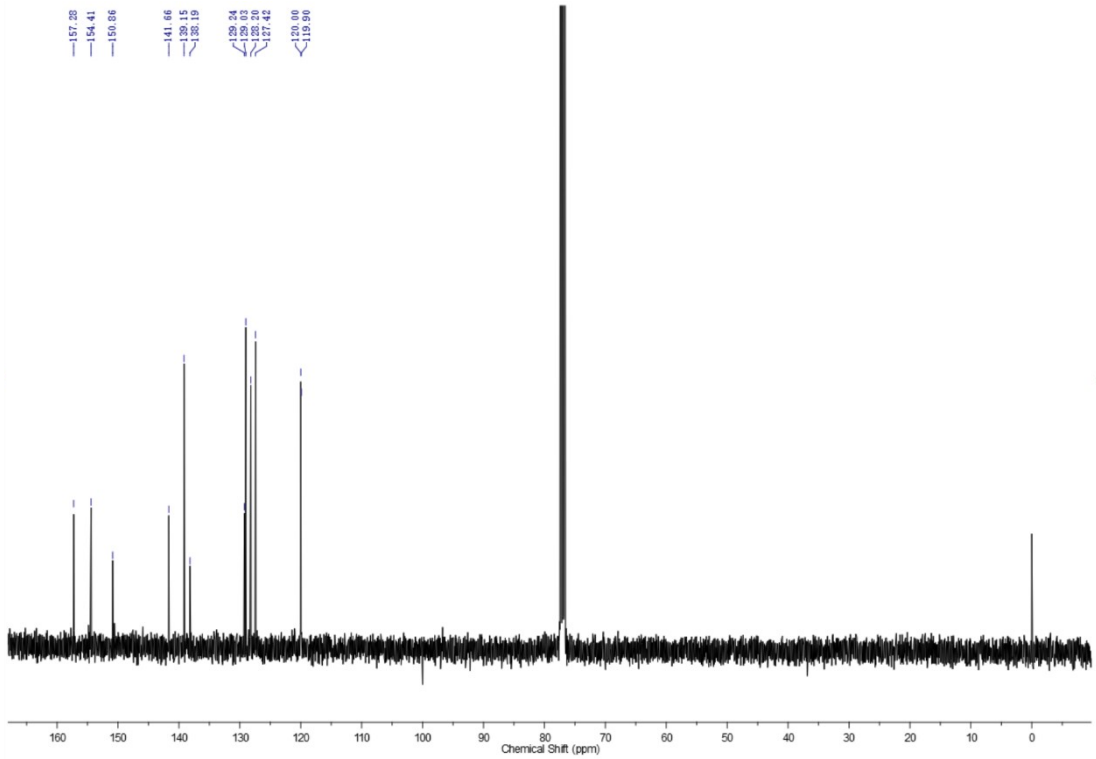

Fig. S2 ^{13}C NMR spectra of ligand **L1** in $CDCl_3$

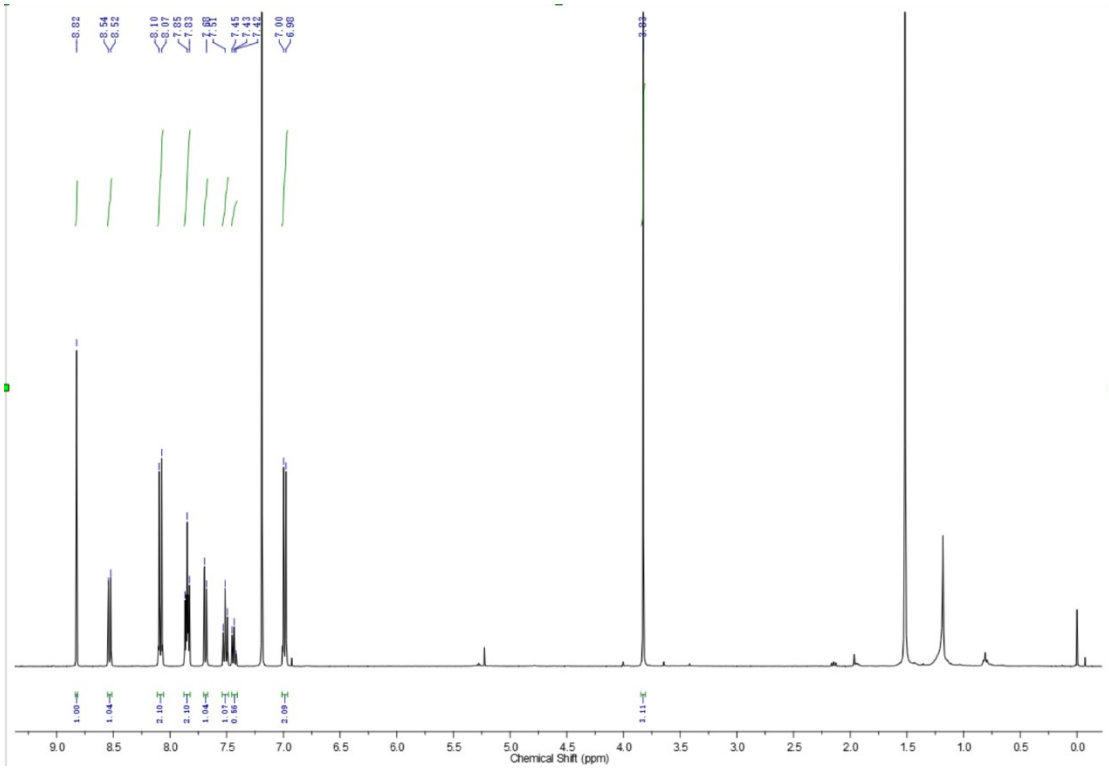

Fig. S3 ^{1}H NMR spectra of ligand **L2** in $CDCl_3$.

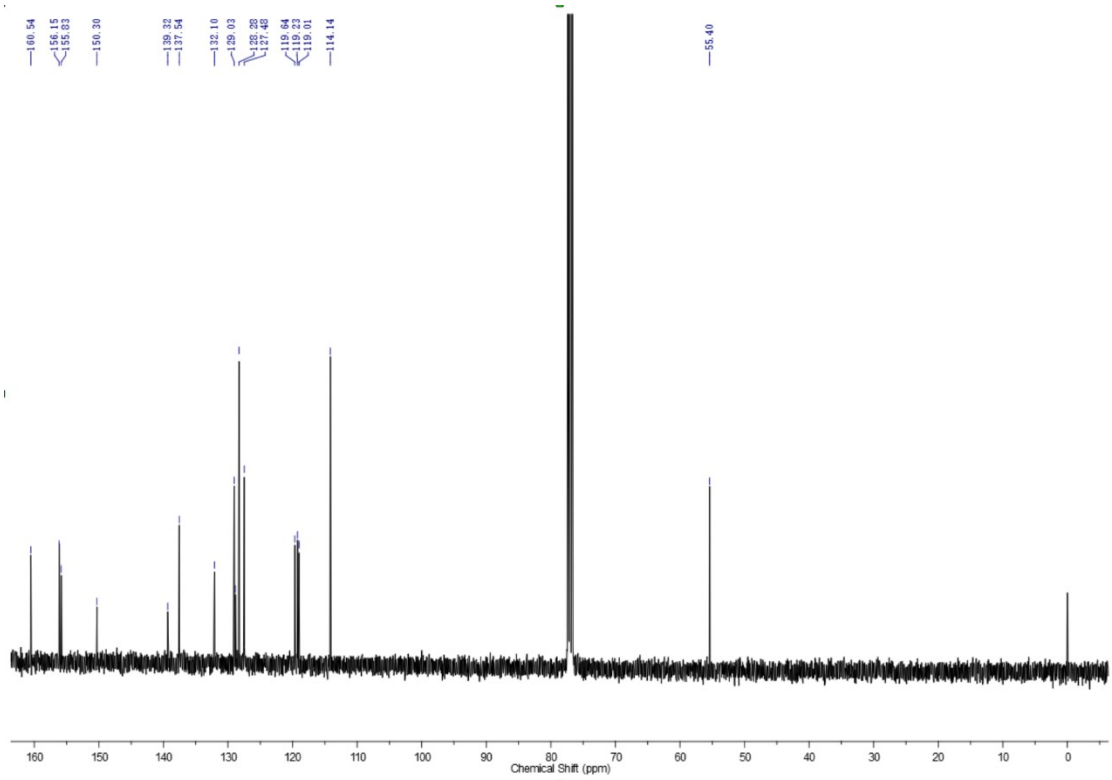

Fig. S4 ^{13}C NMR spectra of ligand **L2** in $CDCl_3$.

Synthesis of Complexes $L1_2$-M and $L2_2$-M

Complex $L1_2$-M [5] (M = Zn [5]. Cu [6]. Ni [5]. Fe [5]. Mn [5]). The Ligand-M was synthesized according to the literature procedures.

Complex $L1_2$-Co. To mixed solvent of $CHCl_3$ (15 mL) and MeOH (15 mL) of ligand **2** (56.24 mg, 107.80 μmol) were added, then a solution of $Co(NO_3)_2 \cdot 6H_2O$ (26.45 mg, 90.89 μmol) in CH_3OH (5.37 mL) was added. After stirring the mixture at 65 °C for 12 h, excess NH_4PF_6 was added to precipitate the complex, which was then filtered, washed with H_2O and then dried in vacuo. The desired complex was obtained (76%) as the black solid: 34.70 mg, 24.93 μmol. ESI-MS (967.11 calcd. For $C_{42}H_{30}CoF_{12}N_6P_2$): m\z 823.15$[M\text{-}PF_6]^+$ (calcd m/z: 823.1584).

Complex $L2_2$-Zn. To mixed solvent of $CHCl_3$ (20 mL) and MeOH (20 mL) of ligand **2** (27.97 mg, 53.60 μmol) were added, then a solution of $Zn(NO_3)_2 \cdot 6H_2O$ (7.98 mg, 26.81 μmol) in CH_3OH (1.28 mL) was added. After stirring the mixture at 65 °C for 12 h, excess NH_4PF_6 was added to precipitate the complex, which was then filtered, washed with H_2O, and then dried *in vacuo*. The desired complex was obtained (80%) as the white solid: 0.03 mg, 21.45 μmol). ^{1}H NMR (400 MHz, CD_3CN, ppm) δ = 8.06 (m, 16H), 7.77 (d, *J* = 8.4 Hz, 4H), 7.52 (d, *J* = 8.4 Hz, 4H), 7.08(d, J = 8.8Hz, 8H), 6.31 (d, J = 8.4Hz, 8H), 3.41(s, 12H); ^{13}C NMR (126 MHz, CD_3CN, ppm): δ = 161.5, 160.1, 155.6, 150.9, 150.8, 141.3, 136.1, 131.9, 130.1, 130.1, 130.0, 128.7, 127.60, 122.4, 122.2, 113.9, 55.4. ESI-MS (1398.55 calcd. For $C_{70}H_{54}ZnF_{12}N_6O_4P_2$): m\z 1257.3140$[M\text{-}PF_6]^+$ (calcd m/z: 1257.3140).

Complex $L2_2$-Cu. To mixed solvent of $CHCl_3$ (18 mL) and MeOH 18 mL of ligand **2 (**34.23 mg, 65.60 μmol) were added, then a solution of $Cu(CH_3COO)_2 \cdot 2H_2O$ (7.63 mg, 32.80 μmol) in CH_3OH (2.60 mL) was added. After stirring the mixture at 65 °C for 12 h, excess NH_4PF_6 was added to precipitate the complex, which was then filtered, washed with H_2O, and then dried in vacuo. The desired complex was obtained (85%) as the pale-yellow solid: 38.95 mg, 27.88 μmol. ^{1}H NMR (600 MHz, CD_3CN, ppm) δ = 8.48 (s, 4H),8.15 (s),6.88 (s),6.33 (s), 4.91(s,12H). ESI-MS (1396.71 calcd. For $C_{70}H_{54}CuF_{12}N_6O_4P_2$): m\z 553.6821$[M\text{-}2PF_6]^+$ (calcd m/z:553.6829).

Complex $L2_2$-Ni. To mixed solvent of $CHCl_3$ (18 mL) and MeOH (18 mL) of ligand **2** (34.23 mg, 65.60 μmol) were added, then a solution of $NiCl_2 \cdot 6H_2O$ (7.63 mg, 32.80 μmol) in CH_3OH (2.60 mL) was added. After stirring the mixture at 65 °C for 12 h, excess NH_4PF_6 was added to precipitate the complex, which was then filtered, washed with H_2O and then dried *in vacuo*. The desired complex was obtained (85%) as the pale-yellow solid: 38.95 mg, 27.88 μmol. ^{1}H NMR (600 MHz, CD_3CN, ppm) δ = 58.86 (s, 4H), 54.90 (s,4H), 49.64 (s, 4H),12.01 (s), 10.19 (s,2H). 7.61 (m),7.24 (s), 4.03(s, 12H). ESI-MS (1391.86 calcd. For $C_{70}H_{54}NiF_{12}N_6O_4P_2$): m\z 551.1874 $[M\text{-}2PF_6]^+$ (calcd m/z:551.1858).

Complex $L2_2$-Co. To mixed solvent of $CHCl_3$ (20 mL) and MeOH (18 mL) of ligand **2** (56.24 mg, 107.80 μmol) were added, then a solution of $Co(NO_3)_2 \cdot 6H_2O$ (15.69 mg, 32.80 μmol) in CH_3OH (1.94 mL) was added. After stirring the mixture at 65 °C for 12 h, excess NH_4PF_6 was added to precipitate the complex, which was then filtered, washed with H_2O and then dried in vacuo. The desired complex was obtained (76%) as the pink solid: 34.70 mg, 24.93 μmol. ^{1}H NMR (600 MHz, CD_3CN, ppm) δ = 107.55 (s, 4H), 69.38 (s, 4H), 37.94 (s, 4H), 27.54 (s, 4H), 15.84 (d), 14.17 (s),12.59 (s), ESI-MS (1392.10 calcd. For $C_{70}H_{54}CoF_{12}N_6O_4P_2$): m\z 1247.4475$[M\text{-}PF_6]^+$ (calcd m/z:1247.3258).

Complex $L2_2$-Mn. To mixed solvent of $CHCl_3$ (21mL) and MeOH (17 ml) of ligand **2 (**35.84 mg, 68.70 μmol) were added, then a solution of $Mn(NTF)_2 \cdot 6H_2O$ (21.14 mg, 34.30 μmol) in CH_3OH 1.79 mL) was added. After stirring the mixture at 65 °C for 12 h, excess NH_4PF_6 was added to precipitate the complex, which was then filtered, washed with H_2O, and then dried in vacuo. The desired complex was obtained (59%) as the green solid: 28.09 mg, 20.24 μmol. ^{1}H NMR (600 MHz, CD_3CN, ppm) δ = 8.84 (s, 4H), 8.44 (s, 4H),8.17 (m), 8.10 (s), 7.76 (s),

6.86 (s),3.83 (s, 12H), ESI-MS (1388.11 calcd. For $C_{70}H_{54}MnF_{12}N_6O_4P_2$): m\z 549.6860[M-2$PF_6$] $^+$ (calcd m/z 549.6871).

Complex L2$_2$-Fe. The **L2$_2$-Fe** [7] was synthesized according to the literature procedures.

NMR and MS spectra of complexes L1$_2$-M and L2$_2$-M

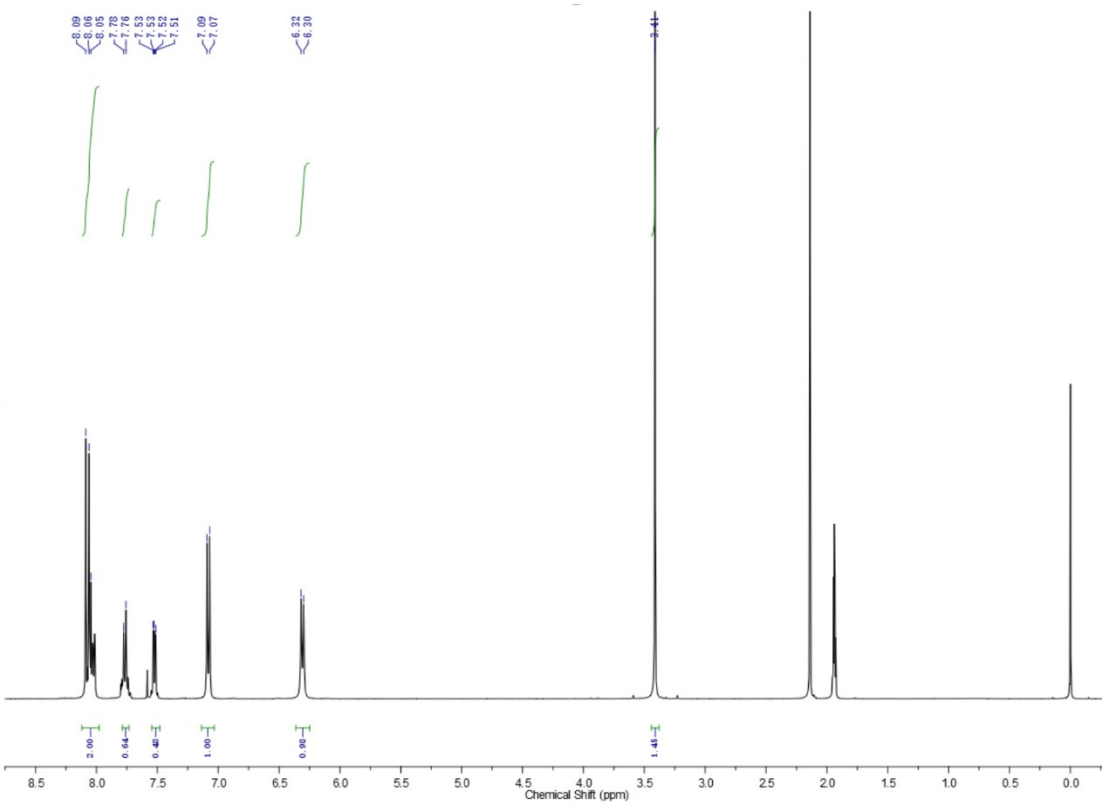

Fig. S5 ^{1}HNMR spectra of complex **L2$_2$-Zn** in CD_3CN.

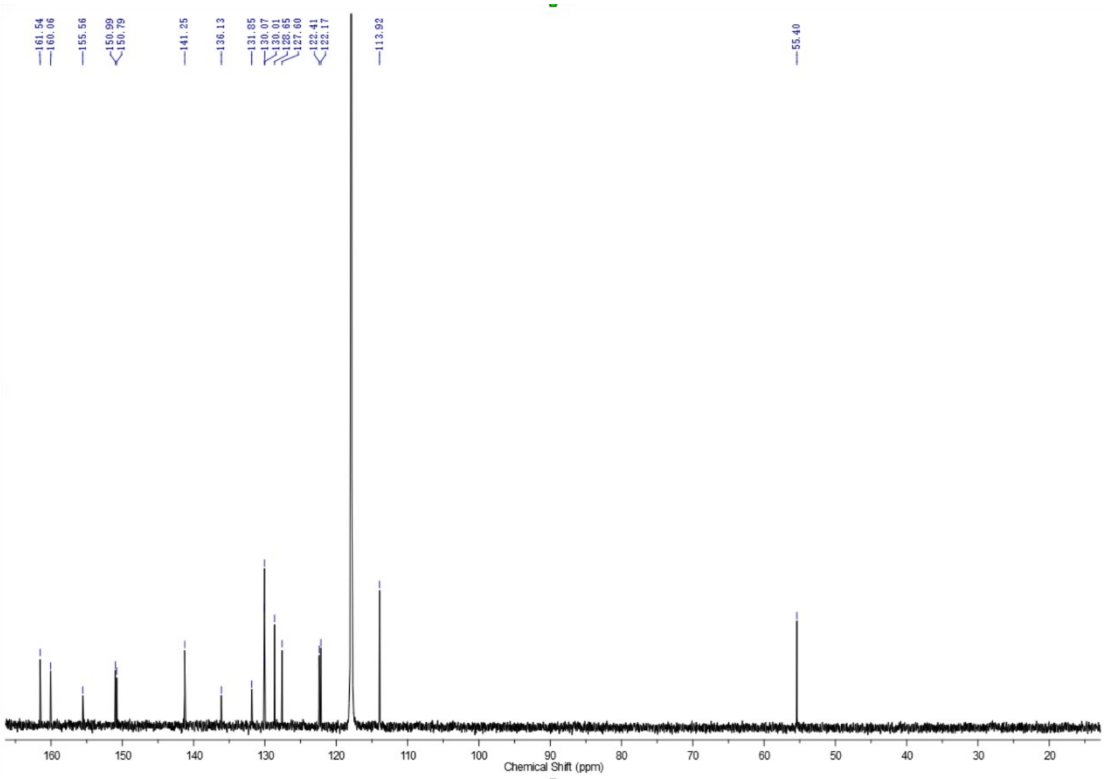

Fig. S6 ^{13}C NMR spectra of complex **L2$_2$-Zn** in CD_3CN.

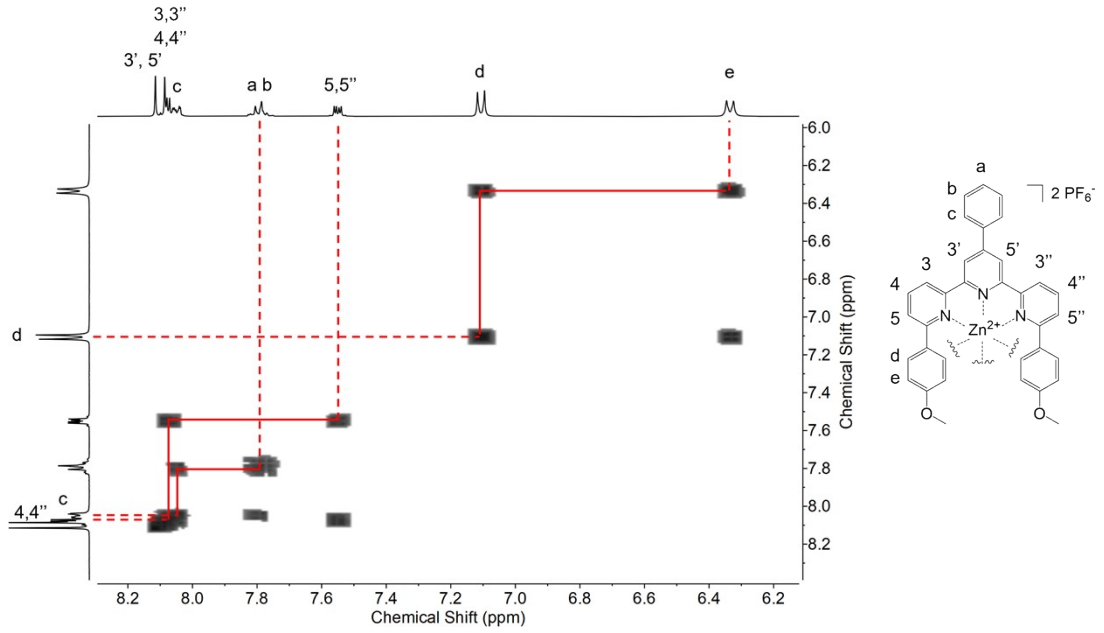

Fig. S7 2D COSY spectra of complex **L2$_2$-Zn** in CD_3CN.

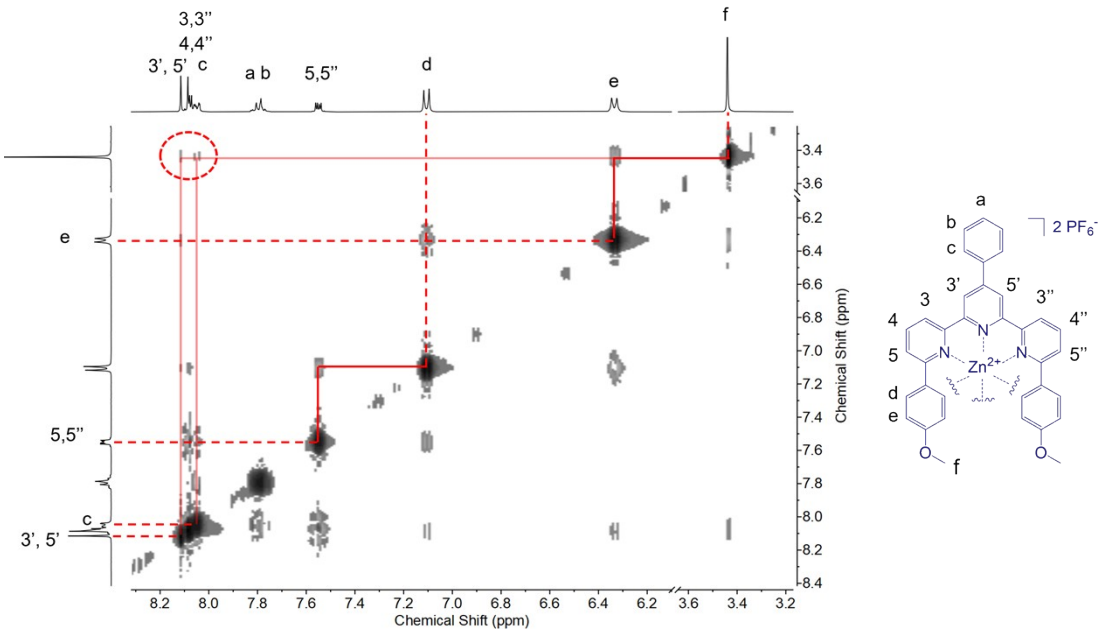

Fig. S8 2D NOESY spectra of complex **L2$_2$-Zn** in CD_3CN.

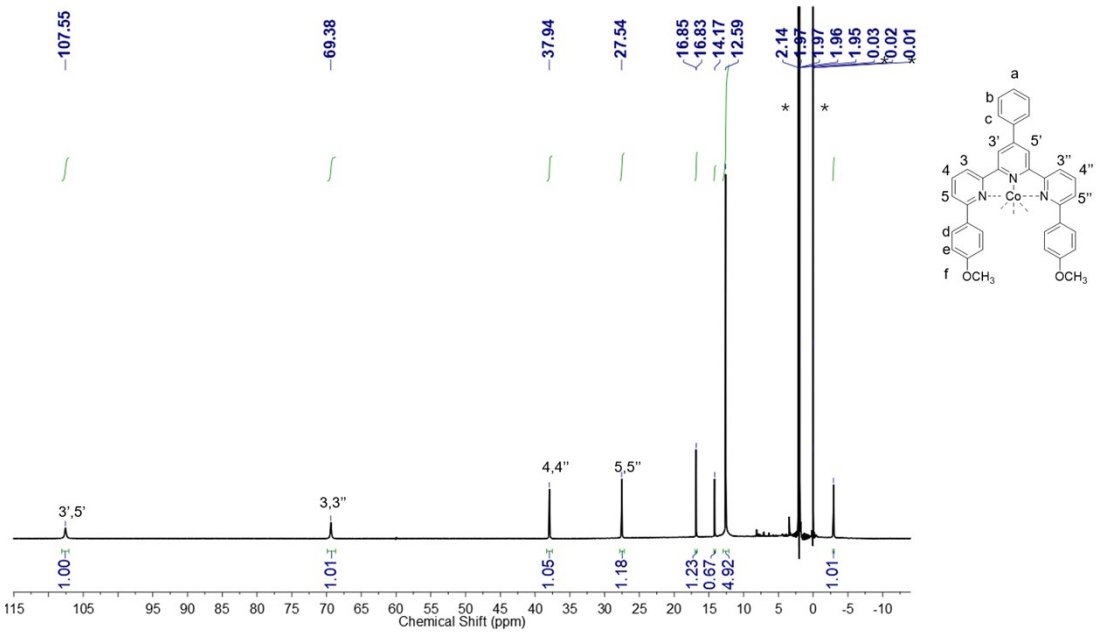

Fig. S9 ^{1}HNMR spectra of complex **L2$_2$-Co** in CD_3CN (* residual acetonitrile solvent, and silicone grease).

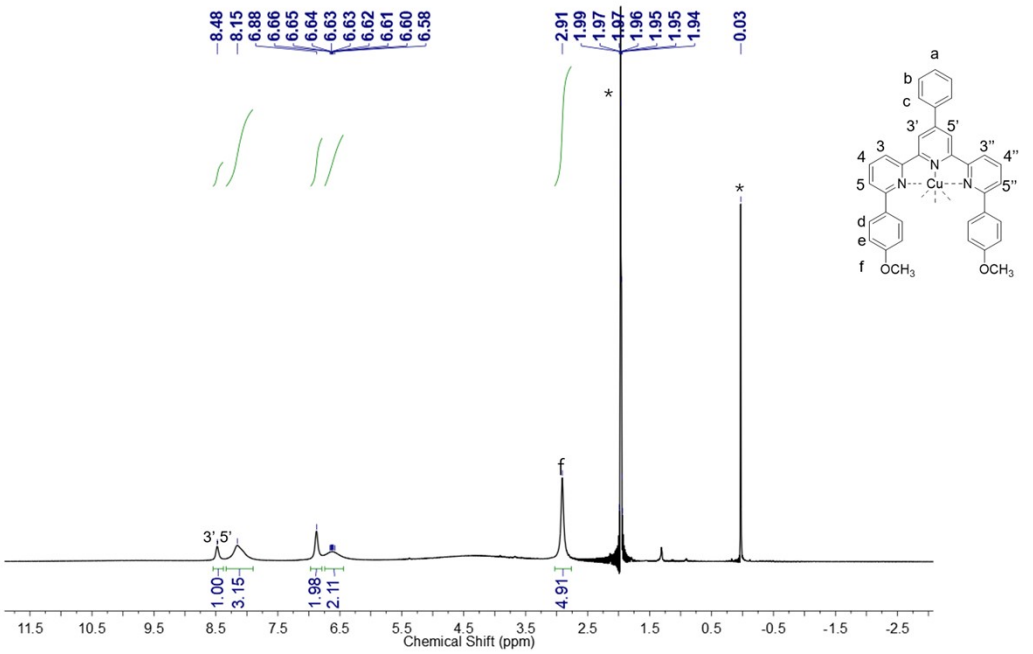

Fig. S10 [1]HNMR spectra of complex **L2$_2$-Cu** in CD_3CN(* residual acetonitrile solvent, and silicone grease).

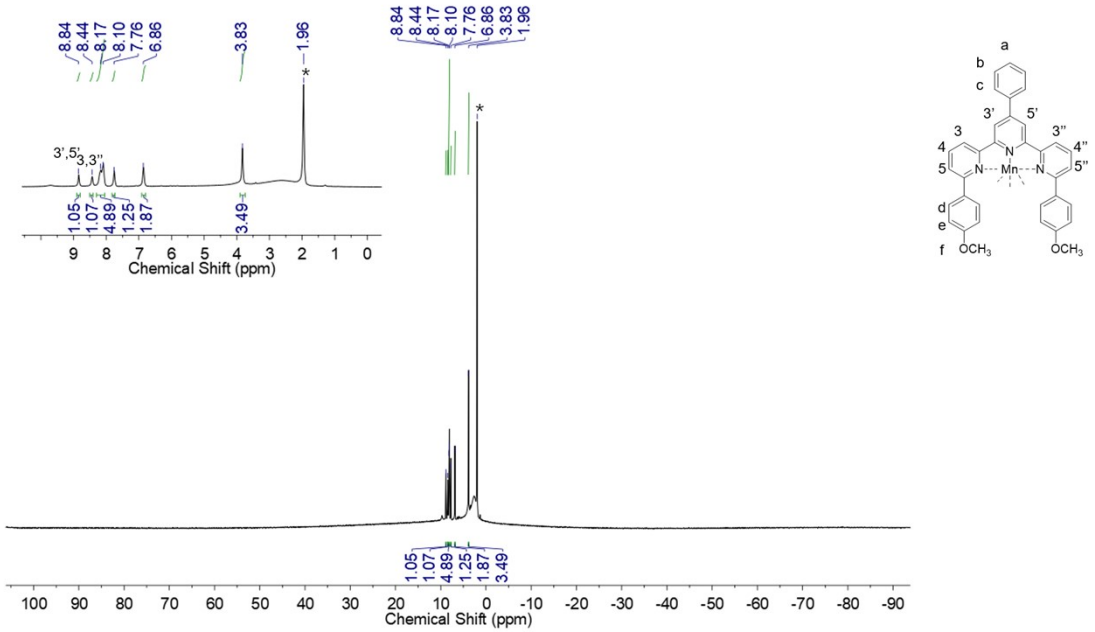

Fig. S11 [1]HNMR spectra of complex **L2$_2$-Mn** in CD_3CN(* residual acetonitrile solvent, and silicone grease).

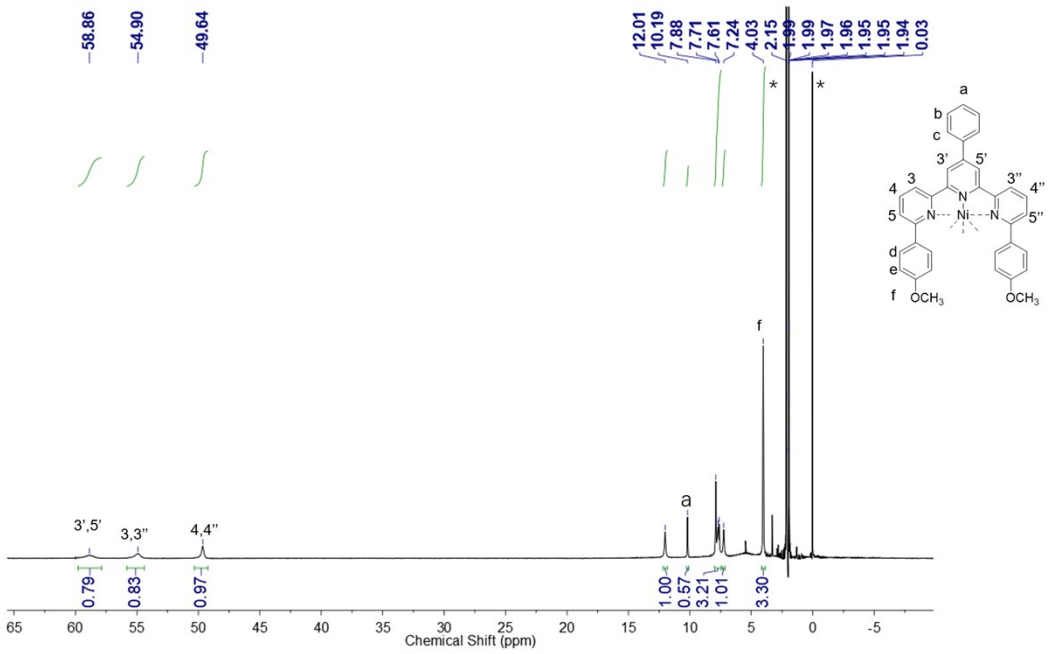

Fig. S12 [1]HNMR spectra of complex **L2$_2$-Ni** in CD_3CN(* residual acetonitrile solvent, and silicone grease).

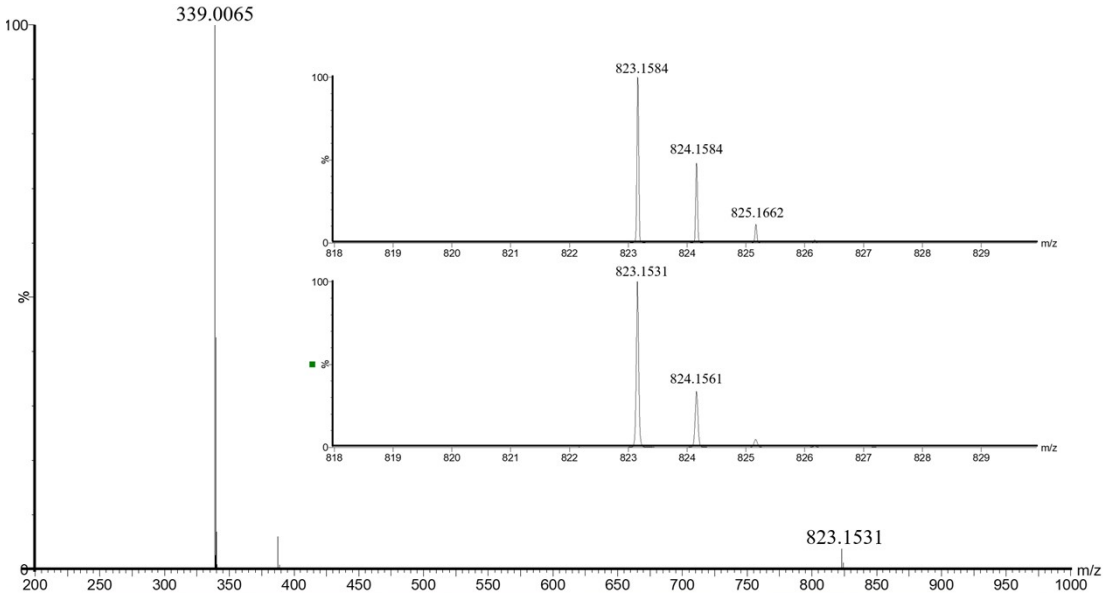

Fig. S13 The ESI-MS spectra of complex **L1$_2$-Co**.

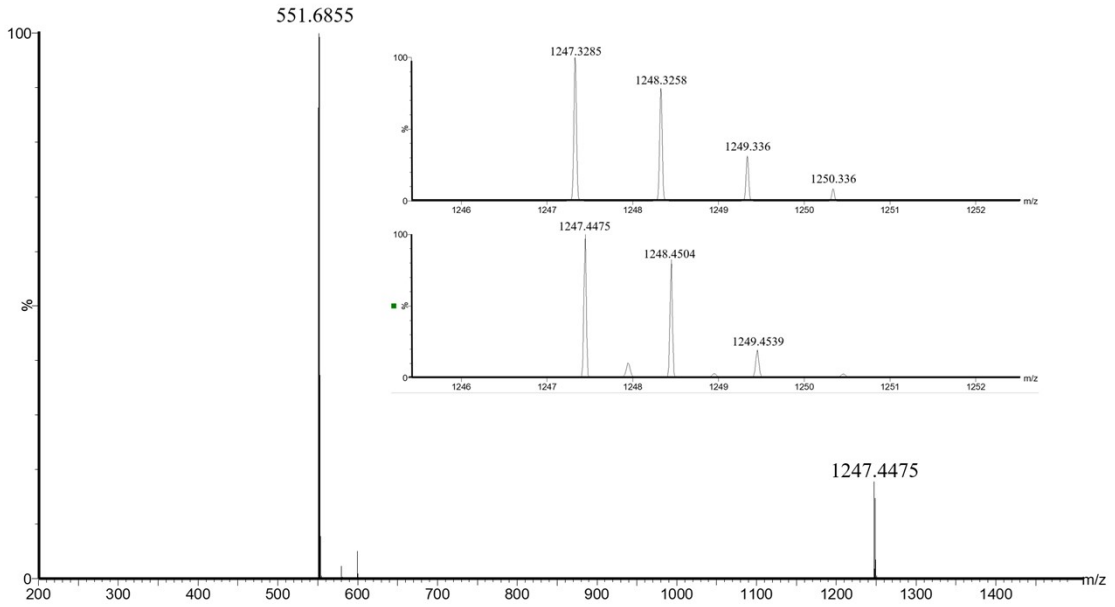

Fig. S14 The ESI-MS spectra of complex **$L2_2$-Co**.

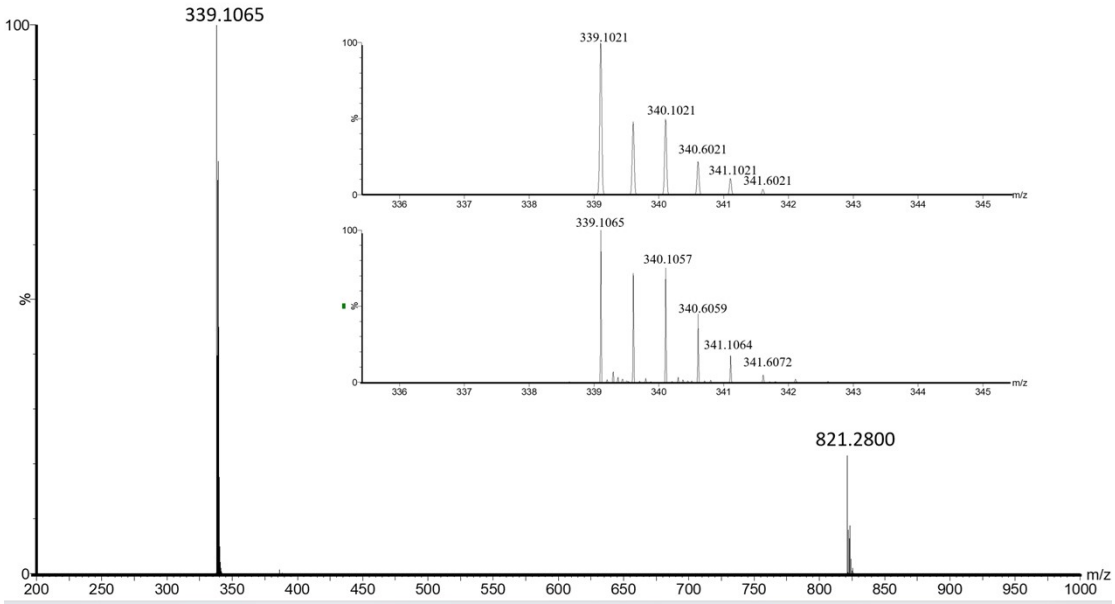

Fig. S15 The ESI-MS spectra of complex **$L1_2$-Ni**.

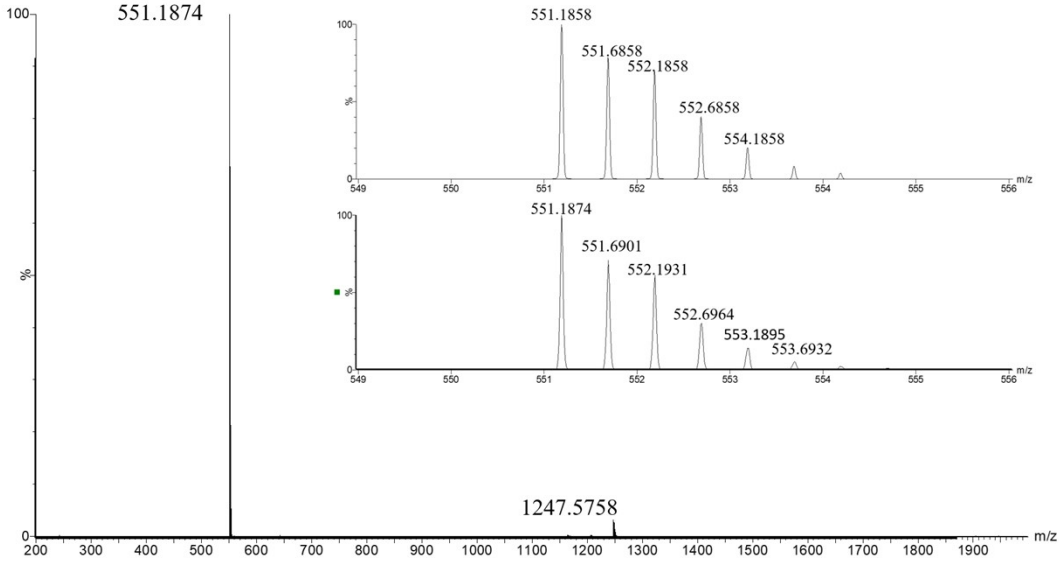

Fig. S16 The ESI-MS spectra of complex **$L2_2$-Ni**.

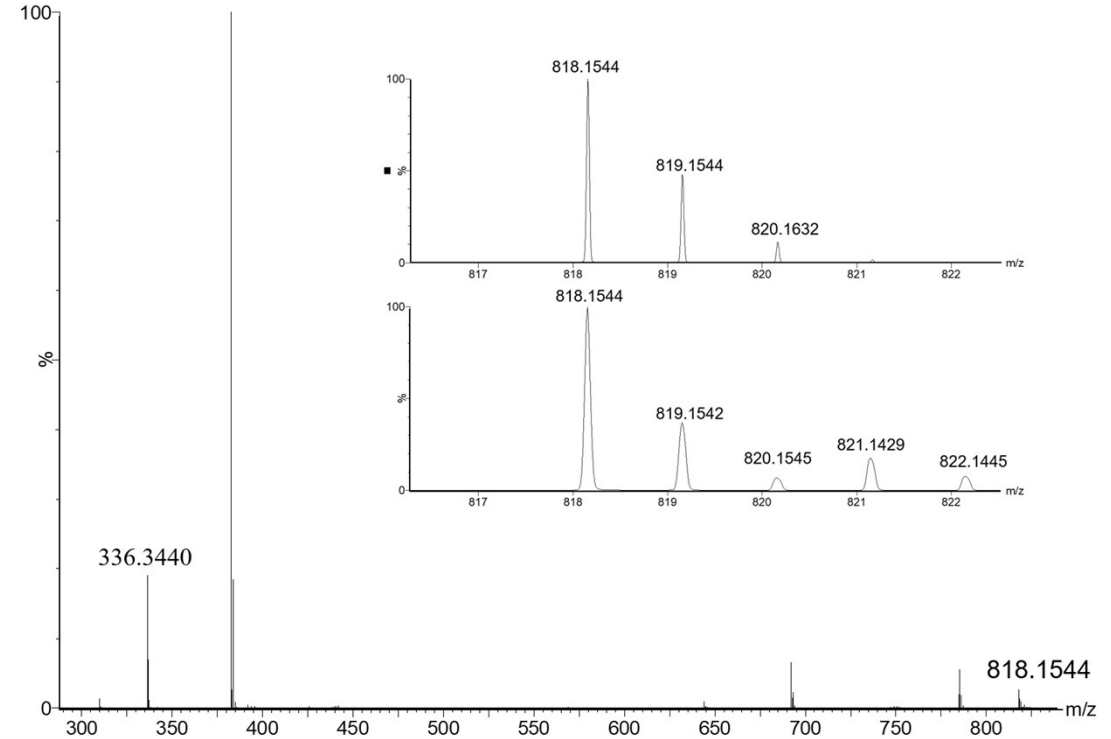

Fig. S17 The ESI-MS spectra of complex **$L1_2$-Mn**.

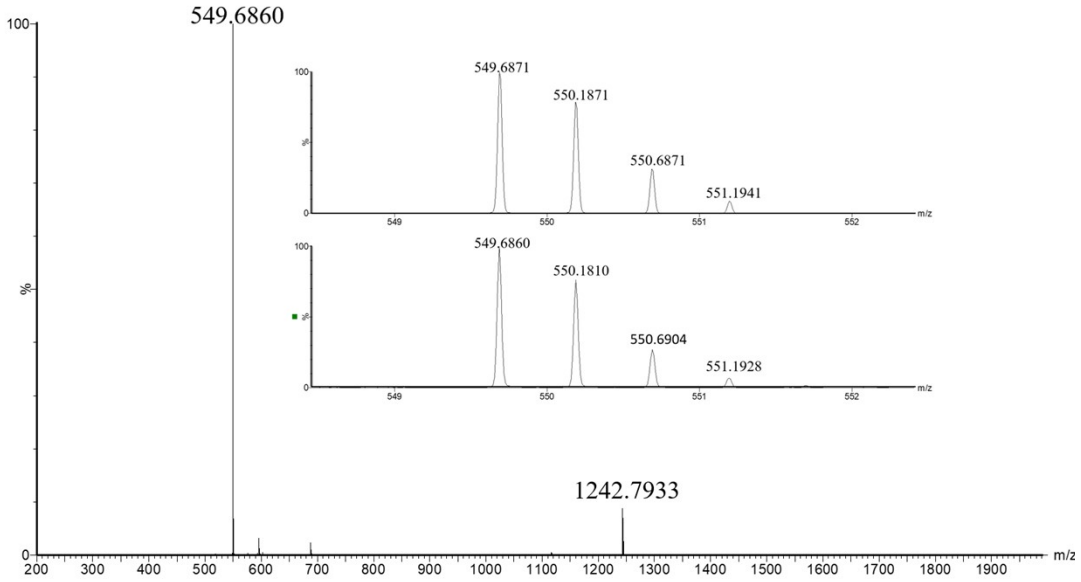

Fig. S18 The ESI-MS spectra of complex **$L2_2$-Mn**.

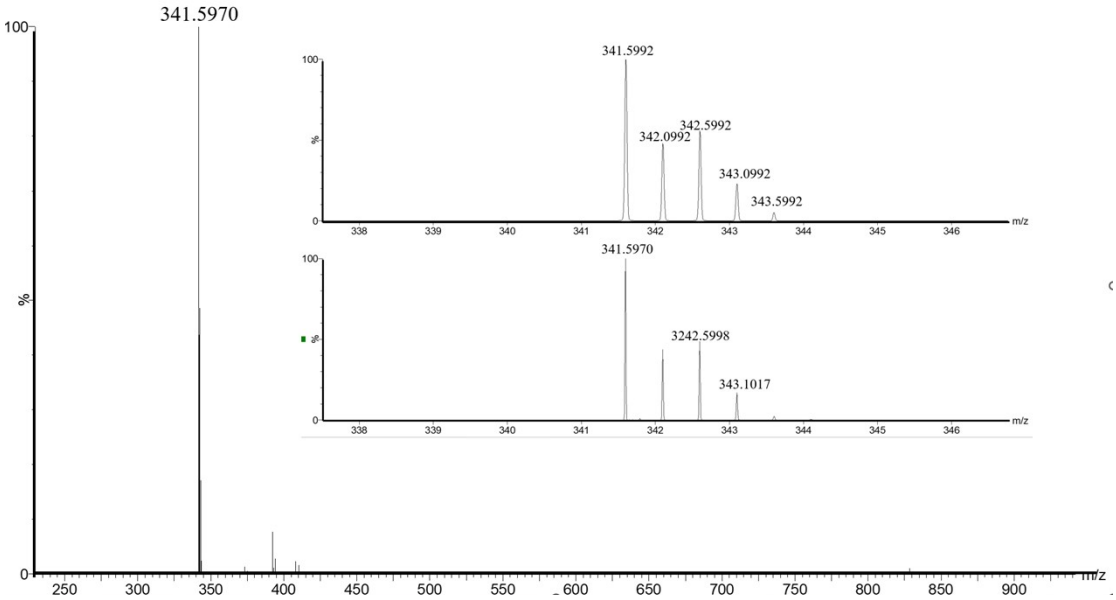

Fig. S19 The ESI-MS spectra of complex **$L1_2$-Cu**.

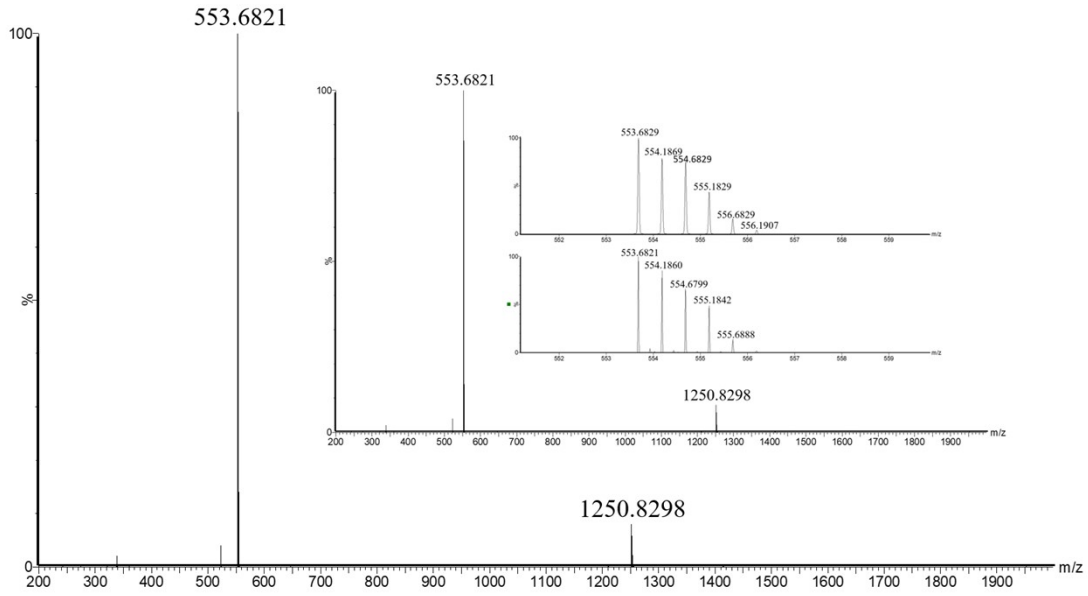

Fig. S20 The ESI-MS spectra of complex **L2$_2$-Cu**.

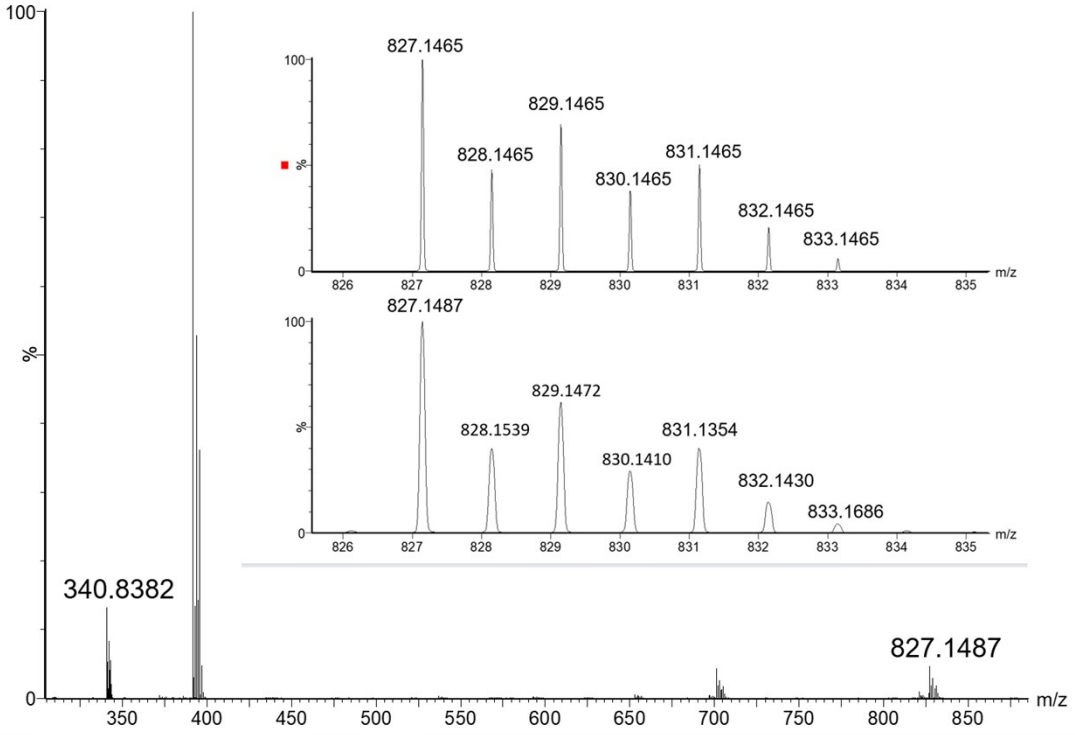

Fig. S21 The ESI-MS spectra of complex **L1$_2$-Zn**.

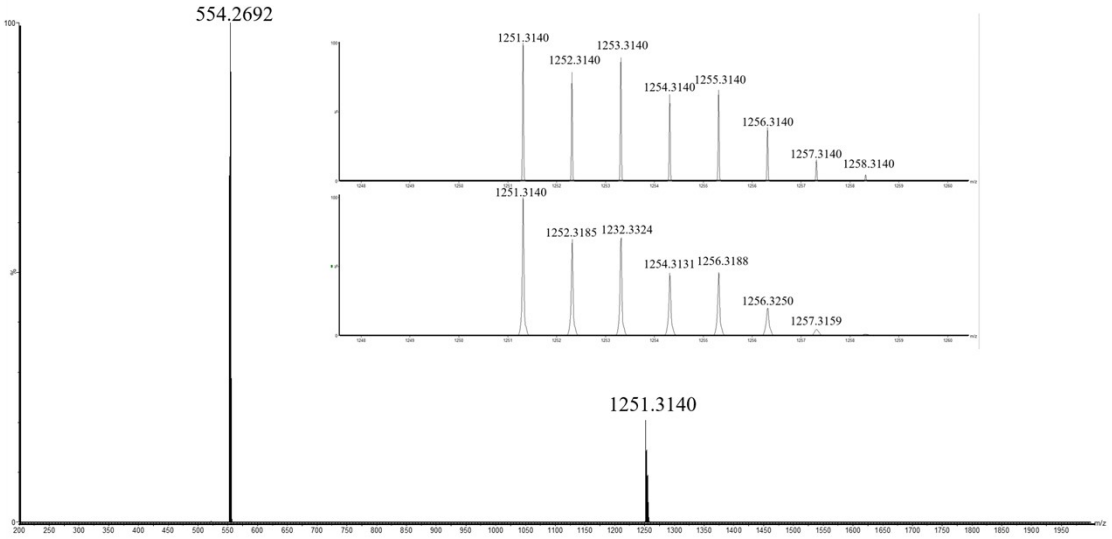

Fig. S22 The ESI-MS spectra of complex **$L2_2$-Zn**.

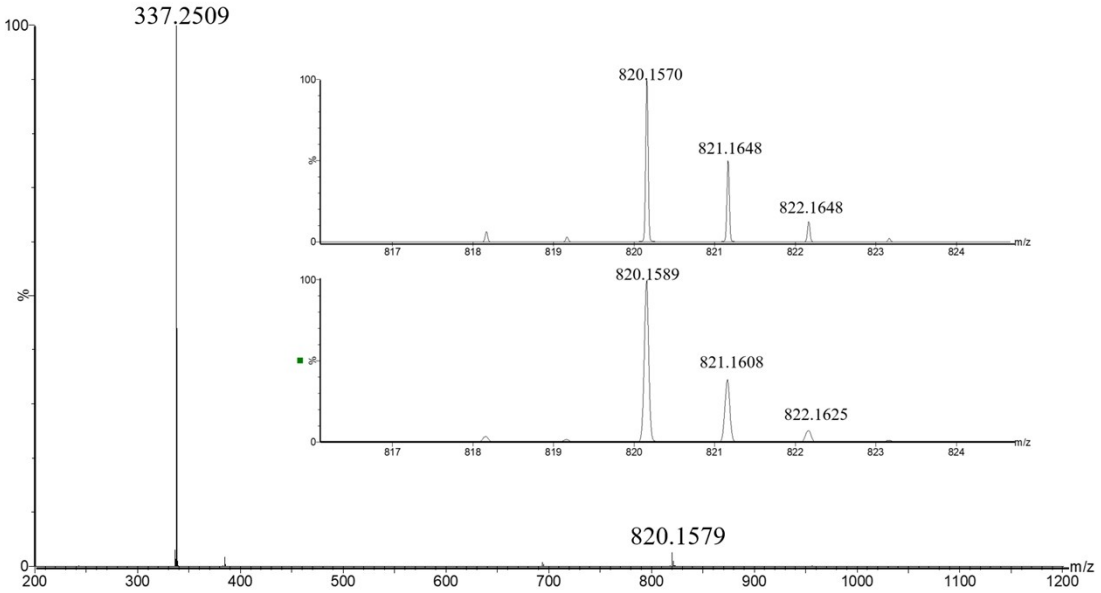

Fig. S23 The ESI-MS spectra of complex **$L1_2$-Fe**.

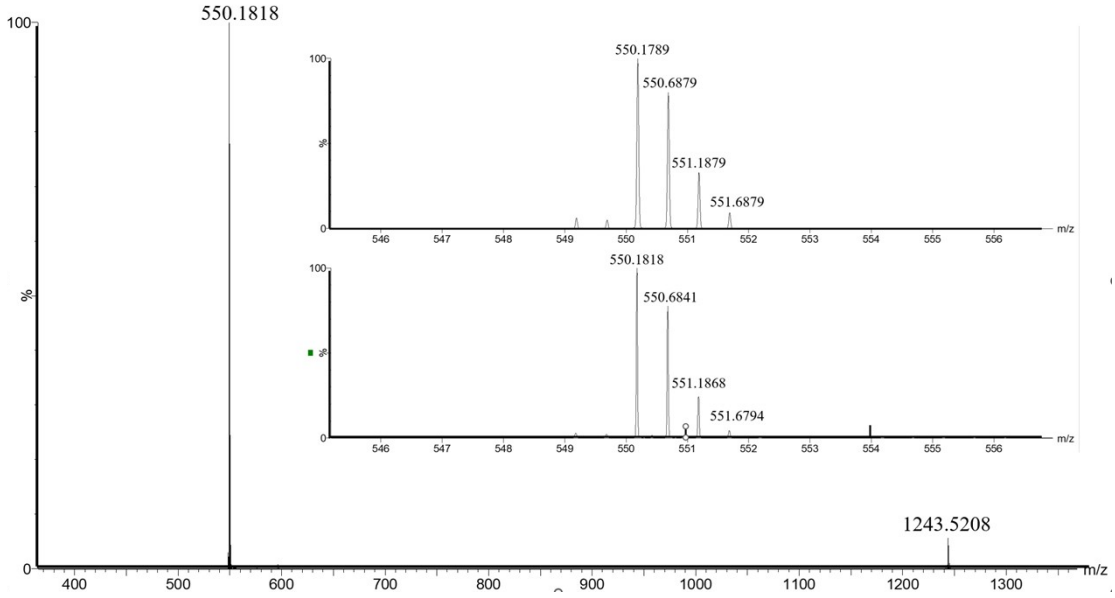

Fig. S24 The ESI-MS spectra of complex **$L2_2$-Fe**.

Crystal structure

Crystals of [**Co(L1)$_2$**] $[PF_6]_2 \cdot CH_3CN$ and [**M**(**L2**)$_2$] $[PF_6]_2 \cdot CH_3CN \cdot H_2O$ (Fe^{2+}, Co^{2+}, Zn^{2+}) grew within seven days by layering H_2O over a CH_3CN solution of complexes. Crystals of **M(L2)$_2$** (Mn^{2+}, Ni^{2+}, Cu^{2+}) grew within seven days by slow evaporation $CHCl_3/CH_3OH$ solution of [**Mn**(**L2**)$_2$] $[(CF_3SO_2)_2N]_2$, [**Ni**(**L2**)$_2$] $[CF_3SO_3]_2$ and [**Cu**(**L2**)$_2$] $[NO_3]_2$, respectively.

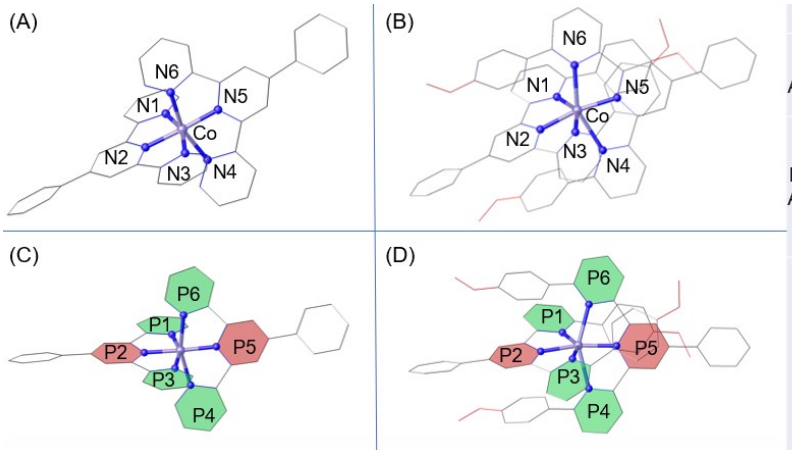

	Angle	$L1_2$-Co	$L2_2$-Co
Bond Angle (°)	N1-Co-N6	92.603	97.717
	N4-Co-N3	90.071	99.365
	N5-Co-N2	177.29	169.17
Dihedral Angle (°)	P2-P1	4.506	11.578
	P2-P3	1.539	26.6
	P5-P4	5.937	25.427
	P5-P6	2.021	8.793
	Average	3.501	18.099
Bond Length (Å)	Co-N1	2.088	2.21
	Co-N2	1.888	2.02
	Co-N3	2.079	2.351
	Co-N4	2.058	2.347
	Co-N5	1.88	2.029
	Co-N6	2.047	2.238
	Average	2.007	2.199

Fig. S25 Molecular structure of **L1$_2$-Co** and **L2$_2$-Co** at room temperature.

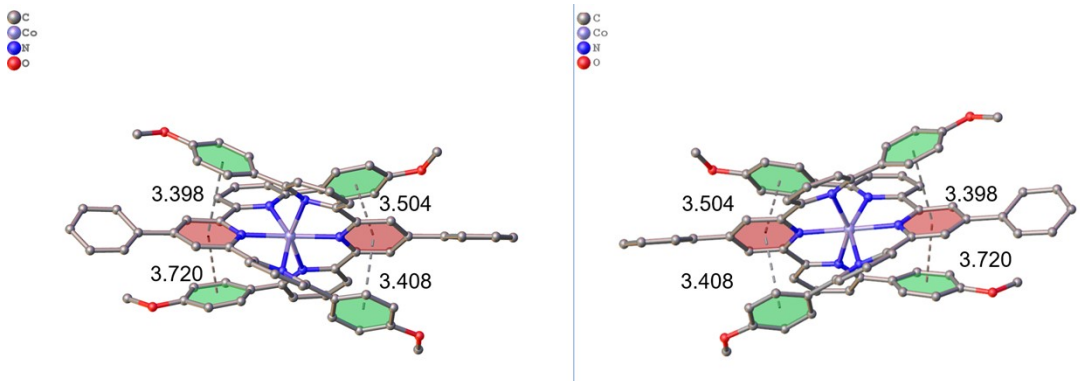

Fig. S26 P and M helical conformation extracted from the crystal structure of **L2$_2$-Co**.

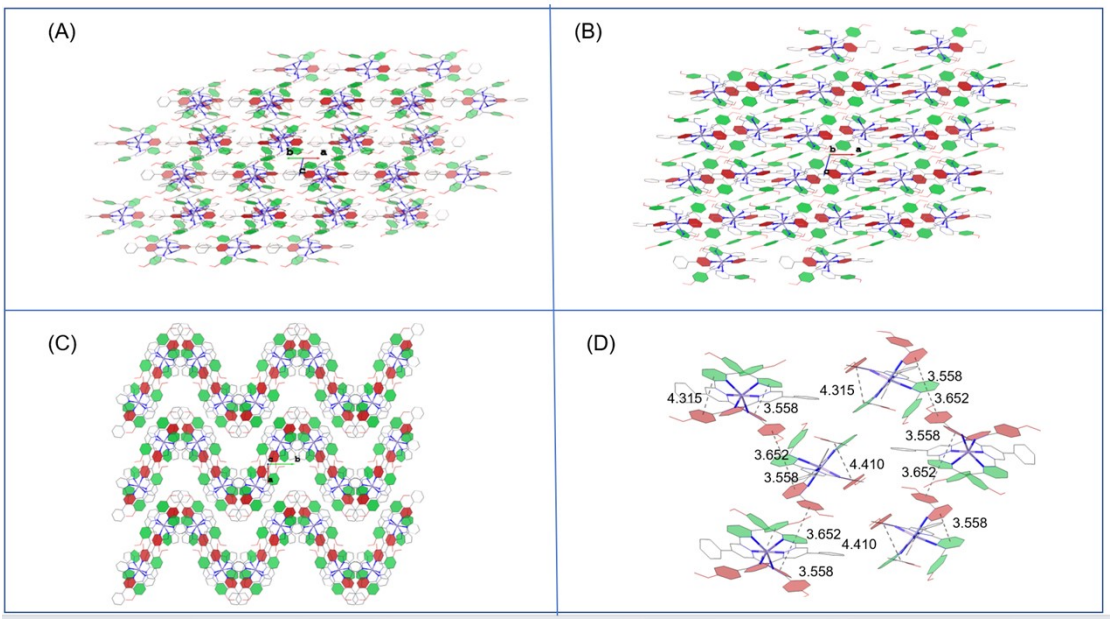

Fig. S27 The views of the π-π stacking interactions of the molecule of complex **$L2_2$-Co**: (a) viewed on 110 from crystal plane, (b) 010 crystal plane, (c) 001 crystal. and (d) π-π stacking interactions of the molecule.

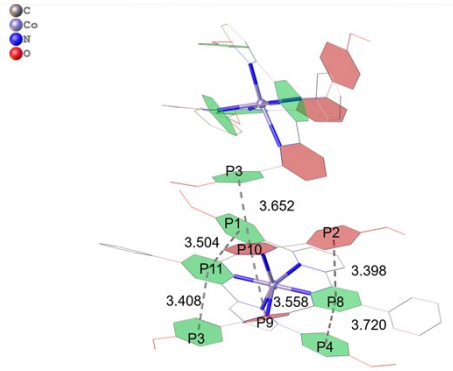

Fig. S28 The views of the intramolecular and intermolecular π-π stacking interactions of the molecule **$L2_2$-Co**.

Table S1 π-π stacking interactions in $L2_2$-Co. P1: C043 → C04W → C042 → C049 → C02K → C01U, P2 : C017 → C00P →C046 → C04M → C05B → C02Q, P3: C03U → C00U → C010 → C036 → C03J → C056, P4 : C6 → C5 → C05K → C0 → C3 → C2, P5 : C03Q → C03P → C03F → C055 → C05F → C03W, P6: C03D → C04G → C024 → C02N → C02U → C04Y, P7: N01B → C058 → C04V → C03I → C02H → C01Q. P8 → N01E → C016 → C03S → C02M → C02O → C00N , P9: N01L → C04C → C04X → C04J → C04A → C02P . P10: N01N → C025 → C01J → C03V → C048 → C00C. P11: N038 → C034 → C02R → C03B → C028 → C01C, P12: N03C → C03G → C03M → C03L → C04I → C026.

Entry	π-π stack	C-C (Å)	α (°)	β (°)	C-plane (Å)	Slippage (Å)	Symmetry operation
1	P1-P11	3.504	9.24	9.86	3.264	1.248	(+X, +Y, +Z)
2	P2-P8	3.398	10.988	36.9	3.373	0.411	(+X, +Y, +Z)
3	P3-P9	3.652	1.504	3.2	3.533	0.844	(+X,1/2-Y, -1/2+Z)
4	P3-P11	3.408	7.401	40.6	3.374	0.487	(+X, +Y, +Z)
5	P4-P8	3.72	12.432	28.4	3.32	1.683	(+X, +Y, +Z)
6	P9-P10	3.558	19.169	59.2	3.518	0.82	(+X, +Y, +Z)

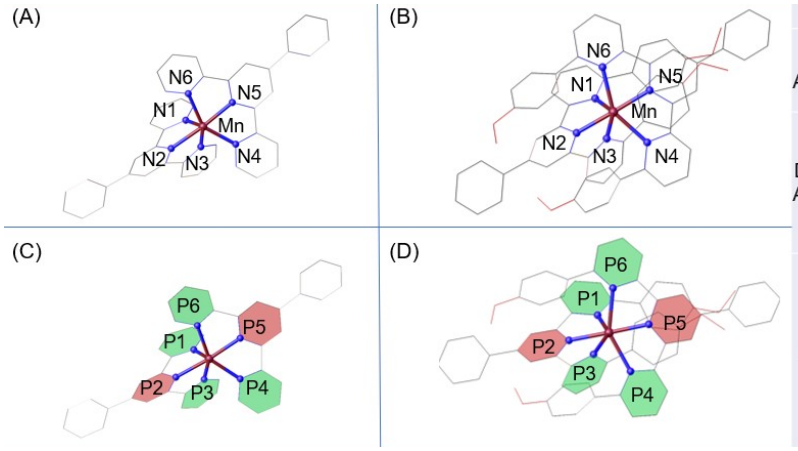

	Angle	$L1_2$-Mn	$L2_2$-Mn
Bond Angle (°)	N1-Zn-N6	92.83	101.92
	N4-Zn-N3	92.333	101.61
	N5-Zn-N2	170.89	152.16
Dihedral Angle (°)	P2-P1	5.145	15.692
	P2-P3	7.853	14.902
	P5-P4	11.04	21.563
	P5-P6	11.24	18.664
	Average	8.819	17.503
Bond Length (Å)	Mn-N1	2.243	2.409
	Mn-N2	2.184	2.148
	Mn-N3	2.254	2.322
	Mn-N4	2.221	2.332
	Mn-N5	2.186	2.133
	Mn-N6	2.245	2.356
	Average	2.222	2.283

Fig. S29 Molecular structure of **$L1_2$-Mn** and **$L2_2$-Mn** at room temperature.

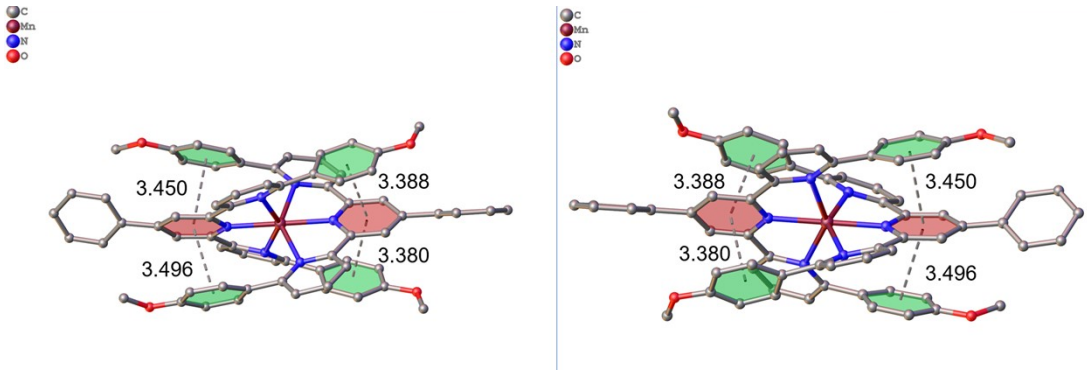

Fig. S30 P and M helical conformation extracted from the crystal structure of **$L2_2$-Mn**.

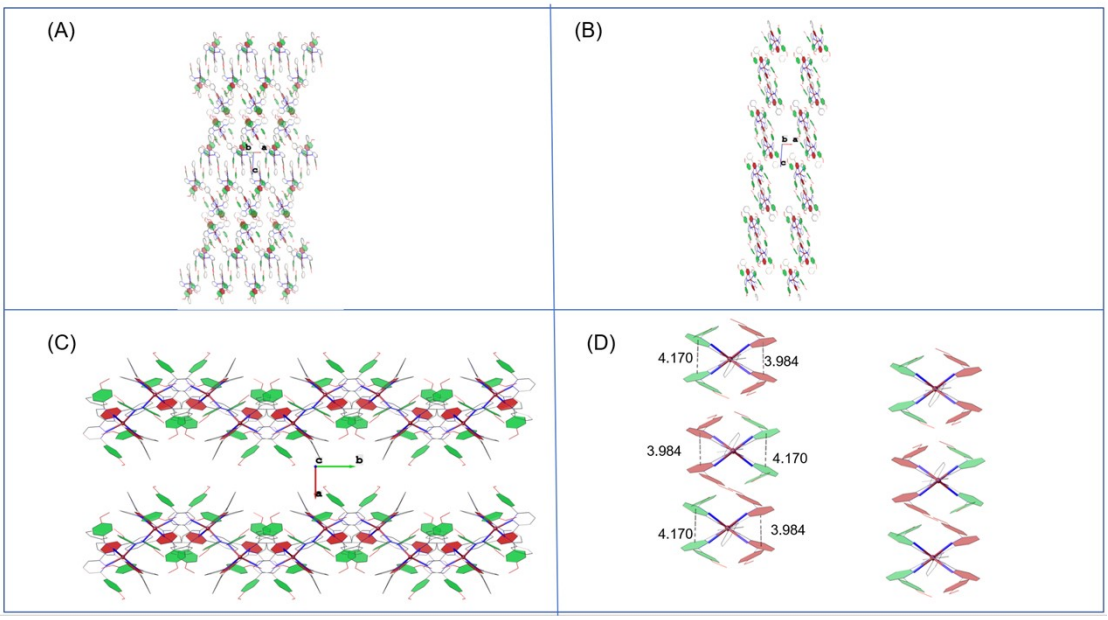

Fig. S31 The views of the π-π stacking interactions of the molecule of complex **$L2_2$-Mn**: (a) viewed on110 from crystal plane, (b) 010 crystal plane, (c) 001 crystal. and (d) π-π stacking interactions of the molecule.

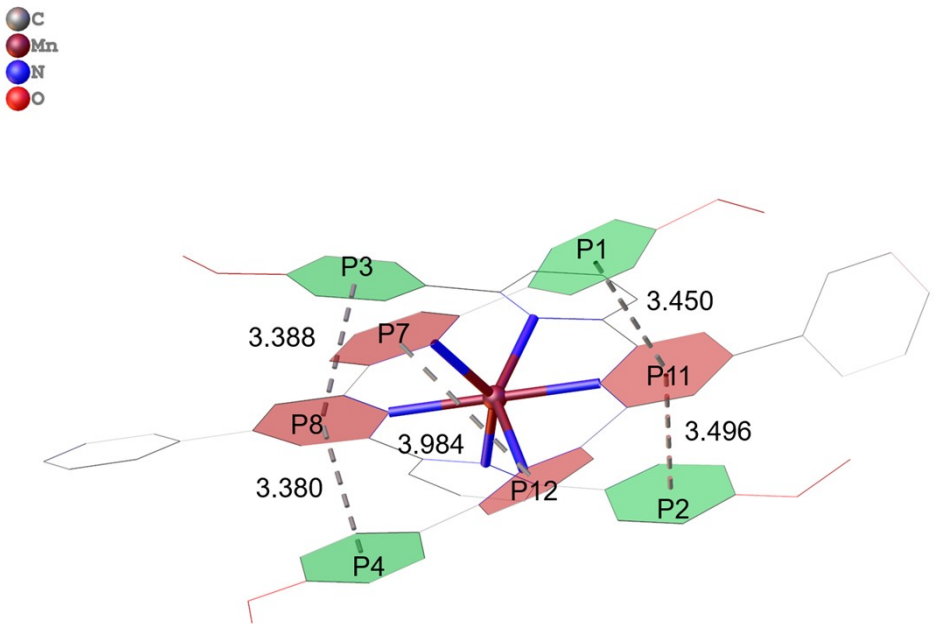

Fig. S32 The views of the intramolecular and intermolecular π-π stacking interactions of the molecule **$L2_2$-Mn**.

Table S2 π-π stacking interactions in $L2_2$-Mn. P1: C17 → C22 → C21 → C20 → C19 → C18 , P2: C29 → C34 → C33 → C32 → C31 → C30 , P3: C29A → C34A → C33A → C32A → C31A → C30A , P4: C17A → C22A → C21A → C20A → C19A → C18A , P5: C4 → C5 → C6 → C1 → C2 → C3 , P6: C4A → C5A → C6A → C1A → C2A → C3A , P7: N1 → C16 → C15 → C14 → C13 → C12 , P8: N2 → C10 → C11 → C7 → C8 → C9 , P9: N3 → C28 → C27 → C26 → C25 → C24 , P10: N4 → C28A → C27A → C26A → C25A → C24A, p11: N5 → C10A → C11A → C7A → C8A → C9A , P12: N6 → C16A → C15A → C14A → C13A → C12A.

Entry	π-π stack	c-c(Å)	α (°)	β (°)	c-plane (Å)	Slippage (Å)	Symmetry operation
1	P1-P11	3.45	7.032	25.6	3.32	0.965	(+X, +Y, +Z)
2	P2-P11	3.496	8.585	24.7	3.298	1.162	(+X, +Y, +Z)
3	P3-P8	3.388	6.586	22.5	3.236	0.877	(+X, +Y, +Z)
4	P4-P8	3.38	7.231	25.1	3.296	0.747	(+X, +Y, +Z)
5	P7-P12	3.984	30.527	74	3.664	1.885	(+X, +Y, +Z)

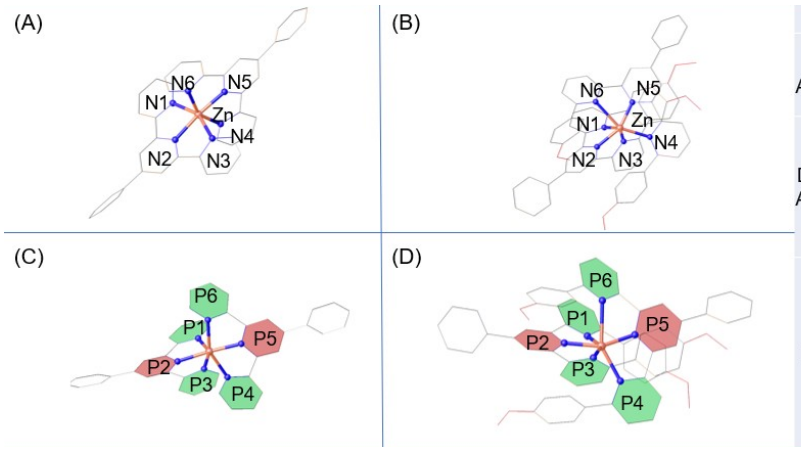

	Angle	$L1_2$-Zn	$L2_2$-Zn
Bond Angle (°)	N1-Zn-N6	85.356	80.63
	N4-Zn-N3	84.823	82.71
	N5-Zn-N2	170.16	175.19
Dihedral Angle (°)	P2-P1	7.397	24.915
	P2-P3	7.9	13.651
	P5-P4	9.539	10.376
	P5-P6	9.763	30.583
	Average	8.650	19.881
Bond Length (Å)	Zn-N1	2.139	2.5059
	Zn-N2	2.0676	2.0272
	ZN-N3	2.223	2.1441
	Zn-N4	2.193	2.4996
	Zn-N5	2.0566	2.013
	Zn-N6	2.184	2.1867
	Average	2.144	2.229

Fig. S33 Molecular structure of **$L1_2$-Zn** and **$L2_2$-Zn** at room temperature.

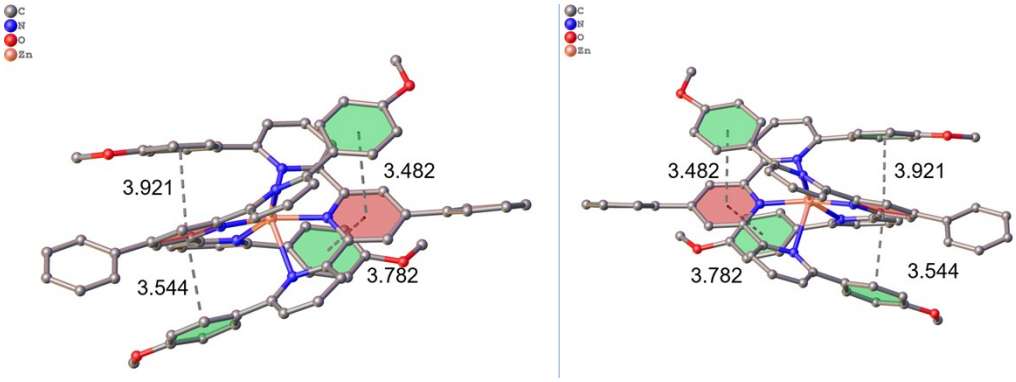

Fig. S34 P and M helical conformation extracted from the crystal structure of **$L2_2$-Zn**.

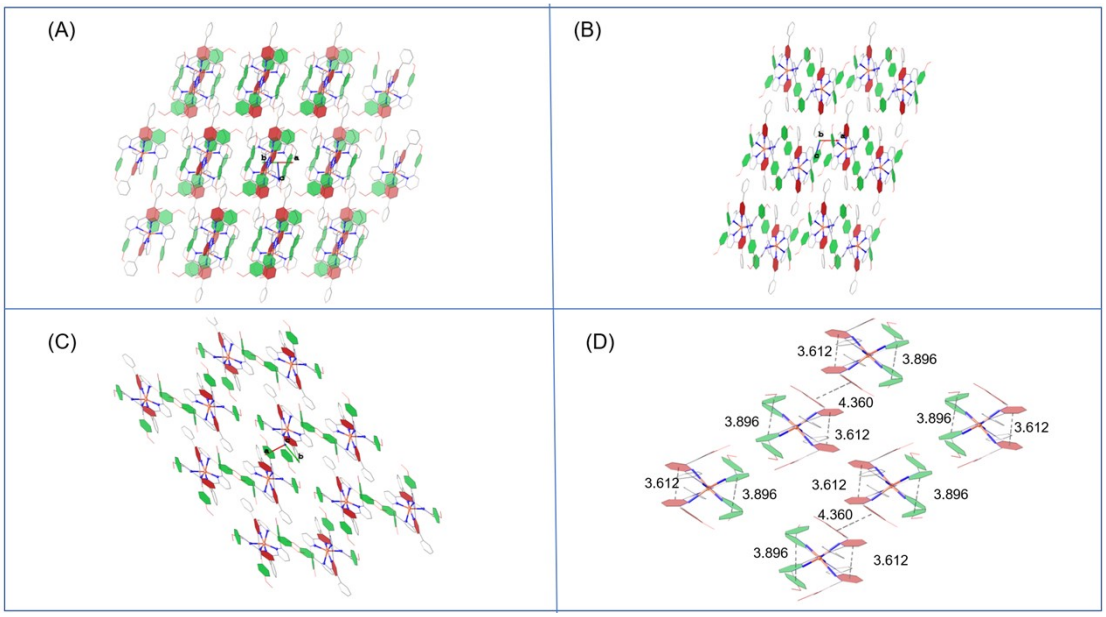

Fig. S35 The views of the π-π stacking interactions of the molecule of complex **$L2_2$-Zn**: (a) viewed on 110 from crystal plane, (b) 010 crystal plane, (c) 001 crystal. and (d) π-π stacking interactions of the molecule.

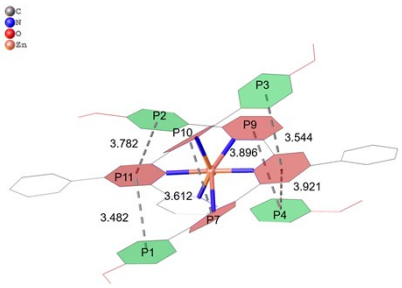

Fig. S36 The views of the intramolecular and intermolecular π-π stacking interactions of the molecule **L2$_2$-Zn**.

Table S3 π-π stacking interactions in **L2$_2$-Zn**. P1**:** C17 → C22 → C21 → C20 → C19 → C18 , P2: C29 → C34 → C33 → C32 → C31 → C30 , P3: C17A → C22A → C21A → C20A → C19A → C18A ,P4: C29A → C34A → C33A → C32A → C31A → C30A , P5: C4 → C5 → C6 → C1 → C2 → C3 , P6: C4A → C5A → C6A → C1A → C2A → C3A , P7: N1 → C16 → C15 → C14 → C13 → C12 , P8: N2 → C10 → C11 → C7 → C8 → C9 , P9 : N2 → C10 → C11 → C7 → C8 → C9 , P10: N4 → C28A → C27A → C26A → C25A → C24A, p11: N5 → C10A → C11A → C7A → C8A → C9A , P12: N6 → C16A → C15A → C14A → C13A → C12A.

Entry	π-π stack	c-c(Å)	α (°)	β (°)	c-plane (Å)	Slippage (Å)	Symmetry operation
1	P1-P11	3.482	3.318	9.9	3.2909	1.17	(+X, +Y, +Z)
2	P2-P10	3.782	11.061	21.38	3.341	1.772	(+X, +Y, +Z)
3	P3-P8	3.544	4.604	0.59	3.2999	1.554	(+X, +Y, +Z)
4	P4-P8	3.921	13.18	22.43	3.249	2.342	(+X, +Y, +Z)
5	P4-P9	3.896	1.469	0.34	3.372	1.951	(+X, +Y, +Z)
6	P7-P10	3.612	11.649	46.6	3.5064	0.972	(+X, +Y, +Z)

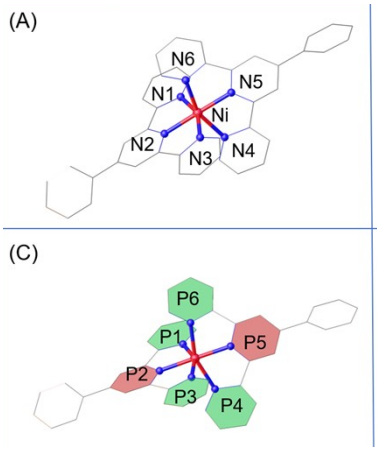

	Angle	L1$_2$-Ni	L2$_2$-Ni
Bond Angle (°)	N1-Ni-N6	92.85	103.9
	N4-Ni-N3	91.79	104.1
	N5-Ni-N2	178.75	177.8
Dihedral Angle (°)	P2-P1	3.35	19.472
	P2-P3	4.624	8.662
	P5-P4	3.059	18.057
	P5-P6	4.287	17.915
	Average	3.83	16.027
Bond Length (Å)	Ni-N1	2.082	2.282
	Ni-N2	1.952	1.967
	Ni-N3	2.073	2.242
	Ni-N4	2.083	2.218
	Ni-N5	1.954	1.972
	Ni-N6	2.076	2.253
	Average	2.037	2.156

Fig. S37 Molecular structure of **L1$_2$-Ni** and **L2$_2$-Ni** at room temperature.

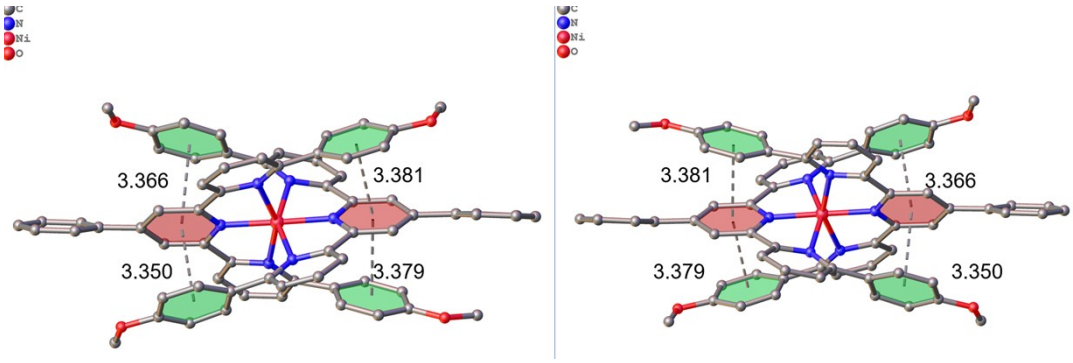

Fig. S38 P and M helical conformation extracted from the crystal structure of **L2$_2$-Ni**.

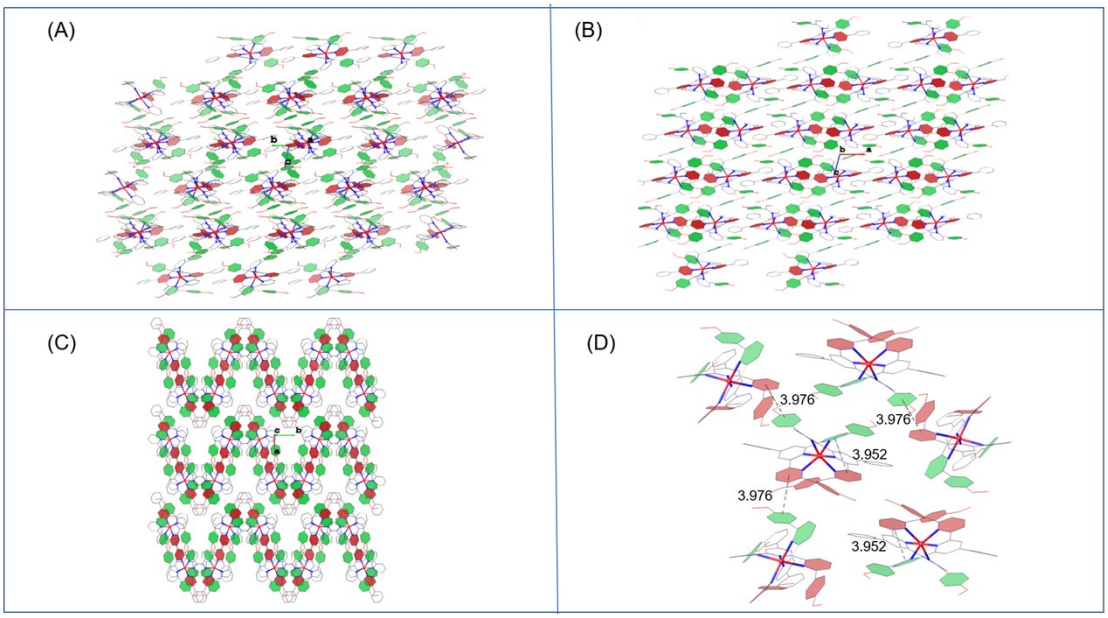

Fig. S39 The views of the π-π stacking interactions of the molecule of complex **L2$_2$-Ni**: (a) viewed on 110 from crystal plane, (b) 010 crystal plane, (c) 001 crystal. and (d) π-π stacking interactions of the molecule.

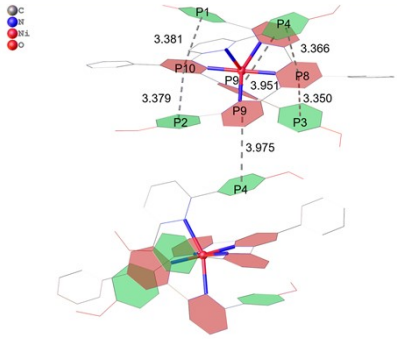

Fig. S40 The views of the intramolecular and intermolecular π-π stacking interactions of the molecule **L2$_2$-Ni**.

Table S4 π-π stacking interactions in **L2$_2$-Ni**. P1: C17 → C22 → C21 → C20 → C19 → C18 , P2: C29 → C34 → C33 → C32 → C31 → C30 , P3: C29A → C34A → C33A → C32A → C31A → C30A ,P4: C17A → C22A → C21A → C20A → C19A → C18A , P5: C4 → C5 → C6 → C1 → C2 → C3 , P6: C4A → C5A → C6A → C1A → C2A → C3A , P7: N1 → C16 → C15 → C14 → C13 → C12 , P8: N2 → C10 → C11 → C7 → C8 → C9 , P9: N3 → C28 → C27 → C26 → C25 → C24 , P10: N5 → C10A → C11A → C7A → C8A → C9A, P11: N4 → C28A → C27A → C26A → C25A → C24A , P12: N6 → C16A → C15A → C14A → C13A → C12A.

Entry	π-π stack	c-c(Å)	α (°)	β (°)	c-plane (Å)	Slippage (Å)	Symmetry operation
1	P1-P10	3.381	9.398	0.857	38.3	0.857	(+X, +Y, +Z)
2	P2-P10	3.391	9.935	48	3.297	0.791	(+X, +Y, +Z)
3	P3-P8	3.35	10.095	60.9	3.292	0.529	(+X, +Y, +Z)
4	P4-P8	3.366	8.206	14	3.355	0.213	(+X, +Y, +Z)
5	P4-P9	3.975	11.061	11.3	3.297	1.638	(+X,3/2-Y, -1/2+Z)
6	P7-P11	3.951	37.254	78.9	3.578	1.677	(+X, +Y, +Z)

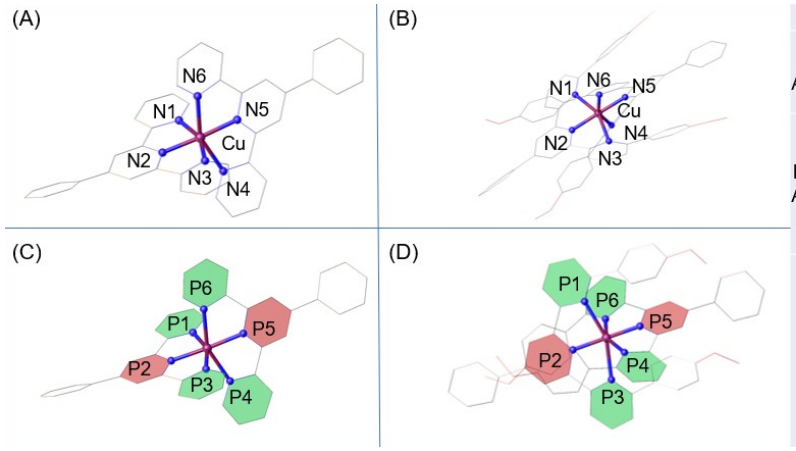

	Angle	$L1_2$-Cu	$L2_2$-Cu
Bond Angle (°)	N1-Cu-N6	98.78	100.92
	N4-Cu-N3	93.54	100.92
	N5-Cu-N2	175.08	178.67
Dihedral Angle (°)	P2-P1	2.546	14.607
	P2-P3	2.737	22.899
	P5-P4	6.503	14.607
	P5-P6	2.937	22.899
	Average	3.681	18.753
Bond Length (Å)	Cu-N1	2.111	2.323
	Cu-N2	1.957	1.915
	Cu-N3	2.131	2.3168
	Cu-N4	2.252	2.323
	Cu-N5	2.01	1.915
	Cu-N6	2.226	2.317
	Average	2.115	2.185

Fig. S41 Molecular structure of **L1$_2$-Cu** and **L2$_2$-Cu** at room temperature.

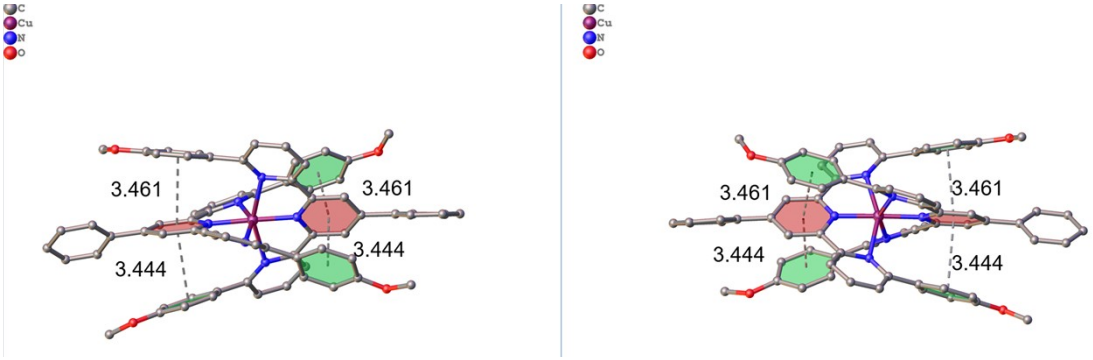

Fig. S42 P and M helical conformation extracted from the crystal structure of **L2$_2$-Cu**.

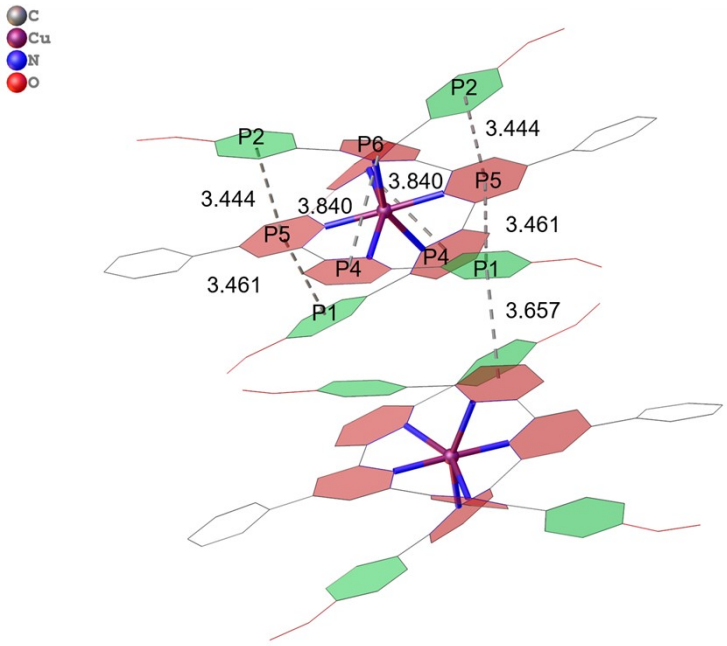

Fig. S43 The views of the intramolecular and intermolecular π-π stacking interactions of the molecule **L2$_2$-Cu**.

Table S5 π-π stacking interactions in **L2$_2$-Cu**. P1: C20 → C21 → C22 → C17 → C18 → C19, P2: C29 → C34 → C33 → C32 → C31 → C30, P3: C4 → C36 → C01E → C37 → C6 → C5, P4: N1 → C16 → C15 → C14 → C13 → C12 , P5: N2 → C10 → C11 → C7 → C8 → C9 , P6: N3 → C28 → C27 → C26 → C25 → C24.

Entry	π-π stack	c-c(Å)	α (°)	β (°)	c-plane (Å)	Slippage (Å)	Symmetry operation
1	P1-P4	3.657	7.835	9.18	3.2712	1.225	(+X,3/2-Y,1-Z)
2	P1-P5	3.461	12.858	36.5	3.2158	1.28	(3/2-X,3/2-Y, +Z)
3	P2-P5	3.444	12.593	49.2	3.4008	0.981	(3/2-X,3/2-Y, +Z)
4	P4-P6	3.84	33.953	70.7	3.5191	1.537	(3/2-X,3/2-Y, +Z)

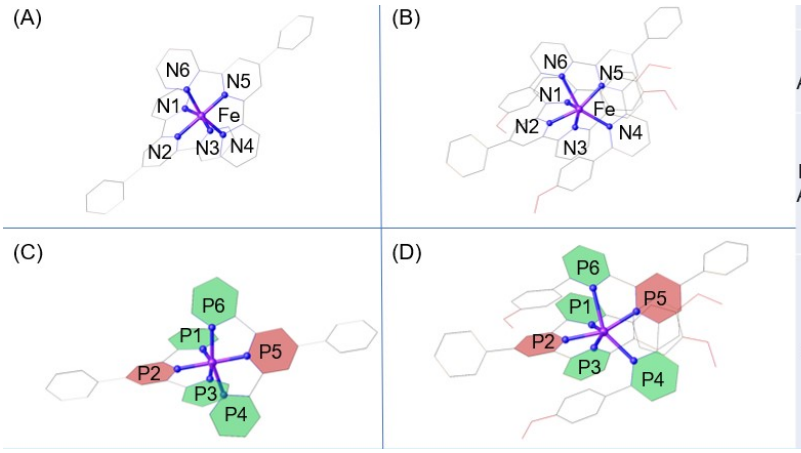

	Angle	$L1_2$-Fe	$L2_2$-Fe
Bond Angle (°)	N1-Fe-N6	91.29	83.51
	N4-Fe-N3	92.56	86.46
	N5-Fe-N2	177.54	156.32
Dihedral Angle (°)	P2-P1	2.912	22.738
	P2-P3	5.598	12.398
	P5-P4	4.04	8.723
	P5-P6	6.721	28.6
	Average	4.818	18.115
Bond Length (Å)	Fe-N1	1.971	2.4057
	Fe-N2	1.876	2.0866
	Fe-N3	1.983	2.1934
	Fe-N4	1.974	2.2316
	Fe-N5	1.875	2.0752
	Fe-N6	1.975	2.4072
	Average	1.942	2.233

Fig. S44 Molecular structure of **L1$_2$-Fe** and **L2$_2$-Fe** at room temperature.

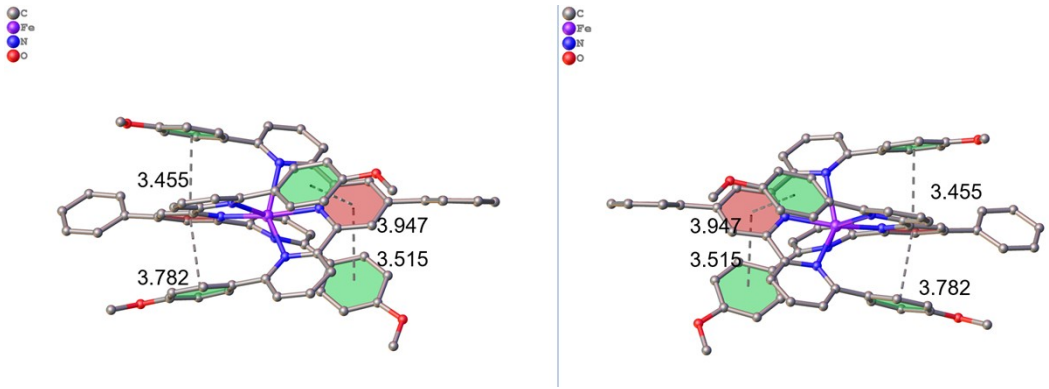

Fig. S45 P and M helical conformation extracted from the crystal structure of **L2$_2$-Fe**.

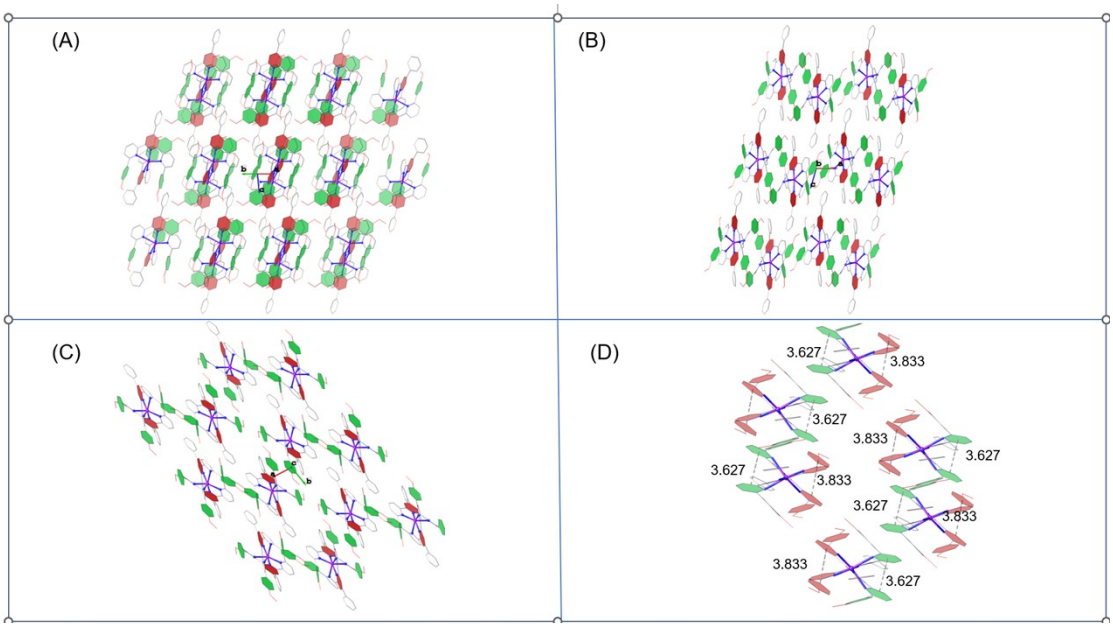

Fig. S46 The views of the π-π stacking interactions of the molecule of complex **L2$_2$-Fe**: (a) viewed on 110 from crystal plane, (b) 010 crystal plane, (c) 001 crystal. and (d) π-π stacking interactions of the molecule.

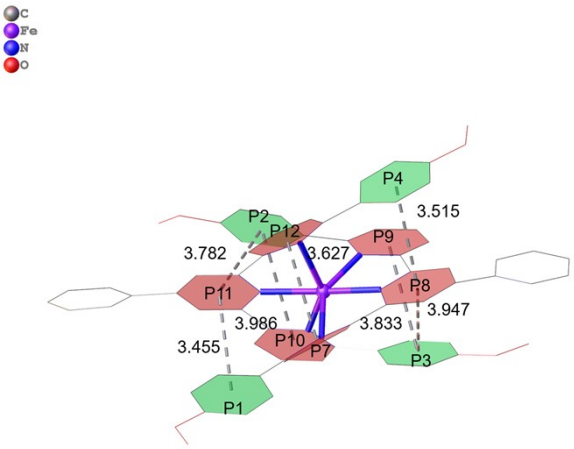

Fig. S47 The views of the intramolecular and intermolecular π-π stacking interactions of the molecule **$L2_2$-Fe**.

Table S6 π-π stacking interactions in **$L2_2$-Fe**. P1**:** C17 → C22 → C21 → C20 → C19 → C18 , P2: C29 → C34 → C33 → C32 → C31 → C30 , P3: C17A → C22A → C21A → C20A → C19A → C18A ,P4: C29A → C34A → C33A → C32A → C31A → C30A , P5: C4 → C5 → C6 → C1 → C2 → C3 , P6: C4A → C5A → C6A → C1A → C2A → C3A , P7: N1 → C16 → C15 → C14 → C13 → C12 , P8: N2 → C10 → C11 → C7 → C8 → C9 , P9: N2 → C10 → C11 → C7 → C8 → C9 , P10: N4 → C28A → C27A → C26A → C25A → C24A, p11: N5 → C10A → C11A → C7A → C8A → C9A , P12: N6 → C16A → C15A → C14A → C13A → C12A.

Entry	π-π stack	c-c(Å)	α (°)	β (°)	c-plane (Å)	Slippage (Å)	Symmetry operation
1	P1-P11	3.455	4.553	13.4	3.248	1.179	(+X, +Y, +Z)
2	P2-P10	3.986	2.562	1.53	3.277	2.404	(+X, +Y, +Z)
3	P2-P11	3.782	10.407	19.57	3.2019	1.833	(+X, +Y, +Z)
4	P3-P8	3.947	13.292	22.3	3.221	2.391	(+X, +Y, +Z)
5	P3-P9	3.833	1.562	2.08	3.8326	1.868	(+X, +Y, +Z)
6	P4-P8	3.515	5.541	3.97	3.2831	1.554	(+X, +Y, +Z)
7	P7-P12	3.515	5.541	77.5	3.5141	0.897	(+X, +Y, +Z)

Table S7 The bond angles of complex **$L1_2$-M** and complex **$L2_2$-M**.

Complex	$L1_2$-Ni	$L2_2$-Ni	$L1_2$-Fe	$L2_2$-Fe	$L1_2$-Cu	$L2_2$-Cu
N (5)- M (1)-N (2)	178.75	177.8	177.54	156.32	175.08	178.67
N (5)-M (1)-N (1)	103.04	103.7	100.8	89.81	89.81	77.3
N (2)-M (1)-N (1)	78.13	77.4	81.31	72.85	78.9	78.093
N (5)-M (1)-N (4)	78.36	77.3	81.45	75.55	76.8	78.093
N (2)-M (1)-N (4)	101.2	104.8	97.33	123.71	102.41	102.7
N (1)-M (1)-N (4)	93.4	80.5	89.74	104.47	90.74	71.317
N (5)-M (1)-N (6)	78.17	77.2	81.24	73	76.58	78.357
N (2)-M (1)-N (6)	92.85	100.7	100.05	88.78	104.69	100.799
N (1)-M (1)-N (6)	92.85	103.9	91.29	83.51	98.78	100.924
N (6)-M (1)-N (4)	156.5	154.5	162.54	147.51	152.52	156.312
N (5)-M (1)-N (3)	100.38	101	96.62	122.4	106.5	100.799
N (2)-M (1)-N (3)	78.45	78	81.27	75.89	78.37	78.357
N (1)-M (1)-N (3)	156.57	155.3	162.58	147.77	157.26	156.312
N (4)-M (1)-N (3)	91.79	104.1	92.56	86.46	93.54	100.924
N (6)-M (1)-N (3)	91.41	82.5	91.66	103.58	87.55	77.055
Complex	$L1_2$-Zn	$L2_2$-Zn	$L1_2$-Co	$L2_2$-Co	$L1_2$-Mn	$L2_2$-Mn
N (5)- M (1)-N (2)	170.893	152.16	177.292	169.17	170.159	175.19
N (5)-M (1)-N (1)	67.672	86.97	98.103	112.165	113.307	102.8
N (2)-M (1)-N (1)	76.866	72.33	79.879	76.299	72.695	72.46
N (5)-M (1)-N (4)	75.865	72.69	79.838	75.706	72.595	73.68
N (2)-M (1)-N (4)	76.036	86.33	101.985	95.563	114.999	108.25
N (1)-M (1)-N (4)	87.584	83.51	88.758	72.589	98.843	106.96
N (5)-M (1)-N (6)	76.133	78.26	80.812	75.814	71.976	72.96
N (2)-M (1)-N (6)	104.603	123.42	97.43	112.855	100.261	108.25
N (1)-M (1)-N (6)	92.83	101.92	92.603	97.717	85.356	80.63
N (6)-M (1)-N (4)	151.407	150.14	160.529	151.488	144.569	146.65
N (5)-M (1)-N (3)	95.773	122.59	102.089	97.505	101.37	110.95
N (2)-M (1)-N (3)	75.121	78.78	79.983	74.449	72.388	73.8
N (1)-M (1)-N (3)	151.913	150.31	159.034	150.29	145.077	146.24
N (4)-M (1)- N (3)	92.333	101.61	90.071	99.365	84.823	82.71
N (6)-M (1)-N (3)	83.896	88.15	89.92	75.568	92.09	109.29

Table S8 The bond lengths of complexes **$L1_2$-M** and **$L2_2$-M**.

Complex	$L1_2$-Ni	$L2_2$-Ni	$L1_2$-Fe	$L2_2$-Fe	$L1_2$-Cu	$L2_2$-Cu
M1-N1	2.082	2.282	1.971	2.4057	2.111	2.323
M1-N2	1.952	1.967	1.876	2.0866	1.957	1.915
M1-N3	2.073	2.242	1.983	2.1934	2.131	2.3168
M1-N4	2.083	2.218	1.974	2.2316	2.252	2.323
M1-N5	1.954	1.972	1.875	2.0752	2.01	1.915
M1-N6	2.076	2.253	1.975	2.4072	2.226	2.317
Complex	$L1_2$-Zn	$L2_2$-Zn	$L1_2$-Co	$L2_2$-Co	$L1_2$-Mn	$L2_2$-Mn
M1-N1	2.139	2.5059	2.088	2.21	2.243	2.409
M1-N2	2.0676	2.0272	1.888	2.02	2.184	2.148
M1-N3	2.223	2.1441	2.079	2.351	2.254	2.322
M1-N4	2.193	2.4996	2.058	2.347	2.221	2.332
M1-N5	2.0566	2.013	1.88	2.029	2.186	2.133
M1-N6	2.184	2.1867	2.047	2.238	2.245	2.356

Table S9 Selected geometric parameters of Complex **$L1_2$-M** and Complex **$L2_2$-M**

	$CoL2_2(PF_6)_2(H_2O)_4$	$CuL2_2(NO_3)_2(H_2O)_4$	$FeL2_2(PF_6)_2(CH_3CN)_{1.5}$	$MnL2_2(NTF)_2$
Formulate	$C_{70}H_{54}CoF_{12}N_6O_4P_2$	$C_{70}H_{54}CuN_8O_{10}$	$C_{73}H_{58.50}F_{12}FeN_{7.5}O_4P_2$	$C_{74}H_{54}F_{12}MnN_8O_{12}S_4$
M	1392.06	1230.75	1450.56	1658.43
Crystal system	monoclinic	tetragonal	monoclinic	monoclinic
Space group	$P2_1/c$	P42/nbc	P -1	P121/c1
a/A	18.2116(5)	19.5981(3)	14.7837(2)	16.4958(5)
b/A	24.5320(6)	19.5981(3)	15.5793(3)	20.9832(7)
c/A	15.6483(4)	33.1820(9)	15.76050(10)	41.0349(14)
α/°	90	90	110.3520(10)	90
β/°	105.614(3)	90	102.5600(10)	93.595(3)
γ/°	90	90	96.5360(10)	90
V/A° ^{3}	6733.1(3)	12744.7(5)	3249.93(8)	14175.7(8)
D_c/g cm^{-3}	1.373	1.283	1.482	1.554
Z	4	8	2	8
Colour	light yellow	blackish black	light orange	light colorless
Habit	needle	prism	prism	block
Dimensions/mm	0.04x0.02x0.01	0.2x0.13x0.11	0.2x0.1x0.06	0.14x0.12x0.11
m(Mo/Cu Ka)/mm^{-1}	0.77	0.82	0.8	0.72
T $_{max,min}$	1.000，0.60401	0.0835, 0.0112	1.000, 0.67645	0.957x 0.945
N_{ind} (Rint)	-0.0999	-0.0282	46115,(0.0496)	33790 (0.0556)
R1[a] ωR2[a]	0.1954,0.2020	0.1856, 0.1907	0.1312, 0.1344	0.1451, 0.1820
GoF	1.16	1.059	1.005	1.047
$\triangle\rho_{min,max}$/e$^-$ A°$^{-3}$	(-)0.678, 0.096	(-)0.835, 0.094	(-)0.682, 0.900	(-)0.595, 0.533
CCDC	2170550	2170552	2170554	2169764

	$NiL2_2(CF_3SO_3)_2(H_2O)_4$	$ZnL2_2(PF_6)2(H2O)_4$	$CoL1_2(PF_6)\ H_2O$
Formulate	$C_{72}H_{54}F_6N_6Ni_{10}S_2$	$C_{74}H_{60}F_{12}N_8O_4P_2Zn$	$C_{42}H_{31}CoF_{12}N_6P_2$
M	1400.04	1480.61	993.11
Crystal system	monoclinic	triclinic	triclinic
Space group	P121/c 1	P -1	P -1
a/A	20.0030(14)	14.82536(16)	13.42
b/A	19.9002(11)	15.58807(16)	17.5883
c/A	17.2847(11)	15.76441(18)	17.7353
α/°	90	110.6557(10)	100.794(1)
β/°	105.098(7)	96.7606(9)	93.906(1)
γ/°	90	96.7606(9)	94.420(1)
V/A° ^{3}	6642.9(8)	3251.48(7)	4085.27(7)
D_c/g cm^{-3}	1.4	1.512	1.615
Z	4	2	4
Color	light green	light colorless	clear dark orange
Habit	needle	block	plate
Dimensions/mm	0.13x0.12x0.1	0.14x0.12x0.1	0.4x0.02x0.08
m(Mo/Cu Ka)/mm^{-1}	0.84	0.8	4.926
T $_{max,min}$	1.00000, 0.93349	0.840, 0.786	1,0.17350
N_{ind} (Rint)	0.1337	0.0335	0.076
R1[a] ωR2[a]	0.1899, 0.2610	0.0453, 0.0422	0.1383,0.1437
GoF	1.022	1.036	1.0066
$\triangle\rho_{min,max}$/e$^-$ A°$^{-3}$	(-)0.592, 0.999	0.1188, 0.1216	0.723, -0.632
CCDC	2170551	2170553	2210926

Table S10 The results of octahedral distortion calculator

Complex	d_{mean}	ζ	Σ	Θ
$L2_2$-Ni	2.1557	0.744414	145.3703	409.5689
$L2_2$-Cu	2.1852	1.079147	147.5754	424.6856
$L2_2$-Co	2.1994	0.698146	164.777	498.798
$L2_2$-Mn	2.299	0.584451	195.7073	562.8937
$L2_2$-Zn	2.2294	1.093747	162.5358	599.4113
$L2_2$-Fe	2.2333	0.692646	168.3102	633.2856

d_{mean} which refers to the average metal–ligand distances in the octahedral coordination sphere. The parameter ζ is the sum of the deviation of 6 unique metal–ligand bond lengths around the central metal atom (*di*) from the average value (d_{mean}). The parameter Σ is the sum of the deviation of 12 unique cis ligand–metal–ligand angles (ϕ_i) from 90°. The parameter Θ is the sum of the deviation of 24 unique torsional angles between the ligand atoms on opposite triangular faces of the octahedron viewed along the pseudo-threefold axis (θ_i) from 60°.

Photophysical properties

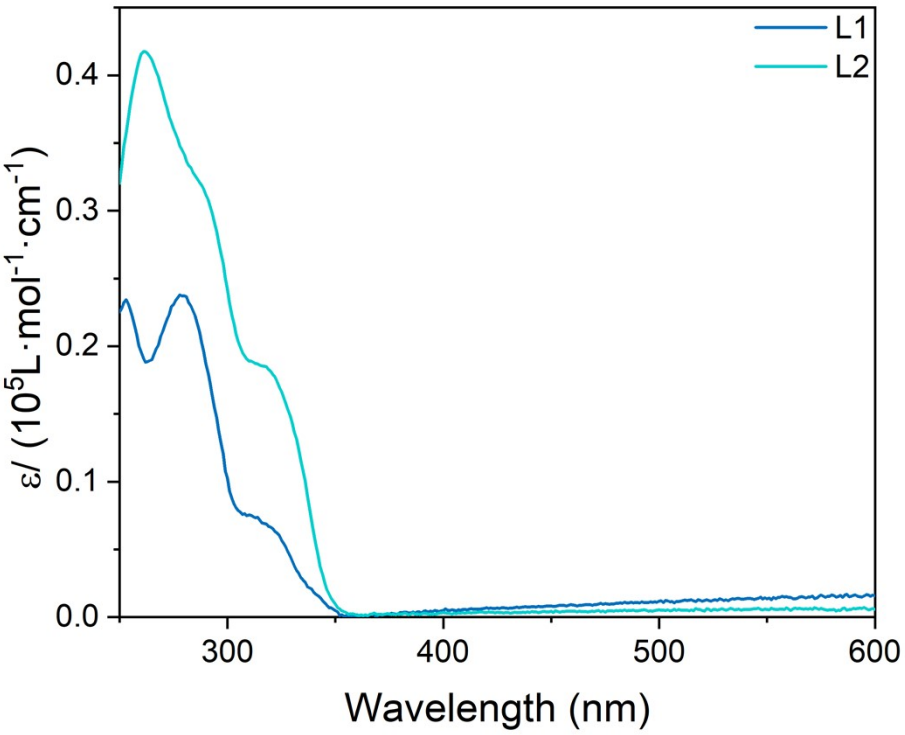

Fig. S48 UV-vis spectra of ligand **L2** (c = 1 × 10^{-5} M) in CH_2Cl_2.

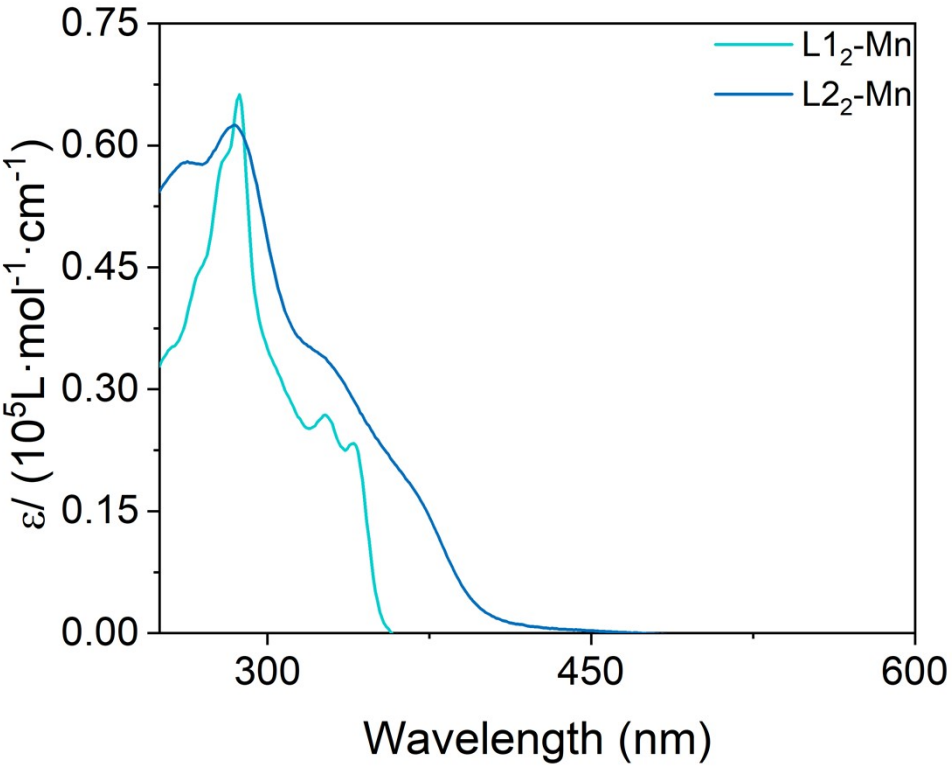

Fig. S49 UV-vis spectra of complex **$L1_2$-Mn** and **$L2_2$-Mn** (c = 1 × 10^{-5} M) in CH_3CN.

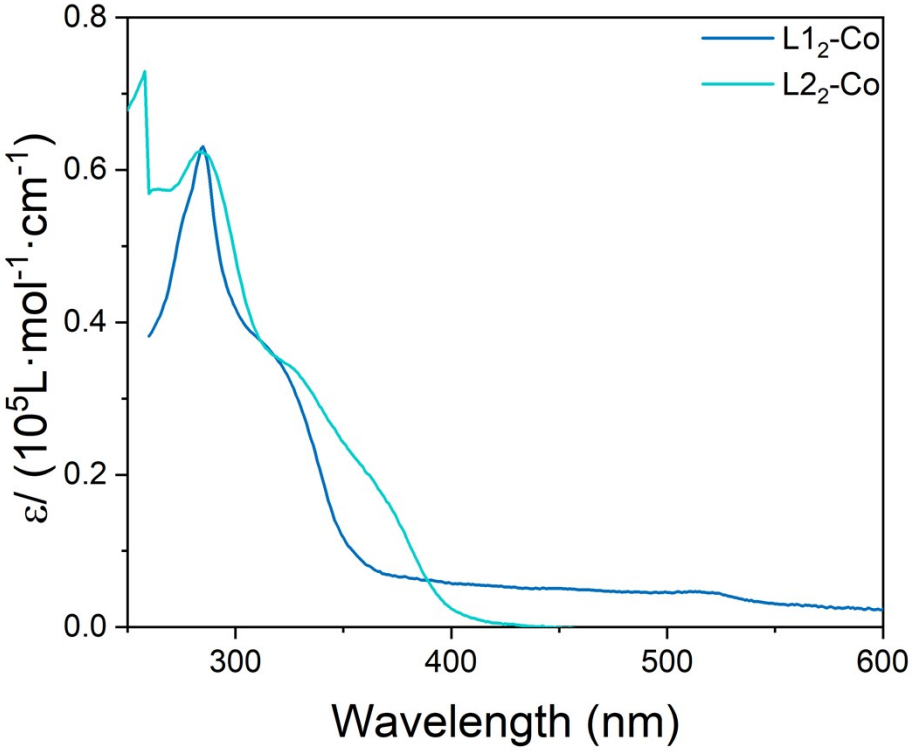

Fig. S50 UV-vis of spectra complex **$L1_2$-Co** and **$L2_2$-Co** (c = 1 × 10^{-5} M) in CH_3CN.

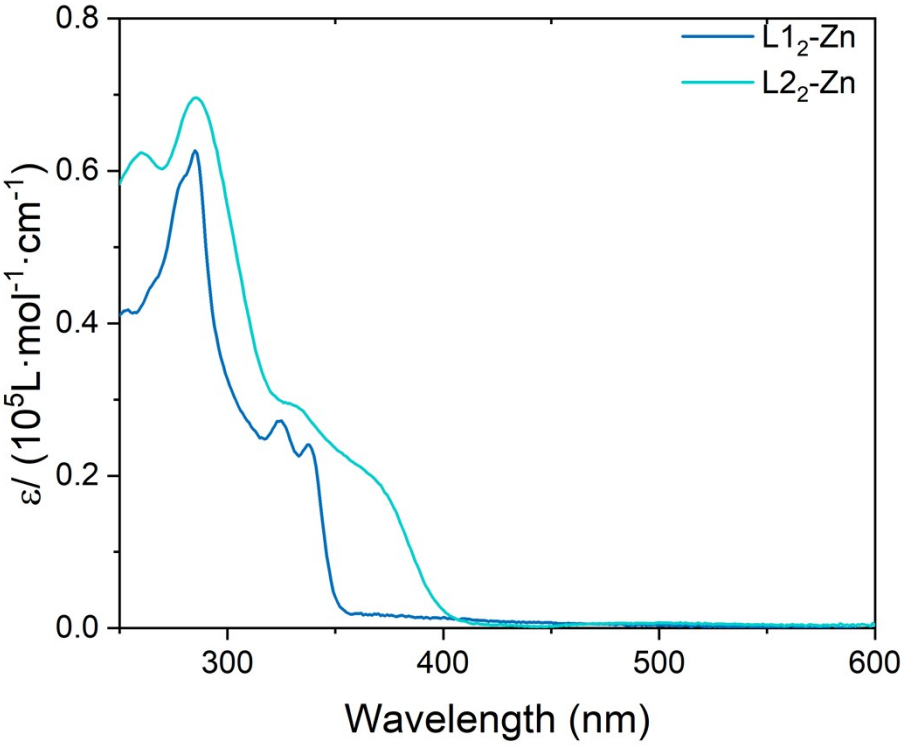

Fig. S51 UV-vis of spectra complex **$L1_2$-Zn** and **$L2_2$-Zn** (c = 1 × 10^{-5} M) in CH_3CN.

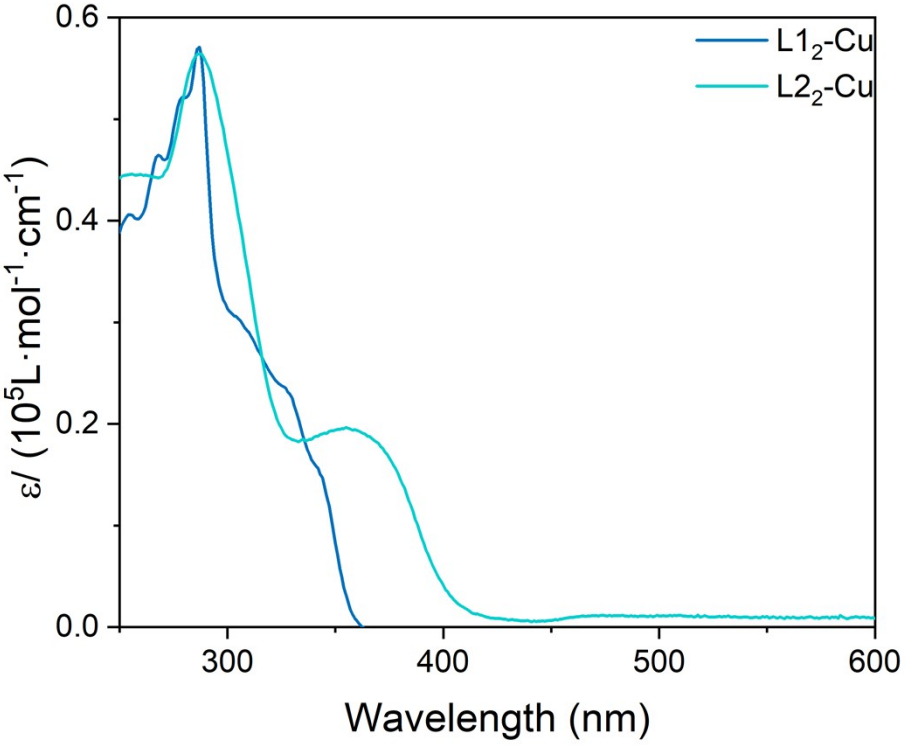

Fig. S52 UV-vis of spectra complex **$L1_2$-Cu** and **$L2_2$-Cu** (c = 1 × 10^{-5} M) in CH_3CN.

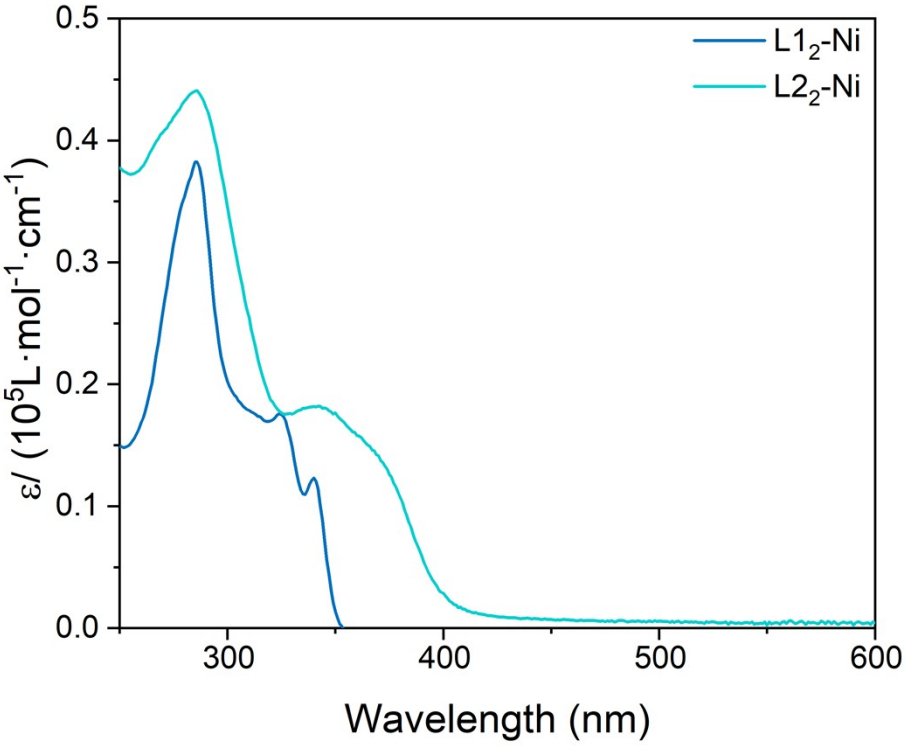

Fig. S53 UV-vis spectra of complex **L1$_2$-Ni** and **L2$_2$-Ni** (c = 1 × 10^{-5} M) in CH_3CN.

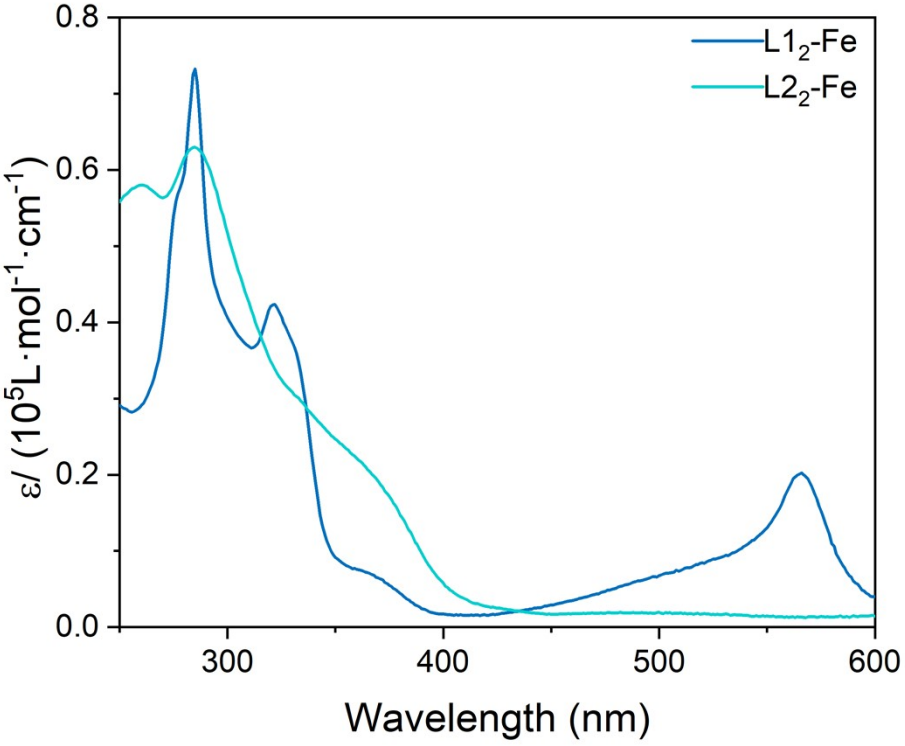

Fig. S54 UV-vis spectra of complex **L1$_2$-Fe** and **L2$_2$-Fe** (c = 1 × 10^{-5} M) in CH_3CN.

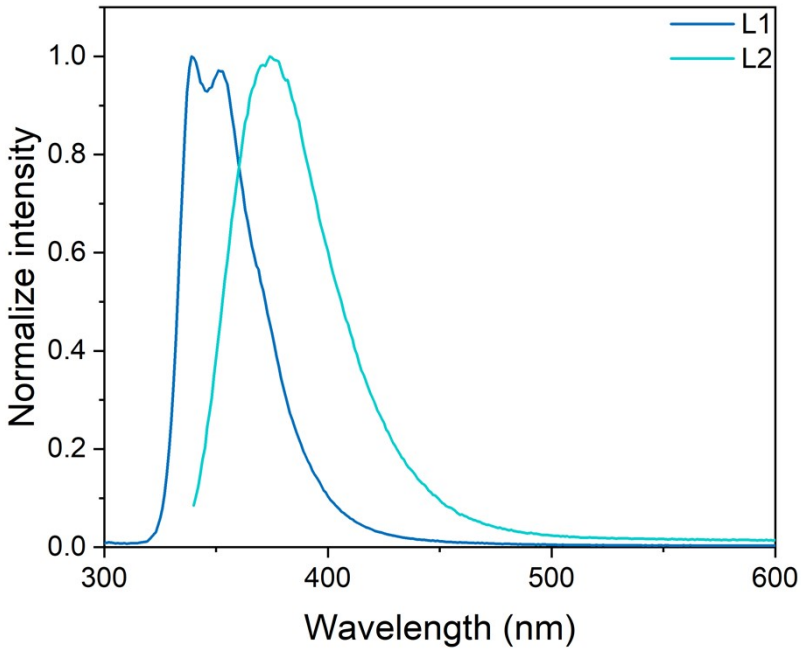

Fig. S55 Normalized fluorescence spectra of ligand **L1** (λ_{ex} = 276nm, c = 1 × 10^{-5} M) and **L2** (λ_{ex} = 320 nm, c = 1 × 10^{-5}M) in CH_2Cl_2.

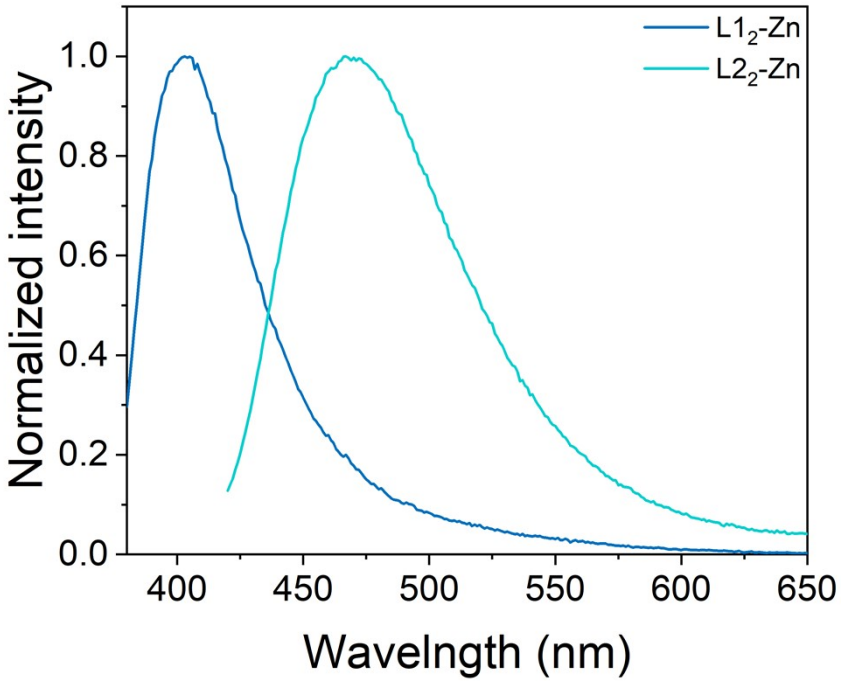

Fig. S56 Normalized spectra of complex **L1$_2$-Zn** (λ_{ex} = 355 nm) and **L2$_2$-Zn** (λ_{ex} = 410 nm) in solid state.

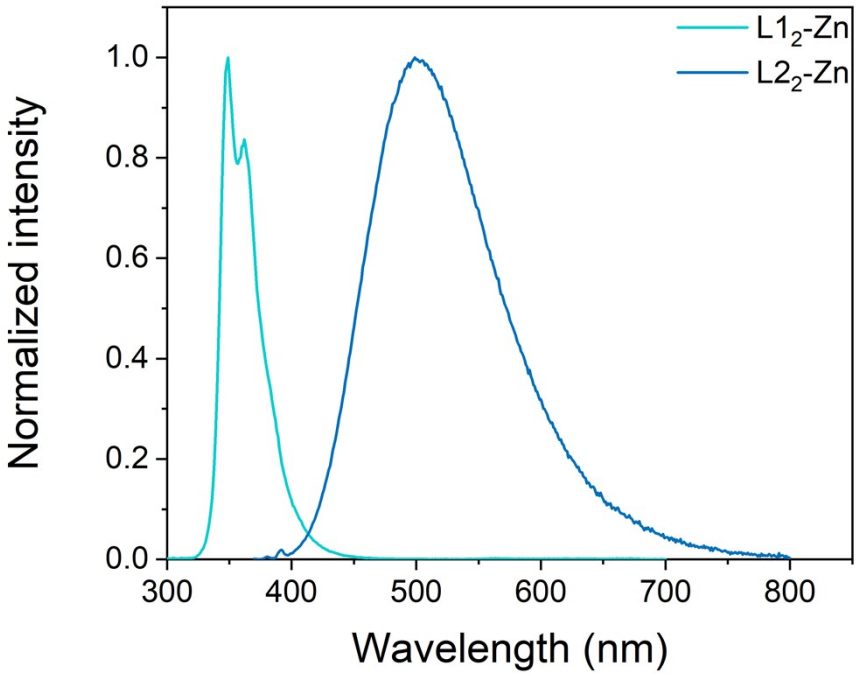

Fig. S57 Normalized fluorescence spectra of complex **L1$_2$-Zn** (λ_{ex} = 280 nm, c = 1 × 10^{-5} M) and **L2$_2$-Zn** (λ_{ex} = 350 nm, c = 1 × 10^{-5}M) in CH_3CN.

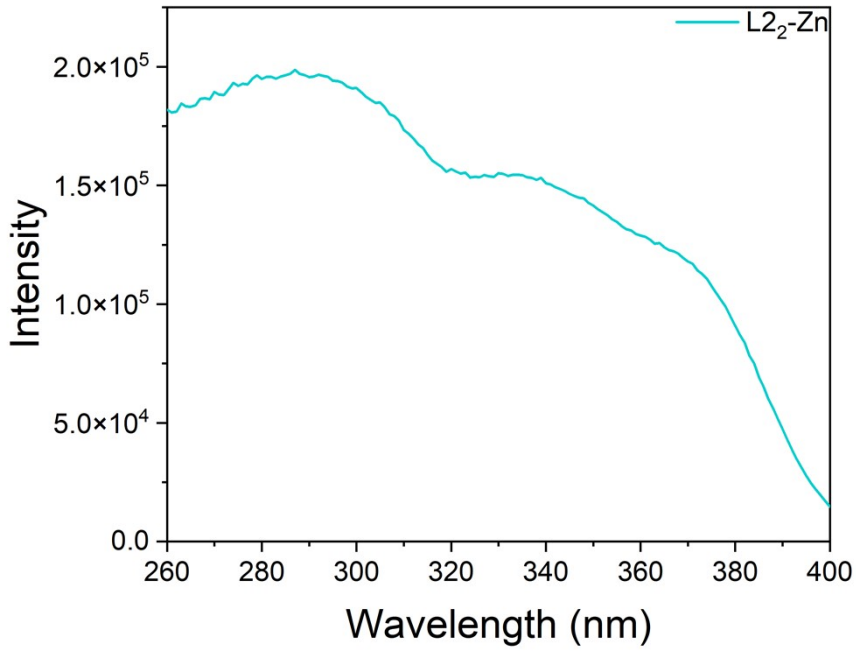

Fig. S58 Fluorescence excitation spectra of complex **L2$_2$-Zn** (λ_{em} = 500 nm, c = 1 × 10^{-5} M) in CH_3CN.

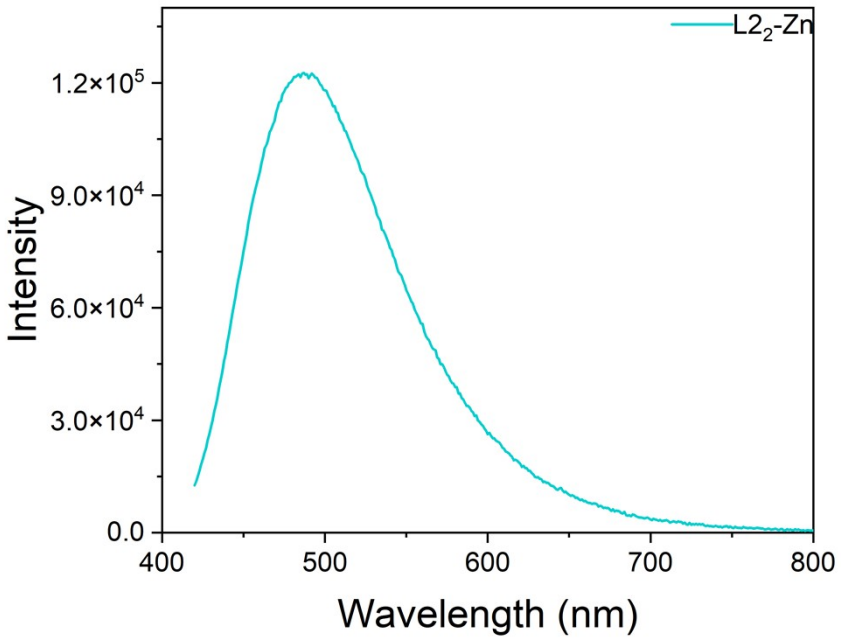

Fig. S59 Fluorescence spectra of complex **L2$_2$-Zn** (λ_{ex} = 400 nm, c = 1 × 10^{-5} M) in CH_2Cl_2.

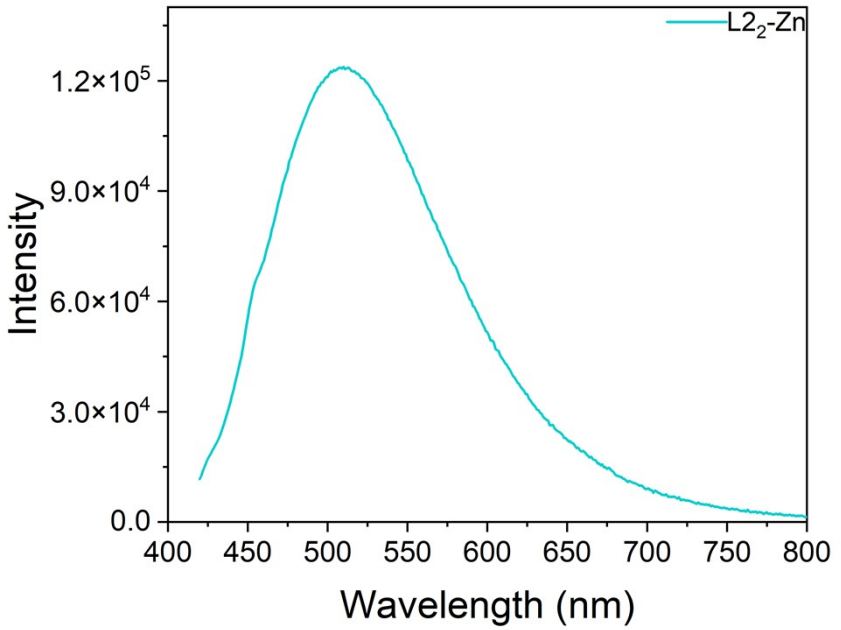

Fig. S60 Fluorescence spectra of complex **L2$_2$-Zn** (λ_{ex} = 400 nm, c = 1 × 10^{-5} M) in DMF.

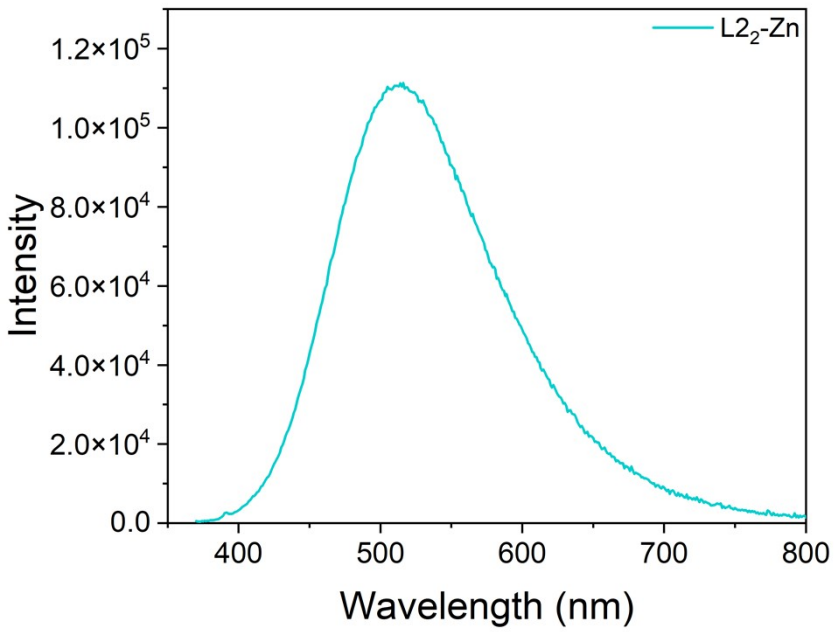

Fig. S61 Fluorescence spectra of complex **L2$_2$-Zn** (λ_{ex} = 400 nm, c = 1 × 10^{-5} M) in DMSO.

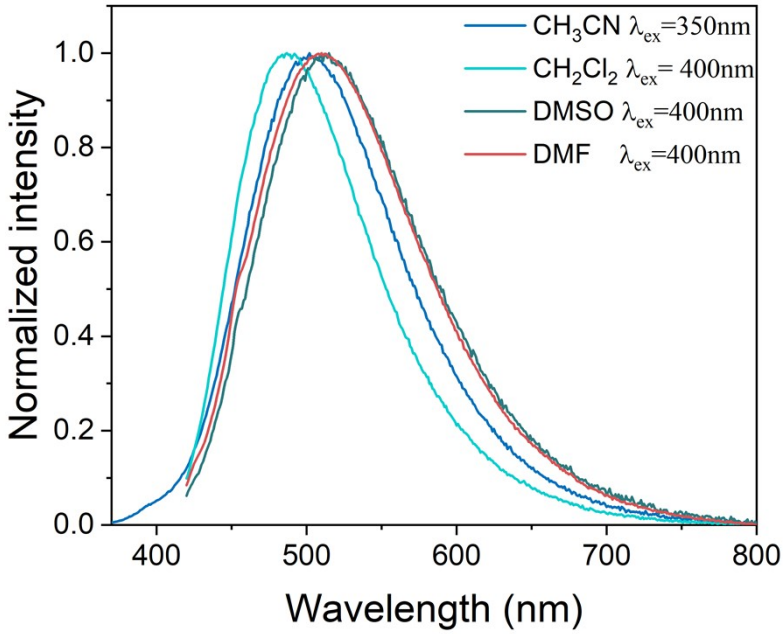

Fig. S62 Normalized fluorescence spectra of complex **L2$_2$-Zn** (c = 1 × 10^{-5} M) in CH_3CN/CH_2Cl_2/DMSO/DMF/CH_3CN).

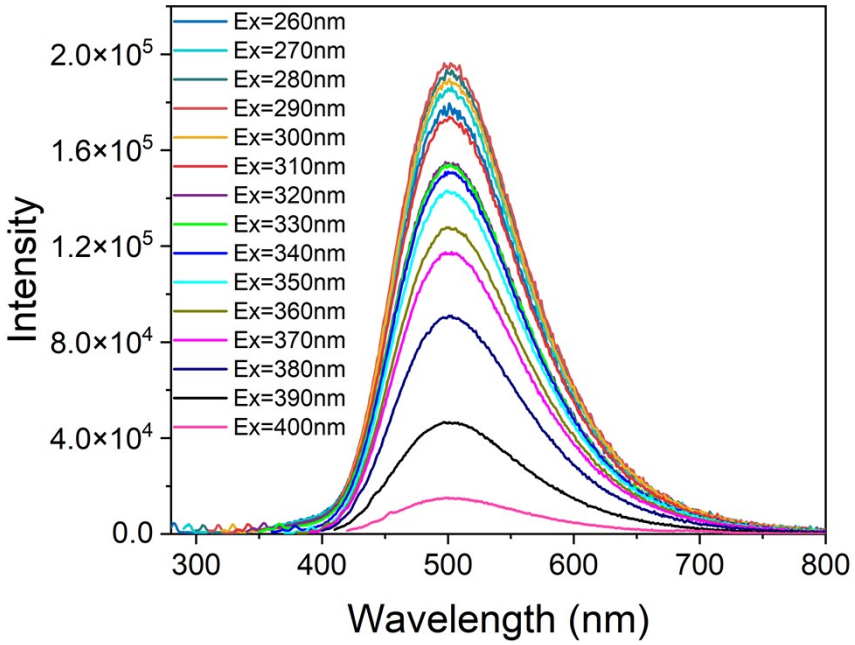

Fig. S63 Fluorescence spectra of complex **$L2_2$-Zn** in CH_3CN (Ex = 260 nm - 400 nm, c = 1 × 10^{-5} M) in CH_3CN.

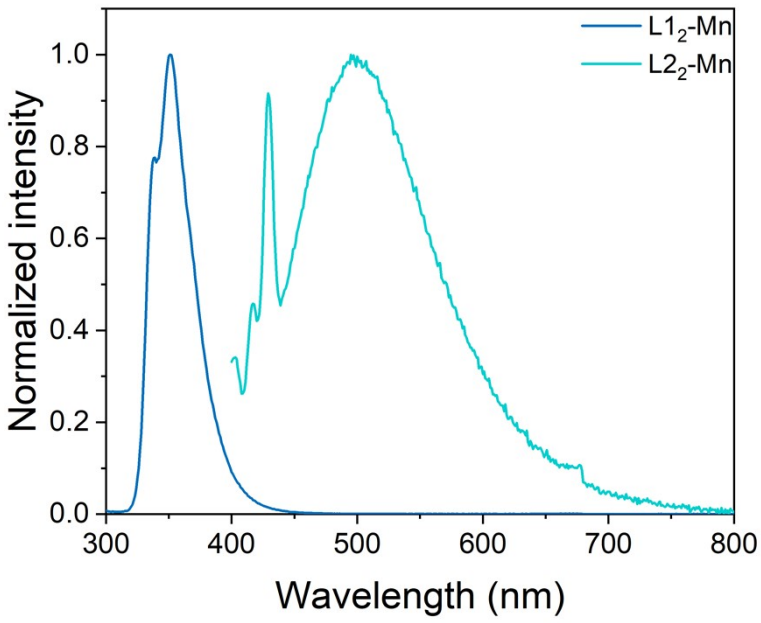

Fig. S64 Normalized fluorescence spectra of complex **$L1_2$-Mn** (λ_{ex} = 280 nm, c = 1 × 10^{-5} M) and **$L2_2$-Mn** (λ_{ex} = 380 nm, c = 1 × 10^{-5} M) in CH_3CN.

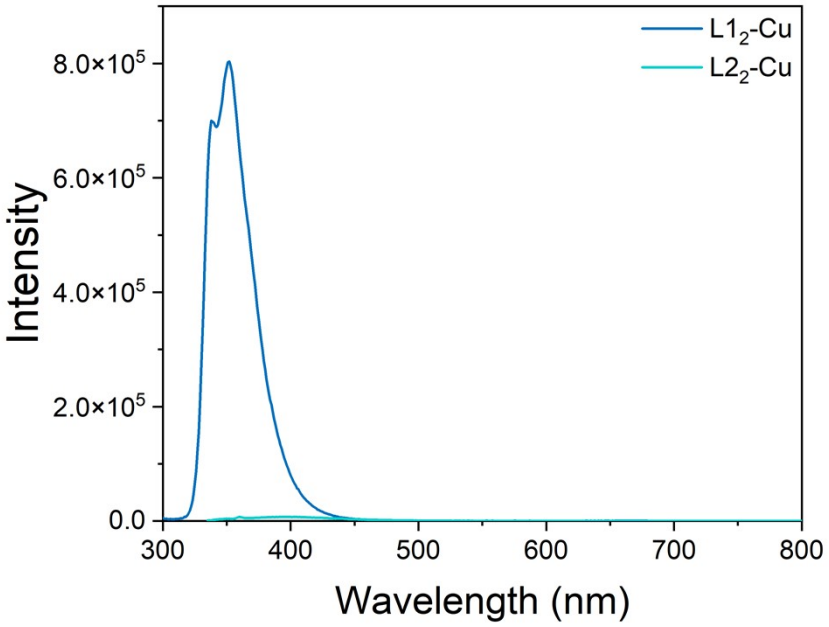

Fig. S65 Fluorescence spectra of complex **L1$_2$-Cu** (λ_{ex} = 280 nm, c = 1 × 10^{-5} M) and **L2$_2$-Cu** (λ_{ex} = 300 nm, c = 1 × 10^{-5} M) in CH_3CN.

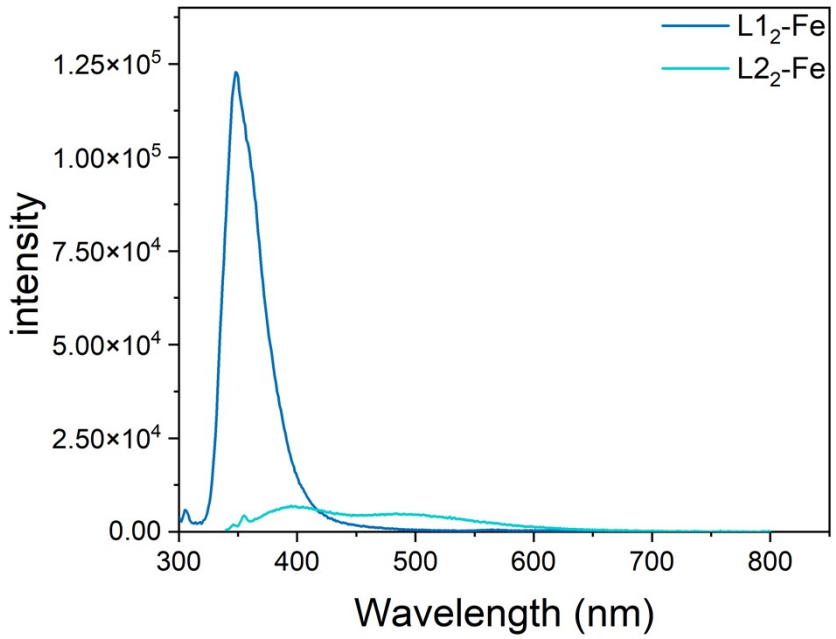

Fig. S66 Fluorescence spectra of complex **L1$_2$-Fe** (λ_{ex} = 280 nm, c = 1 × 10^{-5} M) and **L2$_2$-Fe** (λ_{ex} = 300 nm, c = 1 × 10^{-5} M) in CH_3CN.

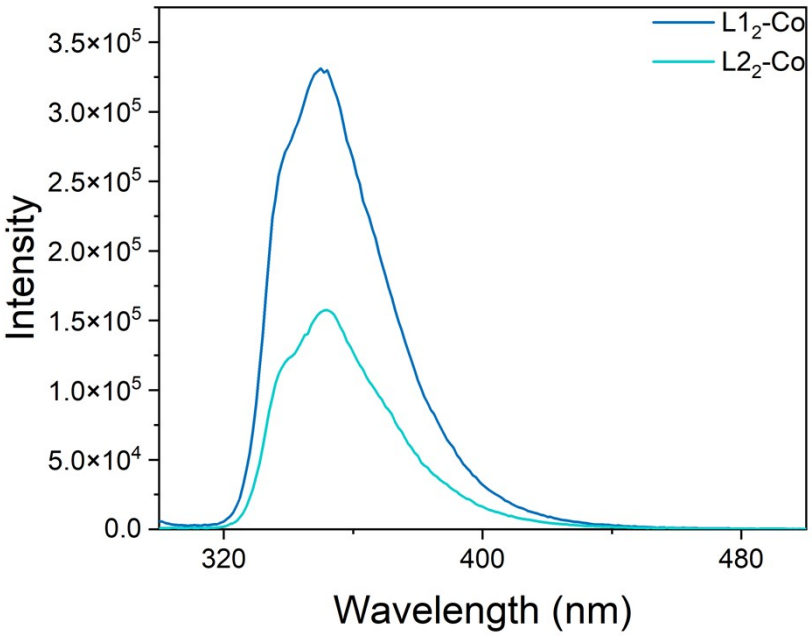

Fig. S67 Fluorescence spectra of complex **L1$_2$-Co** (λ_{ex} = 280 nm, c = 1 × 10^{-5} M) and **L2$_2$-Co** (λ_{ex} = 300 nm, c = 1 × 10^{-5} M) in CH_3CN.

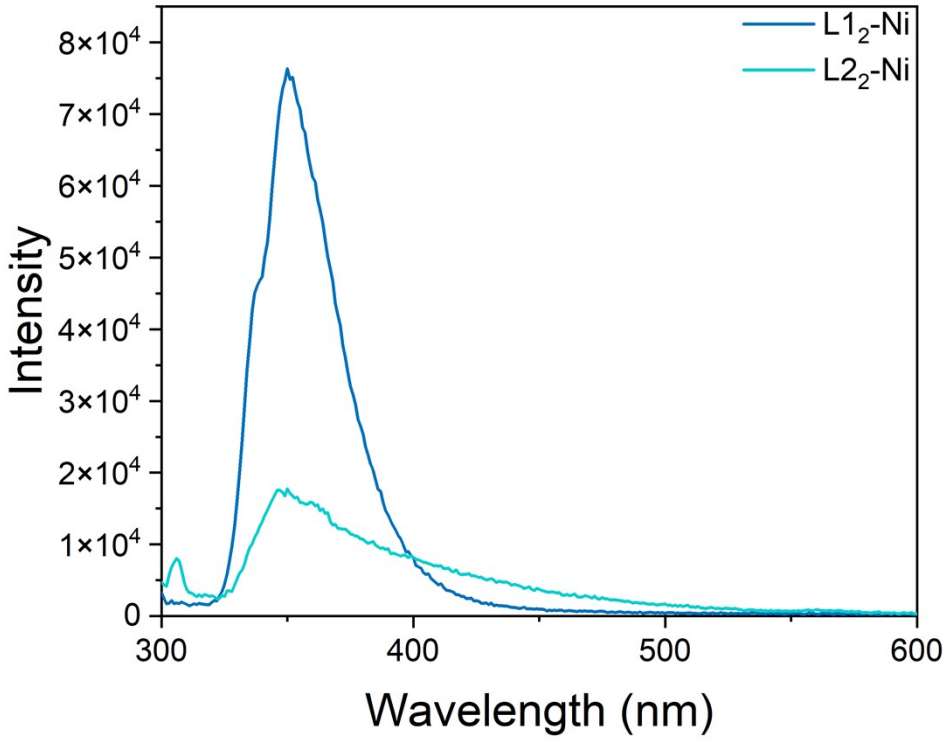

Fig. S68 Fluorescence spectra of complex **L1$_2$-Ni** (λ_{ex} = 280 nm, c = 1 × 10^{-5} M) and **L2$_2$-Ni** (λ_{ex} = 300 nm, c =1 × 10^{-5} M) in CH_3CN.

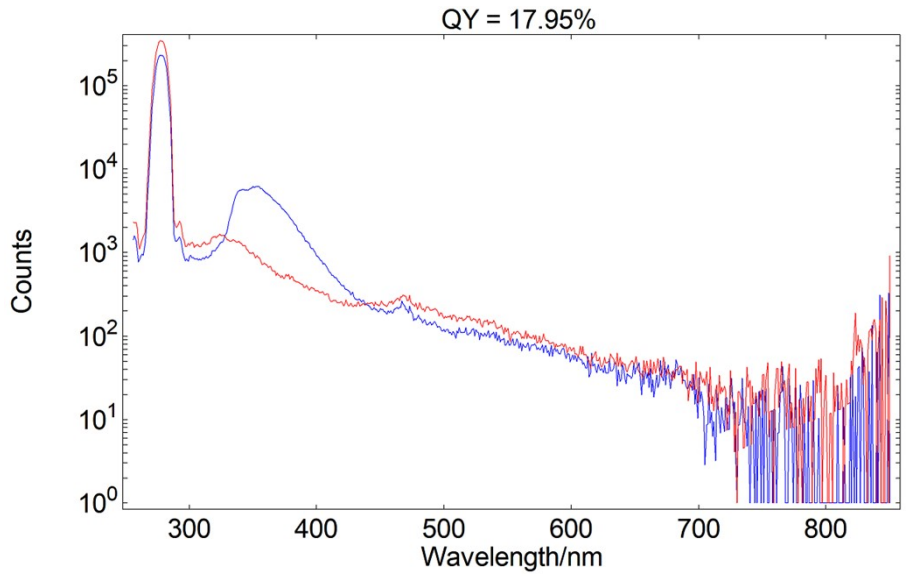

Fig. S69 Absolute fluorescence quantum yield of ligand **L1** (λ_{ex} = 280 nm, c = 1 × 10^{-5} M) in CH_2Cl_2.

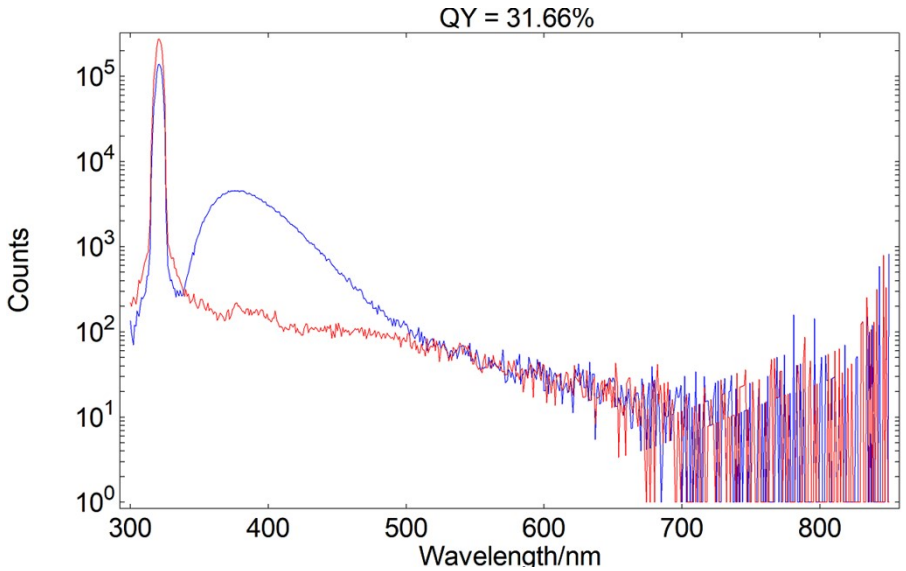

Fig. S70 Absolute fluorescence quantum yield of ligand **L2** (λ_{ex} = 280 nm, c = 1 × 10^{-5} M) in CH_3Cl_2.

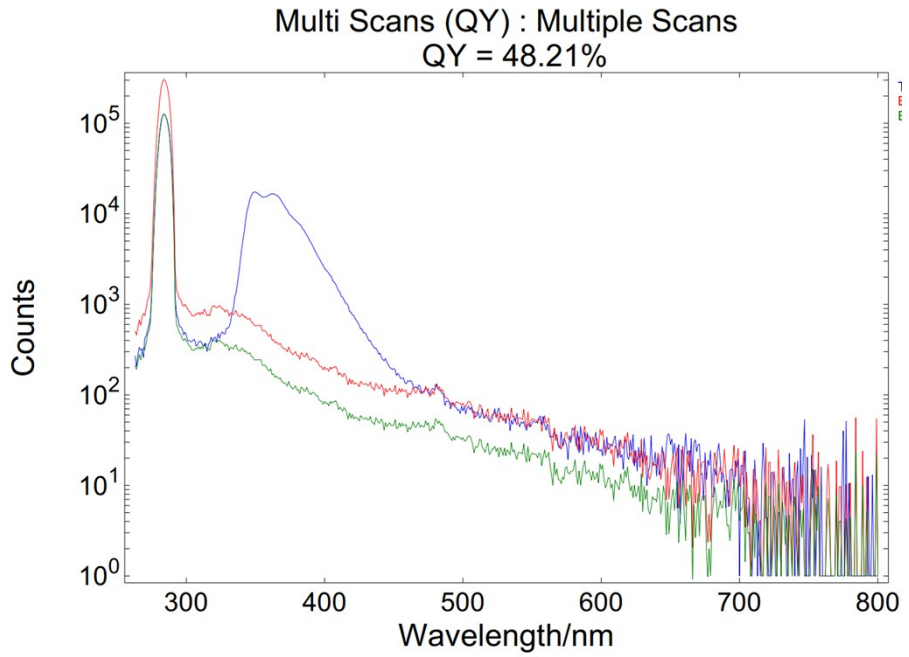

Fig. S71 Absolute fluorescence quantum yield of complex **L1$_2$-Zn** (λ_{ex} = 280 nm, c = 1 × 10^{-5} M) in CH_3CN.

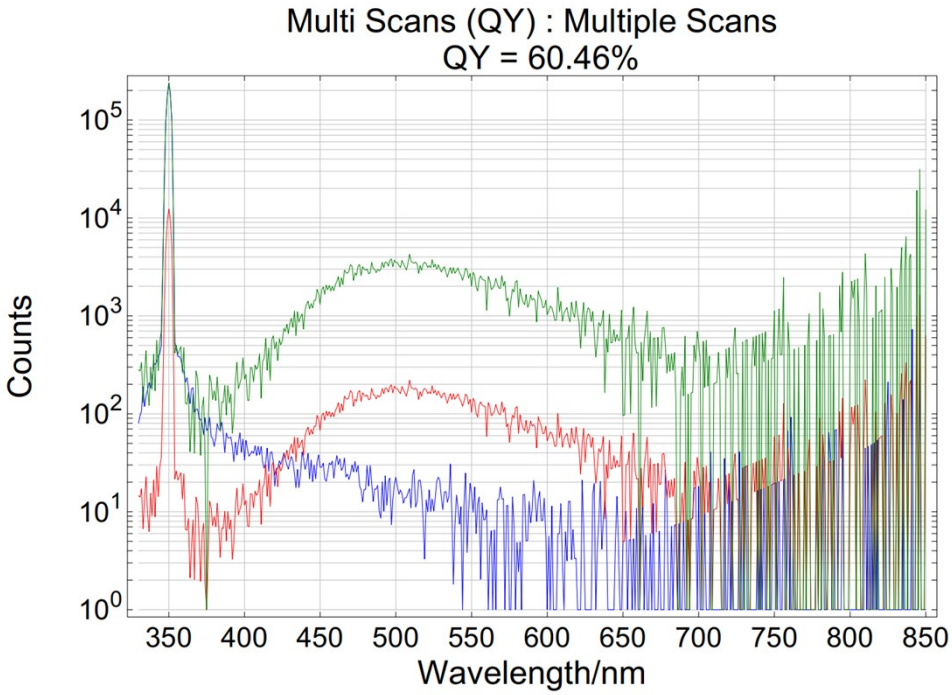

Fig. S72 Absolute fluorescence quantum yield of complex **L2$_2$-Zn** (λ_{ex} = 350 nm, c = 1 × 10^{-5} M) in CH_3CN.

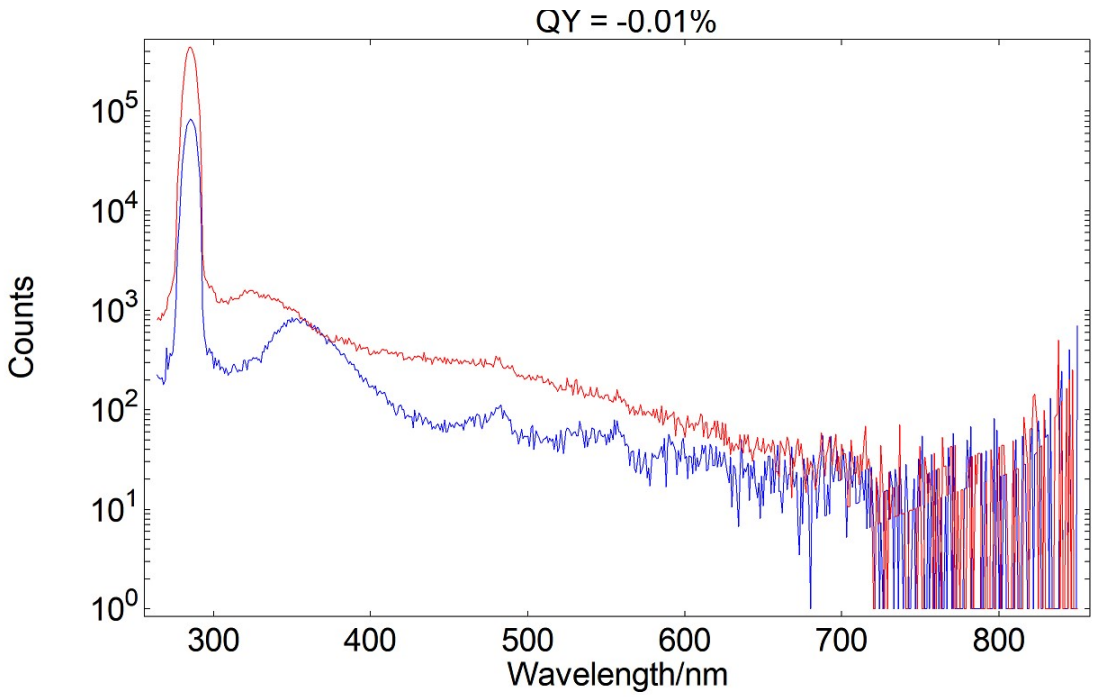

Fig. S73 Absolute fluorescence quantum yield of complex **L1$_2$-Co** (λ_{ex} = 284 nm, c = 1 × 10^{-5} M) in CH_3CN.

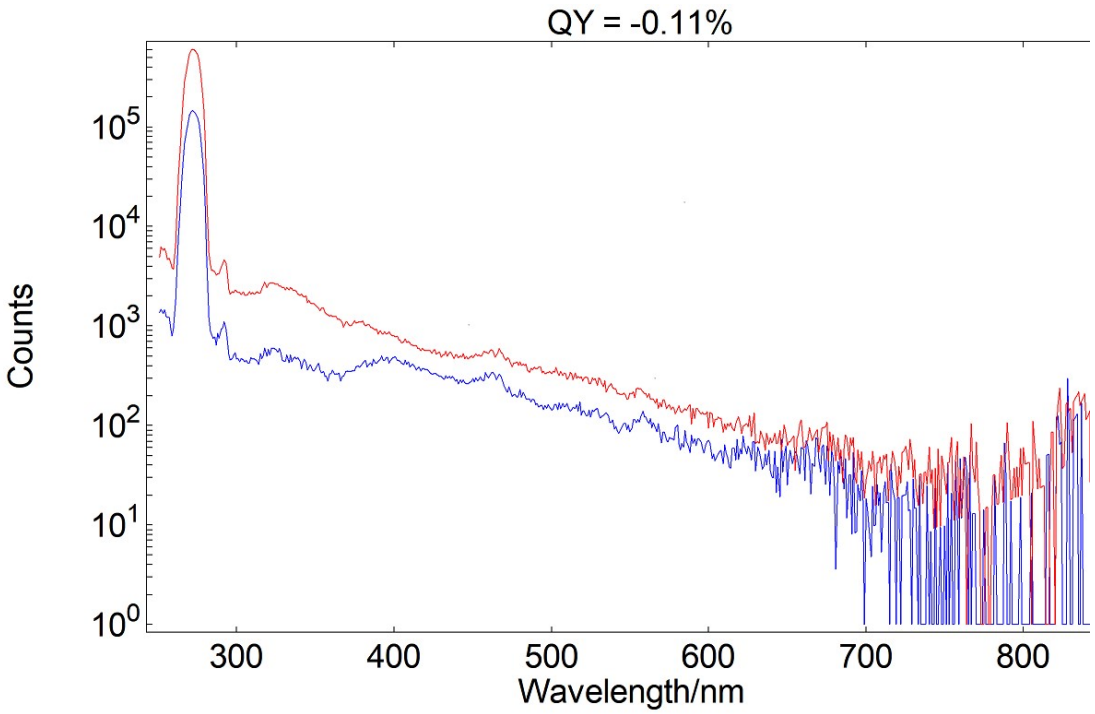

Fig. S74 Absolute fluorescence quantum yield of complex **L2$_2$-Co** (λ_{ex} = 271 nm, c = 1 × 10^{-5} M) in CH_3CN.

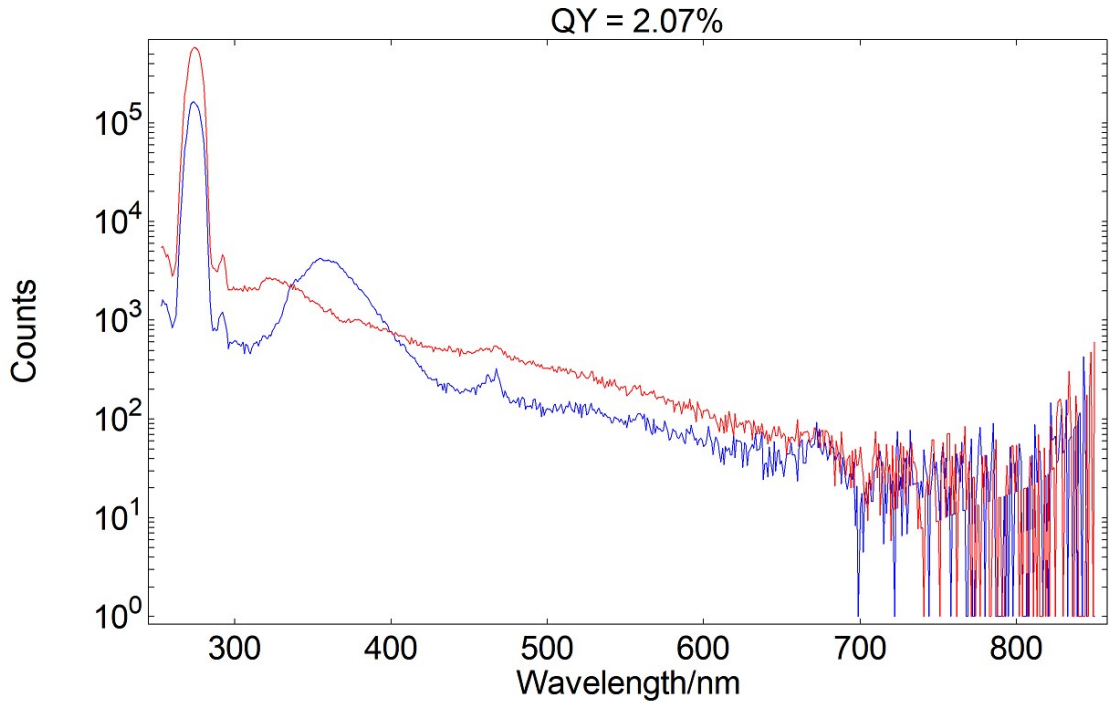

Fig. S75 Absolute fluorescence quantum yield of complex **L1$_2$-Cu** (λ_{ex} = 273 nm, c = 1 × 10^{-5} M) in CH_3CN.

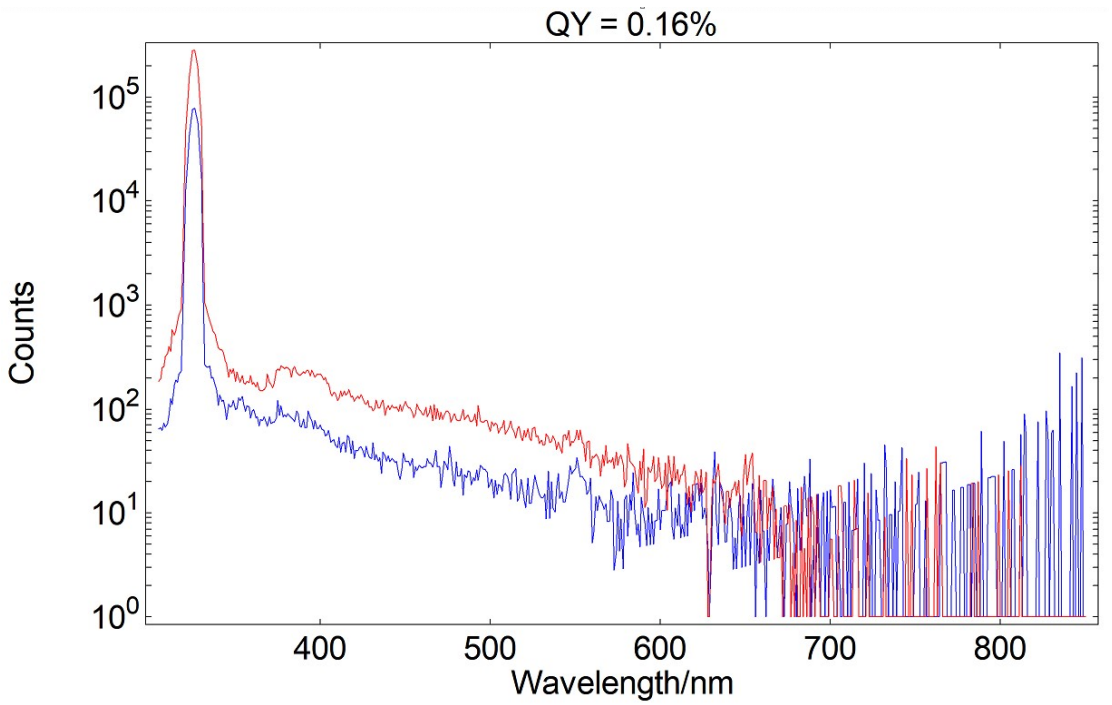

Fig. S76 Absolute fluorescence quantum yield of complex **L2$_2$-Cu** (λ_{ex} = 271 nm, c = 1 × 10^{-5} M) in CH_3CN.

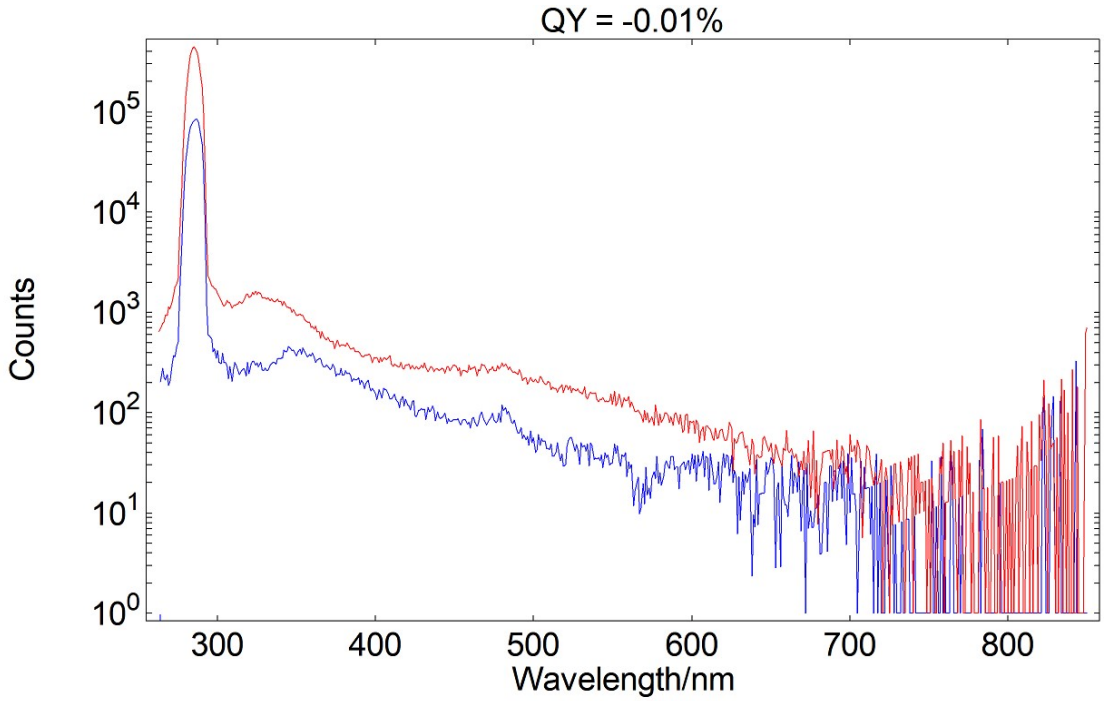

Fig. S77 Absolute fluorescence quantum yield of complex **L1$_2$-Fe** (λ_{ex} = 284 nm, c = 1 × 10^{-5} M) in CH_3CN.

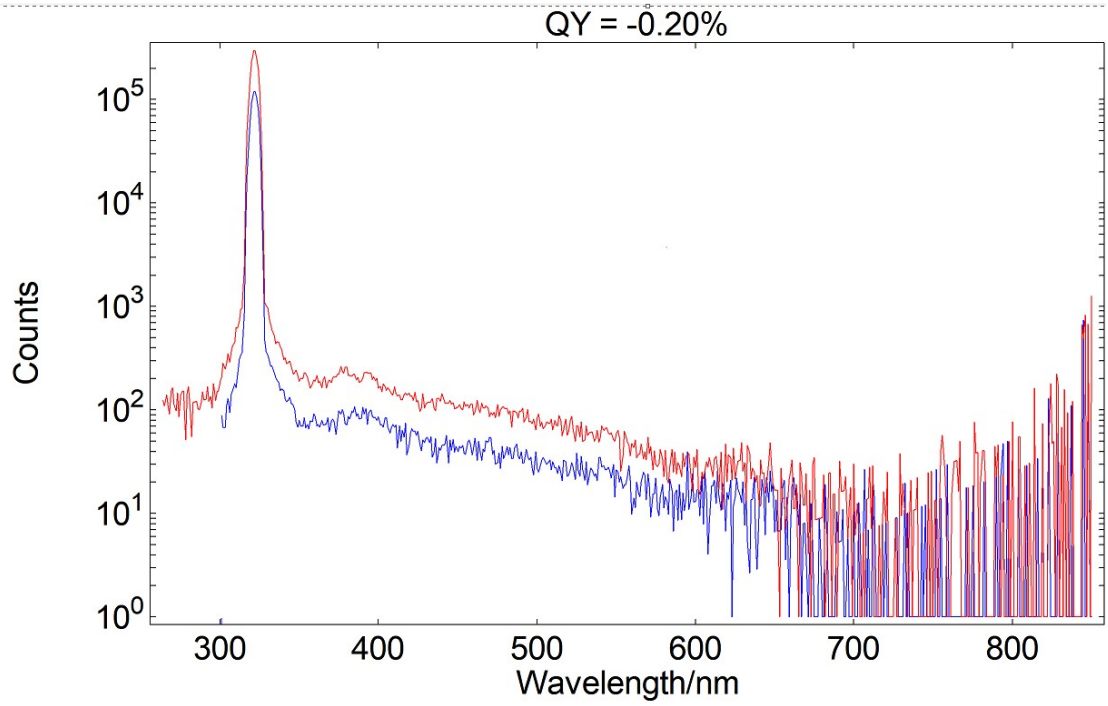

Fig. S78 Absolute fluorescence quantum yield of complex **L2$_2$-Fe** (λ_{ex} = 321 nm, c = 1 × 10^{-5} M) in CH_3CN.

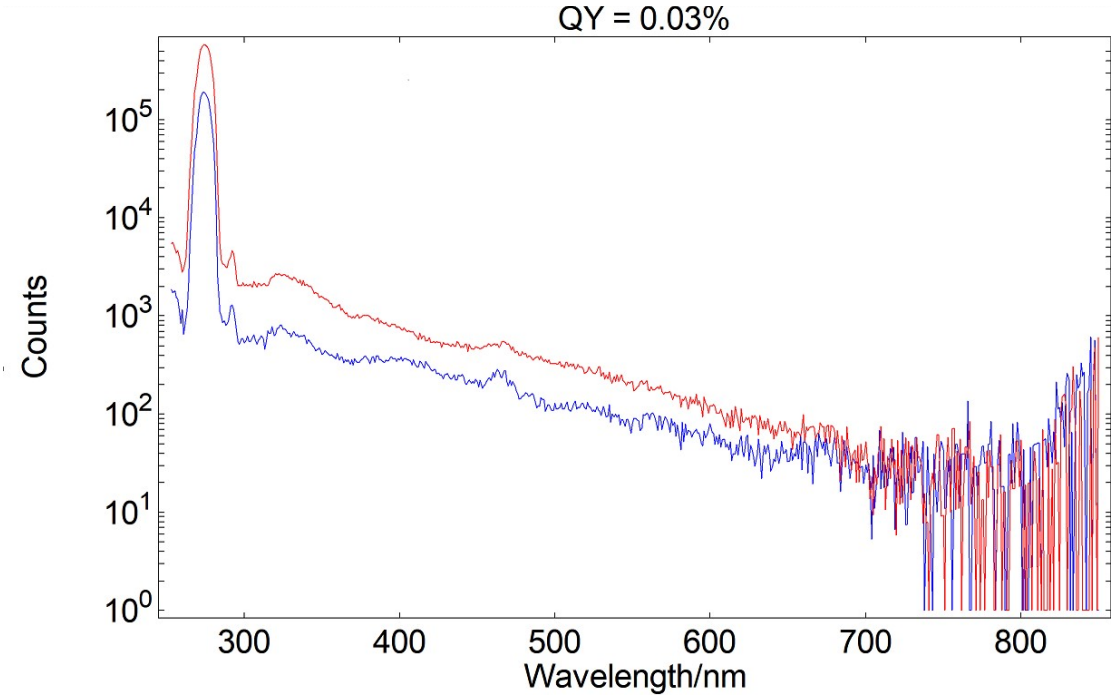

Fig. S79 Absolute fluorescence quantum yield of complex **$L1_2$-Ni** (λ_{ex} = 273 nm, c = 1 × 10^{-5} M) in CH_3CN.

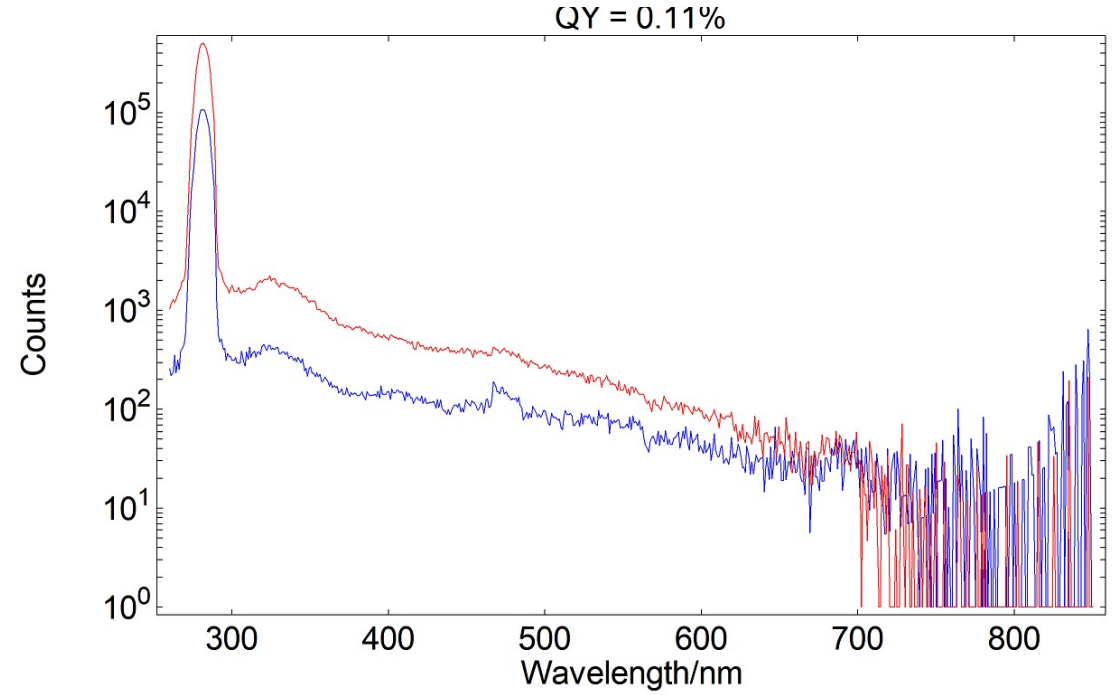

Fig. S80 Absolute fluorescence quantum yield of complex **$L1_2$-Ni** (λ_{ex} = 280 nm, c = 1 × 10^{-5} M) in CH_3CN.

Table S11 Photophysical properties of ligand **L1, L2** and complex **$L1_2$-Zn, $L2_2$-Zn**

	Absorption [a]		Luminescence					
Compound	λ_{max} (nm)	ε_{max} ($M^{-1}\cdot cm^{-1}$)	λ_{ex} (nm) liqud	λ_{max} (nm) Liquid	λ_{ex} (nm) solid	λ_{max} (nm) solid	φ_m(%) [a,b]	solvent
L1	280	23726	281	340	340	393	17.95	CH_2Cl_2
L2	261	41751	325	373	420	450	31.66	CH_2Cl_2
$L1_2$-Zn	285	69500	300	350	352	468	48.21	CH_3CN
$L2_2$-Zn	285	62946	350	500	403	403	60.46	CH_3CN

[a] Air-equilibrated acetonitrile solution in 298K. [b] excitation at 350 nm and uncertainty over the measures is estimated to be 20%.

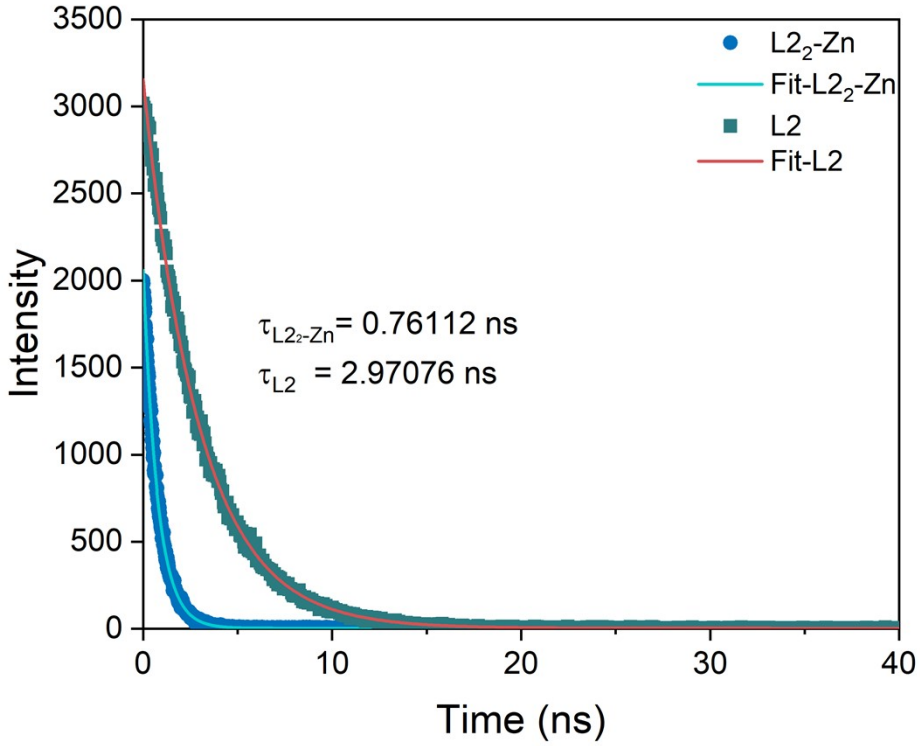

Fig. S81 Time-resolved fluorescence decay curves **L2$_2$-Zn**（ λ_{ex} = 375 nm c = 1 × 10^{-5} M) and **L2**（λ_{ex} = 290 nm ，c = 1 × 10^{-5} M）of persistent emission of in CH_3CN.

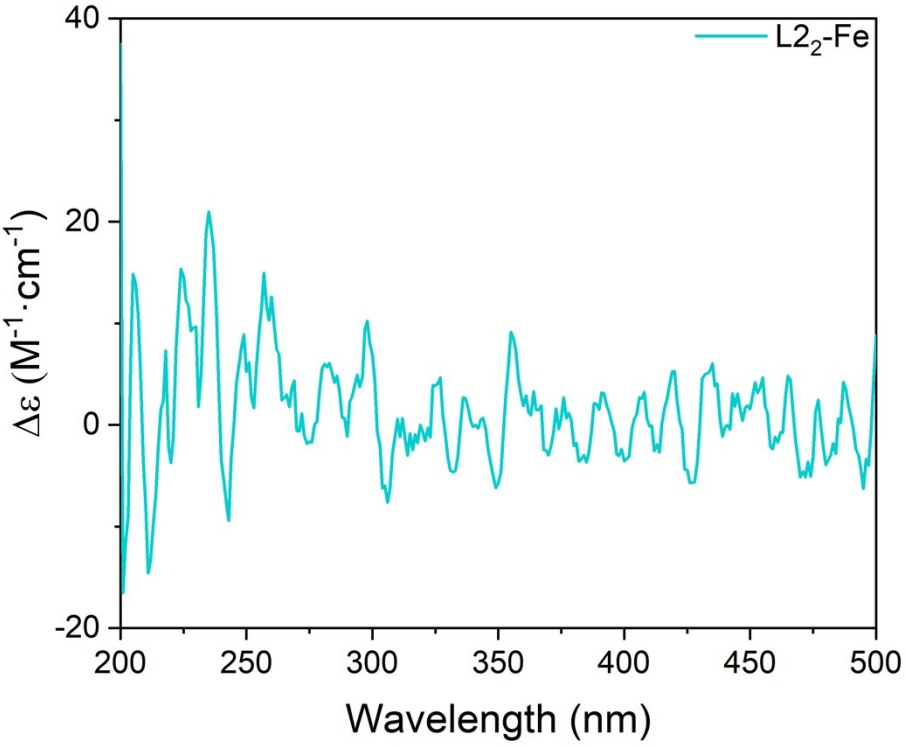

Fig. S82 ECD spectra of L2$_2$-Fe (c = 1 × 10^{-5} M) in CH$_3$CN.

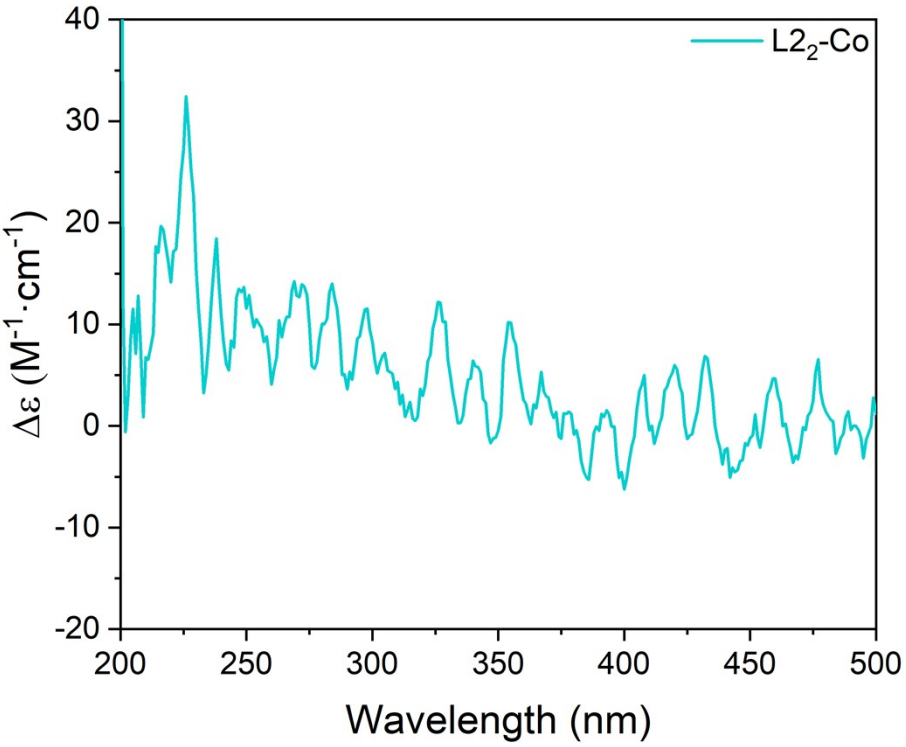

Fig. S83 ECD spectra of L2$_2$-Co (c = 1 × 10^{-5} M) in CH$_3$CN.

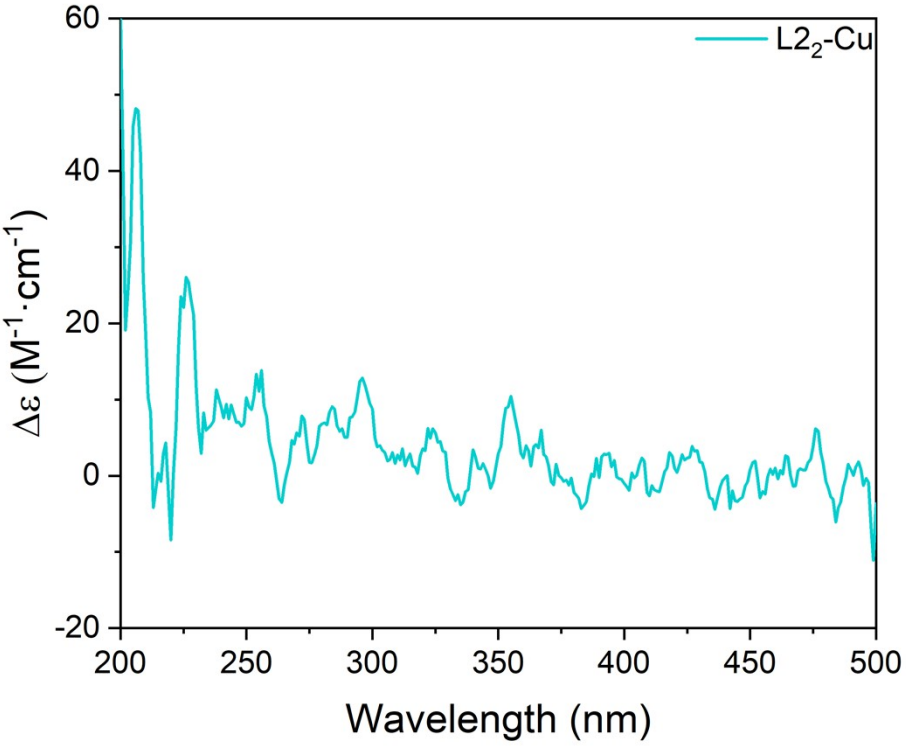

Fig. S84 ECD spectra of L2$_2$-Cu (c = 1 × 10^{-5} M) **in CH$_3$CN.**

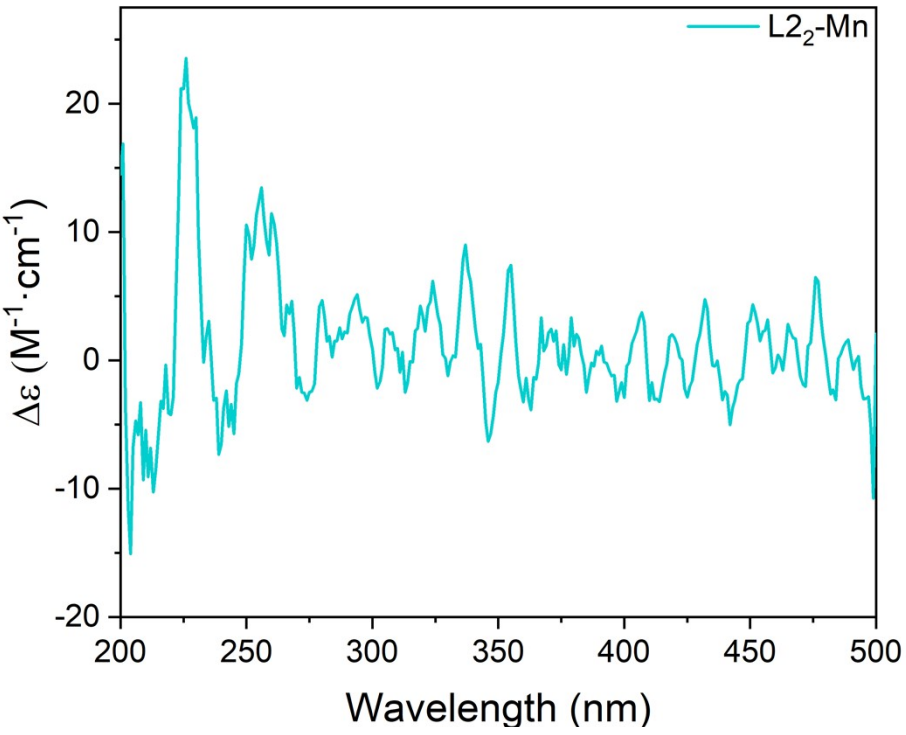

Fig. S85 ECD spectra of L2$_2$-Mn (c = 1 × 10^{-5} M) **in CH$_3$CN.**

.

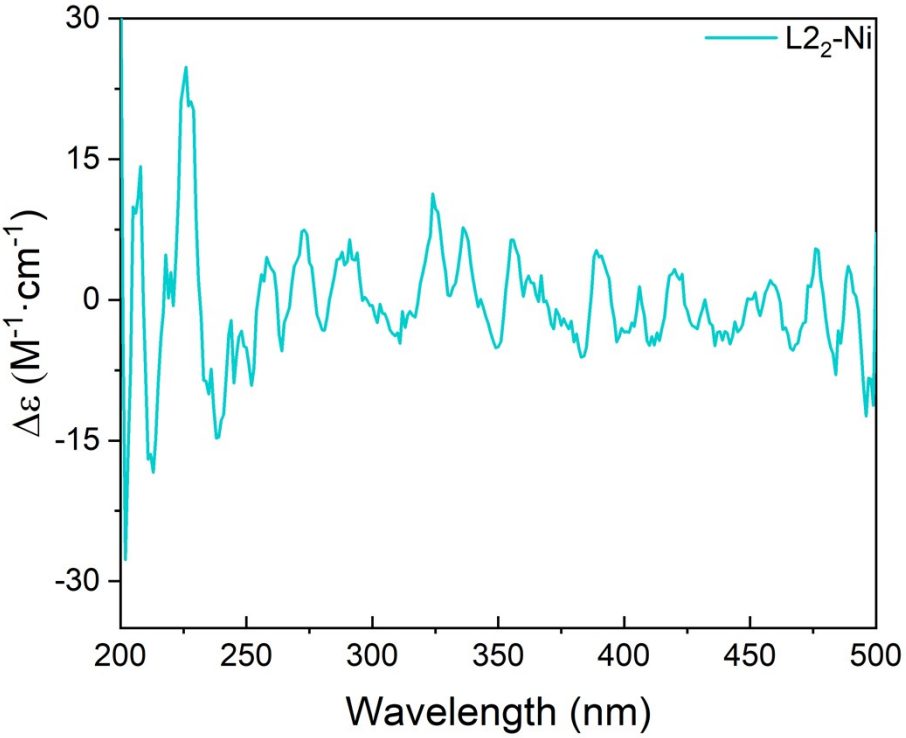

Fig. S86 ECD spectra of L2$_2$-Ni (c = 1 × 10^{-5} M**) in CH$_3$CN.**

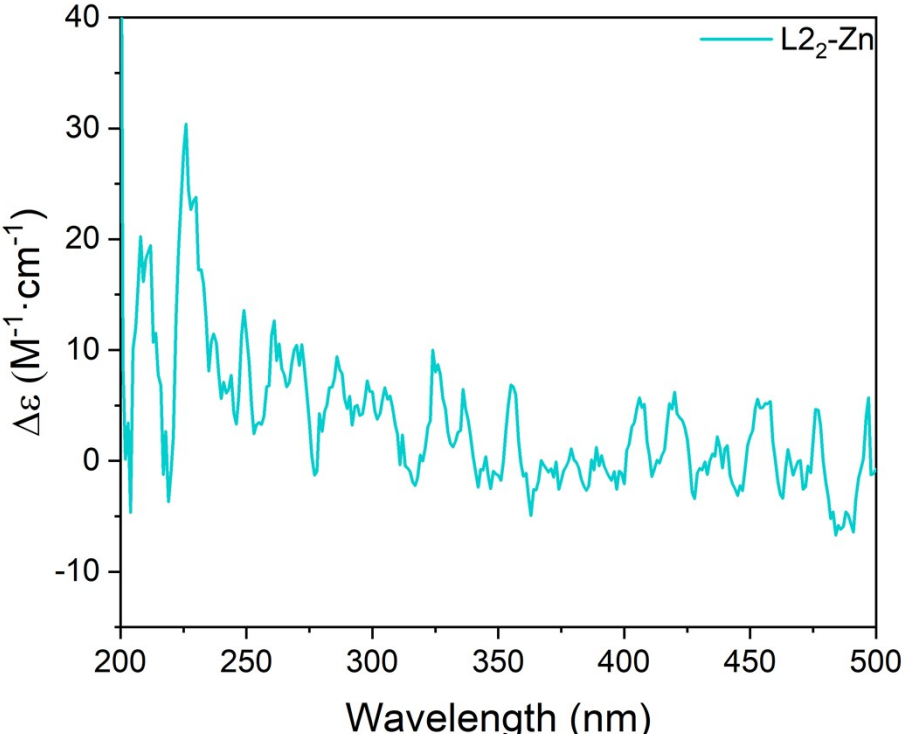

Fig. S87 ECD spectra of L2$_2$-Zn in (c = 1 × 10^{-5} M**) CH$_3$CN.**

Density Functional Theory (DFT) Calculation

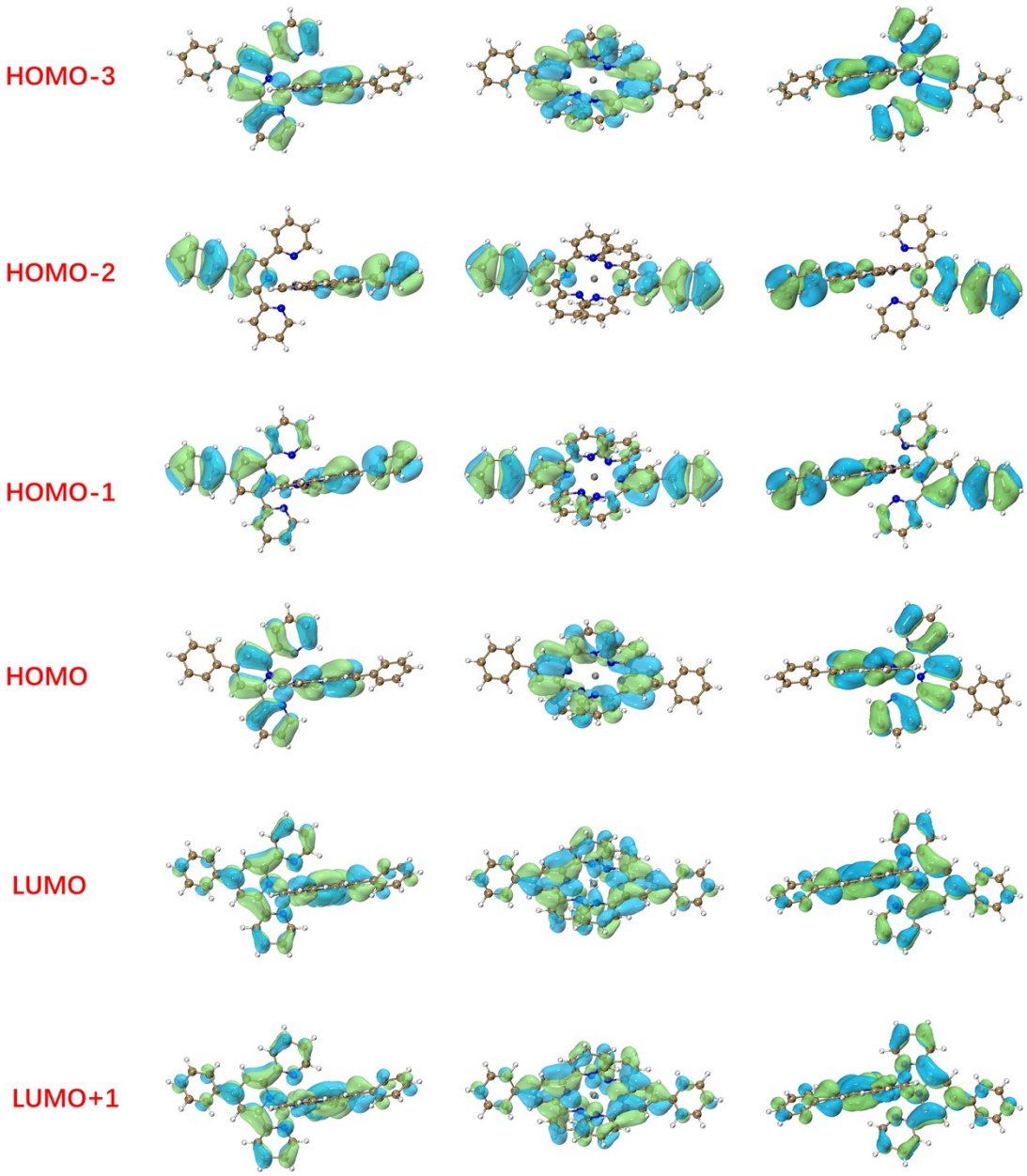

Fig. S88 Frontier molecular orbitals of **$L1_2$-Zn**.

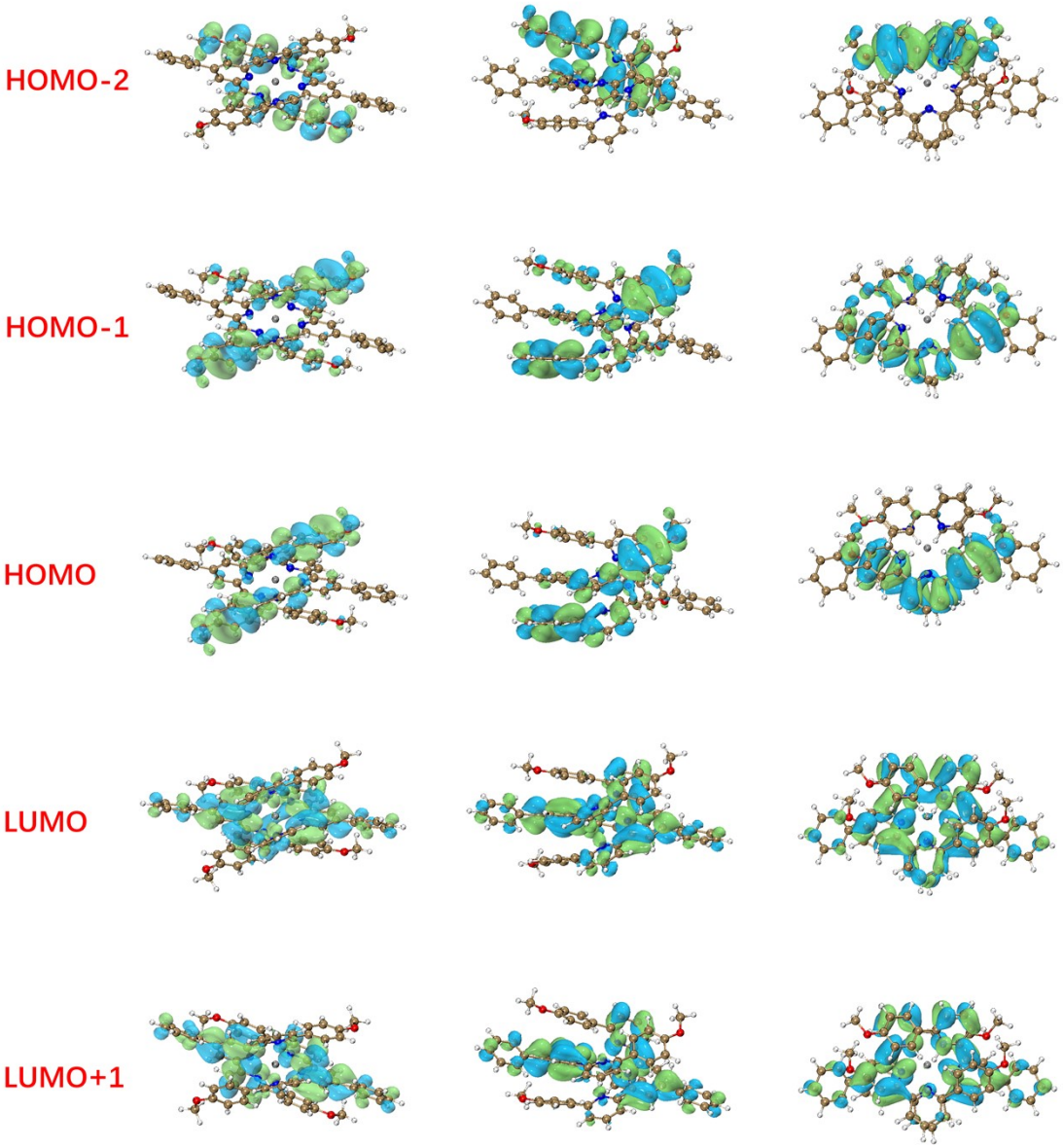

Fig. S89 Frontier molecular orbitals of **L2$_2$-Zn**.

Table S12 The calculated energy levels, oscillator strengths (*f*), and molecular orbital transition analyses of **$L1_2$-Zn** and **$L2_2$-Zn** in CH_3CN.

	State	λ(nm)	f	Assignments
$L1_2$-Zn	S0→S1	312	0.2575	HOMO → LUMO (55.3%)
				HOMO-3 → LUMO+1 (25.7%)
	S0→S2	311	0.3257	HOMO → LUMO+1 (43.3%)
				HOMO-3 → LUMO (32.6%)
	S0→S3	297	0.8845	HOMO-2 → LUMO (54.9%)
				HOMO-1 → LUMO+1 (30.9%)
$L2_2$-Zn	S0→S1	401	0.0038	HOMO → LUMO (92.0%)
				-
	S0→S2	387	0.0011	HOMO-1 → LUMO (63.3%)
				HOMO → LUMO+1 (33.3%)
	S0→S3	382	0.0056	HOMO-2 → LUMO (93.3%)
				-

Table S13 Experimental and calculated optical characteristics for **$L1_2$-Zn** and **$L2_2$-Zn** in CH_3CN.

	Absorption $S_0 \rightarrow S_1$			Emission $S_1 \rightarrow S_0$		
	λ_{exp} (nm)	λ_{calc} (nm)	*f*	λ_{exp} (nm)	λ_{calc} (nm)	*f*
$L1_2$-Zn	338	312	0.2575	349	352	0.5931
$L2_2$-Zn	372	401	0.0038	500	496	0.0036

Reference

[1] G. W. T. M. J. Frisch, H. B. Schlegel, G. E. Scuseria, M. A. Robb, J. R. Cheeseman, G. Scalmani, V. Barone, G. A. Petersson, H. Nakatsuji, X. Li, M. Caricato, A. Marenich, J. Bloino, B. G. Janesko, R. Gomperts, B. Mennucci, H. P. Hratchian, J. V. Ortiz, A. F. Izmaylov, J. L. Sonnenberg, D. Williams-Young, F. Ding, F. Lipparini, F. Egidi, J. Goings, B. Peng, A. Petrone, T. Henderson, D. Ranasinghe, V. G. Zakrzewski, J. Gao, N. Rega, G. Zheng, W. Liang, M. Hada, M. Ehara, K. Toyota, R. Fukuda, J. Hasegawa, M. Ishida, T. Nakajima, Y. Honda, O. Kitao, H. Nakai, T. Vreven, K. Throssell, J. A. Montgomery, Jr., J. E. Peralta, F. Ogliaro, M. Bearpark, J. J. Heyd, E. Brothers, K. N. Kudin, V. N. Staroverov, T. Keith, R. Kobayashi, J. Normand, K. Raghavachari, A. Rendell, J. C. Burant, S. S. Iyengar, J. Tomasi, M. Cossi, J. M. Millam, M. Klene, C. Adamo, R. Cammi, J. W. Ochterski, R. L. Martin, K. Morokuma, O. Farkas, J. B. Foresman, and D. J. Fox, Gaussian 09, Revision D.01; Gaussian, Inc.: Wallingford CT, 2013.

[2] S. Grimme, J. Antony, S. Ehrlich, H. Krieg, The Journal of chemical physics 2010, 132, 154104.

[3] Tian Lu, Feiwu Chen, J. Comput. Chem., 2012, 33, 580-592.

[4] Humphrey, W., Dalke, A. and Schulten, K., “VMD - Visual Molecular Dynamics” J. Molec. Graphics 1996, 14.1, 33-38.

[5]. McMurtrie, J.; Dance, I., Crystal packing in metal complexes of 4′-phenylterpyridine and related ligands: occurrence of the 2D and 1D terpy embrace arrays. CrystEngComm 2009, 11 (6).

[6]. Zhang, Y.; Zhou, P.; Liang, B.; Huang, L.; Zhou, Y.; Ma, Z., Effects of counterions of colorful sandwich-type zinc(II) 4′-phenyl-terpyridine compounds on photoluminescent and thermal properties. Journal of Molecular Structure 2017, 1146, 504-511.

[7]. Brauchli, S. Y.; Constable, E. C.; Harris, K.; Haussinger, D.; Housecroft, C. E.; Rosel, P. J.; Zampese, J. A., Towards catenanes using pi-stacking interactions and their influence on the spin-state of a bis(2,2':6',2"terpyridine)iron(II) domain. Dalton Trans 2010, 39 (44), 10739-48.

[8].Ketkaew, R.; Tantirungrotechai, Y.; Harding, P.; Chastanet, G.; Guionneau, P.; Marchivie, M.; Harding, D. J., OctaDist: a tool for calculating distortion parameters in spin crossover and coordination complexes. Dalton Trans 2021, 50 (3), 1086-1096.